Shibaura Institute of Technology

Graduate School of Engineering and Science

Doctor thesis

Precision Control of Piezo Electric Actuator

Tran Vu Minh

Student ID: NB12506

Major: Functional Control System

Supervisor: Professor Xinkai Chen.

September 2015

Abstract

This dissertation is concerned with piezo electric actuators (PEA), especially modelling and displacement control of them. Piezo electric actuators have been widely used in micro and nanopositioning applications due to their fine resolution, rapid responses, and large actuating forces. Unfortunately, piezo electric actuators exhibit strong hysteresis nonlinearity that reduces the accuracy and that may lead to the instability of the whole system. The control of piezo electric actuators to overcome the hysteresis phenomenon has emerged as a hot topic in recent years.

The main object of this thesis is the control design to overcome the hysteresis phenomenon so that the system can track the reference signal. To solve the problem, mathematical models of the hysteretic system are discussed and controllers are developed for micro-position tracking control of the PEAs. Tracking performance of compensated system is validated using experimental results.

The hysteresis nonlinearity is described by 3 kinds of modelling methods, which are second order linear model, Prandlt-Ishlinskii (PI) hysteresis model, and pseudo discrete-time Bouc-Wen model. Accuracy of the models is shown by experiments.

Based on these models, four model-based control methods are proposed. The feedforward compensation, which is based on identified PI model, is introduced. Because the feedforward compensation technique runs on open-loop fashion, the positioning accuracy is low. In order to improve the performance of PEA, PI control, model predictive control (MPC), and adaptive model predictive control (AMPC) are discussed. Experimental results show that PI control and MPC have better performances than feedforward compensation even though they are based on linear identified model. Lastly, a model reference adaptive control using pseudo discrete-time Bouc-Wen model is proposed. This method can guarantee the closed-loop system stability. Experimental results show the effectiveness of proposed method.

Acknowledgements

I would like to convey my special thanks to my supervisor Professor Xinkai Chen of Department of Electronic and Information Systems, College of Systems Engineering and Sciences, Shibaura Institute of Technology, for his kindness, encouragements, enthusiastic guidance, helpful advices and technical supports.

I would also like to thanks to all students in Systems Control laboratory, Omiya campus, Shibaura Institute of Technology. Special thanks to my all Vietnamese friends. Without their help, this work would not have been possible.

Contents

List of Figures

List of Tables

Notation

$G(z)$: Transfer function of linear PEAs model

$Y(z)$: Displacement

$U(z)$: Applied voltage

z : z-transformation

a_1, a_2, b_1, b_2 : Plant parameters

$u(t), u(k)$: Input

$y(t), y(k)$: Output

$F_r[u](k)$: Play operator

r_i : Threshold

A : A constant

$p(r)$: The density function

N : Number of play operators

$\mu(r_i)$: Weighted coefficients for the threshold r_i

$z(t)$: Hysteresis term

$\alpha_m, \beta_m, \gamma_m, n$: Hysteresis parameters

λ and ϑ : Known parameters

Δt : Sampling period

α_0 : Small positive constant

$\hat{A}$: A constant

$\hat{\mu}(\hat{r}_i)$: Coefficients of the inverse operator

$\hat{r}_i$: Thresholds of inverse operators

$y_{di}(k)$: Reference outputs

K_p : Proportional gain

K_i : Integral gain

P : Cost function

$\hat{y}(k \mid i)$: The ith step predicted output from time step k

$\Delta\hat{u}(k \mid i)$: The ith step predicted incremental input from time step k

N_p : Number of predicted steps

ω and ρ : Weighting coefficients

$x(k)$: The state vector

A, B, C : Known system matrices

$\Delta u(k)$: Control increment

α, β, γ : Unknown hysteresis parameters

$e(k)$: Tracking error

$u_x(k)$: Input variable

$\hat{y}(k)$: Estimated output

$\hat{\alpha}(k)$, $\hat{\beta}(k)$, $\hat{\gamma}(k)$: Estimated parameters

$\varepsilon(k)$: Estimated error

$D(k)$: Norm

Γ : Adaptive gain

$L(k)$: Lyapunov function

B_1, B_2, C_1, C_2, C_3 : Positive constant

Acronyms

PEAs	Piezoelectric actuators
ARX	Auto-regressive exogenous
PI model	Prandlt-Ishlinskii hysteresis model
MRC	Maxwell resistive capacitor model
MPC	Model predictive control
AMPC	Adaptive model predictive control
MRAC	Model reference adaptive control
LM	Levenberh-Marquardt algorithm.

(This page intentionally left blank)

Chapter 1: Introduction

Piezo electric actuators (PEA) have been widely used in the fields of micro and nanopositioning such as atomic force microscopes [1], [2], [3], adaptive optics [4], computer components [5], machine tools [6], aviation [7], internal combustion engines [8], micromanipulators [9] due to their sub nanometer resolution, large actuating force, and rapid response. However, PEA possesses a natural unavoidable hysteresis phenomenon which is nonsmooth nonlinearity. Because of the unknown hysteresis, the performance of PEA is limited especially for those cases requiring speed and accurateness [10]. If the actuators run in an open-loop fashion, the positioning accuracy cannot be achieved. Therefore, control of systems considering hysteresis nonlinearities is important and the development of control techniques to overcome the hysteretic effects is a challenging task.

The goal of this thesis is to design controllers to overcome the hysteresis phenomenon so that the system can track the reference signal. To achieve the goal, a linear model and mathematical models of the hysteretic system are discussed. These models are then utilized in control methods to improve the performance of PEAs. Tracking performance of compensated system is validated using experimental results.

1.1 Working Principles of Piezo Electric Actuator

Pierre and Jacques Curie discovered the piezo electric effect in 1880. Pierre Curie had previously studied the relations of pyro electricity and crystal symmetry, and this must be the

driving force to seek electrification from pressure. In the following year, Lippmann predicted the existence of the inverse piezo electric effect from thermodynamic considerations, and then the Curies verified this before the end of 1881 [11].

Piezo electric actuators are based on the inverse piezo electric effect. In inverse piezo electric effect, voltage is applied to an asymmetrical crystal lattice, causing the material to deform in a certain direction [12].

1.2 Hysteresis

Hysteresis is the time-based dependence of a system's output on current input and past input. In PEAs, hysteresis exists in voltage-displacement relationship as shown in Fig. 1.1. It can be seen in that the hysteresis can be treated as composed of three types of components, which are the major loop that spans the whole input range, the minor loop that only spans portions of input range, and the initial loading curve.

Hysteresis occurs in both relatively static operations and dynamic operations. If the influence of the rate of change of the input can be ignored, then the hysteresis is referred to as rate independent, otherwise rate dependent. As hysteresis being the major nonlinearity of PEAs, compensation of hysteresis has always been a major concern in modelling and control of PEAs.

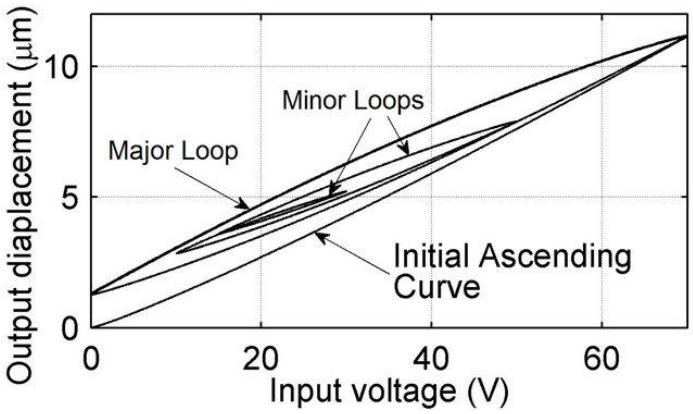

Fig. 1.1 Hysteresis of a PEA

1.3 Modelling of PEAs

With the emergence of PEAs in industry, which are capable of generating larger displacement under applied voltage, significant efforts have been made in the study of

electromechanical behavior of piezoelectric actuators. Piezo electric actuators have been used in the design of different advanced structures, e.g. large-scale space structures, aircraft structures, satellites, and so forth. Because of the importance of their application, the modelling of piezoelectric actuators has received significant attention from the research community.

The linear electromechanical model reported in [13] is an early example of PEA models. But it cannot represent the nonlinear behaviors in PEA due to its linear and static nature. Researchers have developed a lot of models for describing the hysteresis nonlinearities characteristic. In order to describe the basic physical principle of smart materials, physics-based models try to establish the hysteresis model through the relationship of energy, displacement and so on [14], [15] and [16]. The physics-based model of one hysteretic system usually cannot be applied in another system [17]. So, the physics-based model lacks generality. Starting from the characteristics of the hysteresis curve, some hysteresis models try to describe the hysteresis curve directly by using the effective mathematical model. These models can be classified as differential-equation-based hysteresis models and operator-based hysteresis models. Prandlt-Ishlinskii (PI) model is based on the sum of elementary stop or play operators [18], [19], [20] and [21]. The accurateness of PI model depends on the number of these operators. Preisach model and Krasnosel'skii- Pokrovskii model are parameterized by a pair of threshold variables [22], [23], [24], [25] and [26]. Applications of Bouc-Wen model to simulate the hysteresis are reported in [27], [28], and [29]. Wen [27] applies Bouc-Wen model for hysteresis in vibration of mechanical systems. Ismail et al. [28] adopt Bouc-Wen model to describe hysteresis nonlinearity in magneto rheological dampers. Lin and Yang [30] use Bouc-Wen model to model hysteresis behavior in piezoelectric actuators. Researches on Duhem model can be found in [31], [32], and [33].

1.3.1 Preisach Model

The Preisach model is a commonly used hysteresis model employs a simple integral formula to describe the hysteresis effect,

$$y(t) = \int\int \mu(\alpha,\beta)\hat{\gamma}_{\alpha,\beta}[u(t)]d\alpha d\beta \tag{1.1}$$

where $\mu(\alpha,\beta)$ is the weighting function of the hysteresis operator with two parameters α and β which correspond to "up" and "down" switching value of input, respectively. $u(t)$ is

the input voltage. $\hat{\gamma}_{\alpha,\beta}[u(t)]$ is the relay operator. Outputs of relay operator only have two values $+1$ and -1, which is shown in Fig. 1.2.

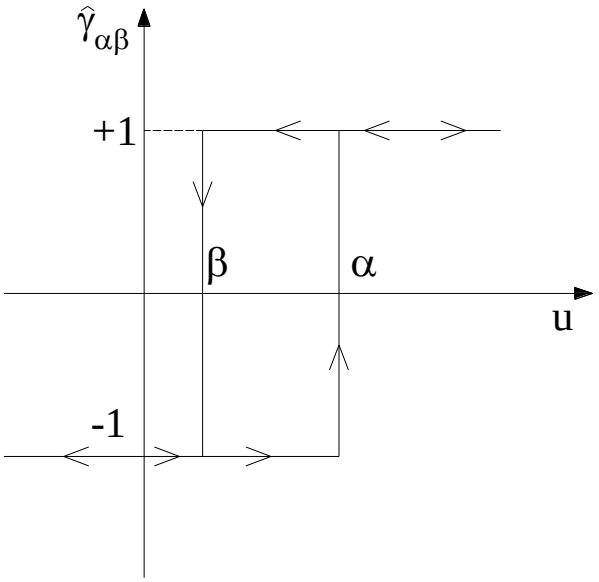

Fig. 1.2 Relay operator

The hysteresis can be regarded as the integral of the hysteresis operator in the α-β plane, as shown in Fig. 1.3.

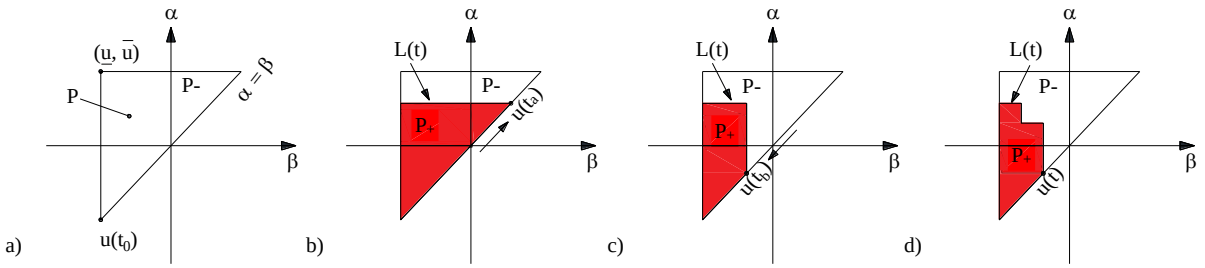

Fig. 1.3 Hysteresis mapping in Preisach model

When the input voltage increases monotonically from $u(t_0)$ to $u(t_a)$, the interference line L(t) moves horizontally from $\alpha = \alpha_{\min}$ to $\alpha = u(t_a)$. In the integral region below the interference line, $\hat{\gamma}_{\alpha,\beta}[u(t)] = 1$; and above this line, $\hat{\gamma}_{\alpha,\beta}[u(t)] = -1$. Therefore, the output displacement $y(t)$ can be written as

$$y(t) = \iint_{p_+} \mu(\alpha,\beta)\,d\alpha d\beta - \iint_{p_-} \mu(\alpha,\beta)\,d\alpha d\beta \tag{1.2}$$

As the input voltage decreases monotonically from $u(t_a)$ to $u(t_b)$, the interference line L(t) moves vertically from $\beta = u(t_a)$ to $\beta = u(t_b)$. To the left of the interference line, $\hat{\gamma}_{\alpha,\beta}[u(t)] = 1$ and to the right, $\hat{\gamma}_{\alpha,\beta}[u(t)] = -1$. In general, the output of the hysteresis equals to the integral of the hysteresis weighting function in the P+ region, and this leads to the memory effect of hysteresis. The Preisach model can describe a wide range of hysteresis accurately, but the lack of physical meaning makes it difficult to understand. Also, digital implementation requires lots of calculations.

1.3.2 Prandlt-Ishlinskii Hysteresis Model

One of the well-known operator-based models, which is used to characterize the hysteresis in PEAs and other types of smart materials, is the classical PI model that utilizes two essential hysteresis operators, namely, the play operator and the stop operator.

1.3.2.1 PI Model Using Stop Operator

The rate-independent stop operator is illustrated in Fig. 1.4. Conceptually, this operator determines the linear stress-strain $(u\,; w)$ relationship as in the Hook's law, when the stress is less than the yield stress, r. In analytical form, assume that $C_m[0, K]$ is the space of piece-wise monotone functions. For arbitrary input $u(k) \in C_m[0, K]$ and $r \geq 0$, where $0 < k_0 < k_1 < ... < k_n < K$ are intervals in $[0, K]$ such that the function u is monotone on each subintervals $[k_i, k_{i+1}]$ the output of the stop operator is expressed as

$$E_r[u; w_{-1}](0) = e_r(u(0) - w_{-1})$$

$$E_r[u; w_{-1}](k) = e_r(u(k) - u(k_i) + E[u; w_{-1}](k_i)) \tag{1.3}$$

$$e_r(u) = \min(r, \max(-r, u)) \tag{1.4}$$

Then the output of the Prandlt-Ishlinskii hysteresis model using stop operator is defined by

$$y(k) = \int_0^R p(r) E_r[u\,; w](k)\, dr \tag{1.5}$$

where $p(r)$ is the density function, satisfying $p(r) \geq 0$, and R is a positive constant.

The Prandlt-Ishlinskii hysteresis model (1.5) is approximated by the discrete form as follows:

$$y(k) = \sum_{i=1}^{N} \mu(r_i) E_{r_i}[u; w](k) \tag{1.6}$$

where N is the number of the adopted stop operators for modelling, and $\mu(r_i)$ are the weighted coefficients for the threshold r_i.

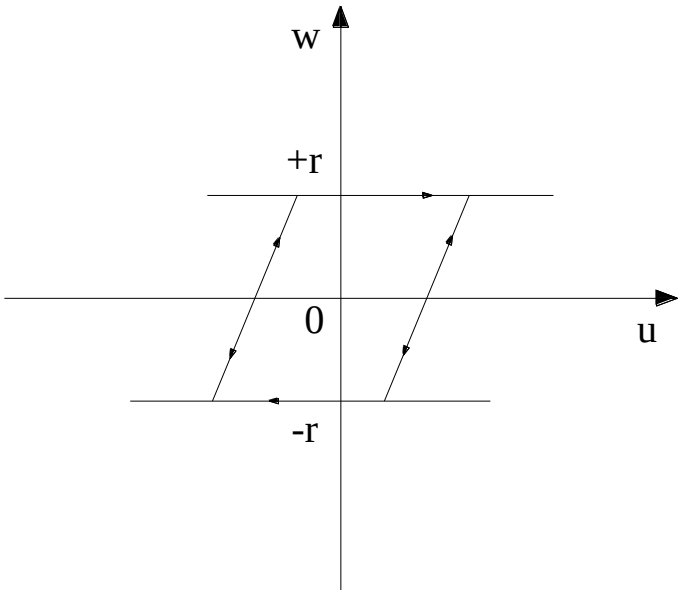

Fig. 1.4 Stop operator

1.3.2.2 PI Model Using Play Operator

The rate-independent play operator is demonstrated in Fig. 1.5. This operator implies the reciprocating motion of a piston inside a cylinder with length $2r$, where the instantaneous position of center of piston is defined by u and w as input and output subsequently. In analytical form, for any input $u(k) \in C_m[0, K]$ and $r \geq 0$, the play operator is inductively defined by

$$F_r[u; w_{-1}](0) = f_r(u(0) - w_{-1})$$

$$F_r[u; w_{-1}](k) = f_r(u(k), F[u](k_i)) \tag{1.7}$$

$$f_r(u, w_{-1}) = \max(u - r, \min(u + r, w)) \tag{1.8}$$

where w_{-1} defines the initial state.

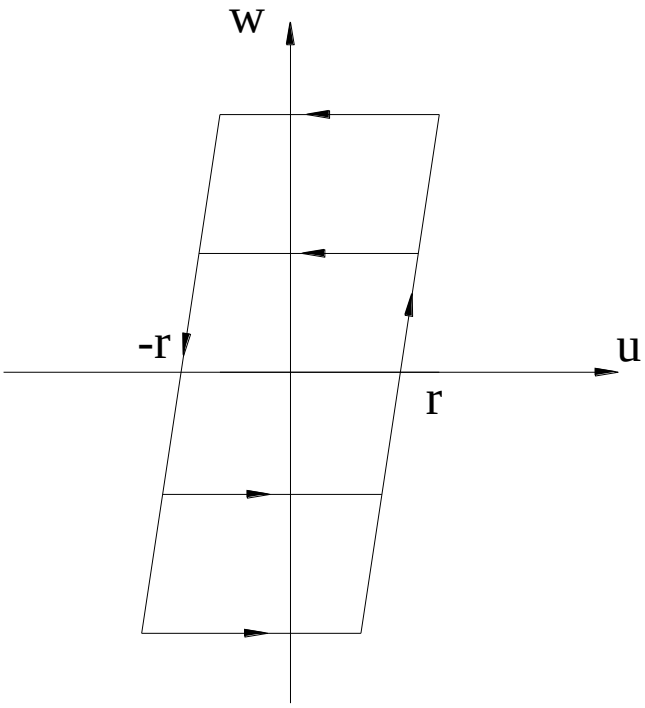

Fig. 1.5 Play operator

Then the output of the Prandlt-Ishlinskii hysteresis model using play operator is defined by

$$y(k) = Au(k) + \int_0^R p(r) F_r[u](k)dr \tag{1.9}$$

where A is a constant, $p(r)$ is the density function, satisfying $p(r) \geq 0$, and R is a positive constant.

The discrete form of classical PI model using play operator can be written as follows:

$$y(k) = Au(k) + \sum_{i=1}^{N} \mu(r_i) F_{r_i}[u](k) \tag{1.10}$$

where N is the number of the adopted play operators, and $\mu(r_i)$ are the weighted coefficients for the threshold r_i.

It should be note that the classical PI model can only describe the symmetric hysteresis. To be able to describe the asymmetric hysteresis curve, the classical PI model has to be modified.

1.3.3 Maxwell Resistive Capacitor Model (MRC)

Similar to the PI hysteresis model, the MRC hysteresis model represents the hysteresis by putting n spring-slider elements in parallel, each of which consists of a linear spring with stiffness k_i in series with a Coulomb friction block having a breakaway force f_i (see Fig. 1.6). The constitutive behavior of the Maxwell-slip friction model can be described by

$$\dot{x}_i(t) = \begin{cases} 0 & if \quad k_i[x(t) - x_i(t)]\operatorname{sgn}\dot{x}(t) < f_i \\ \dot{x}(t) & if \quad k_i[x(t) - x_i(t)]\operatorname{sgn}\dot{x}(t) \geq f_i \end{cases} \tag{1.11}$$

$$f(t) = \sum_{i=1}^{n} k_i(x(t) - x_i(t)) \tag{1.12}$$

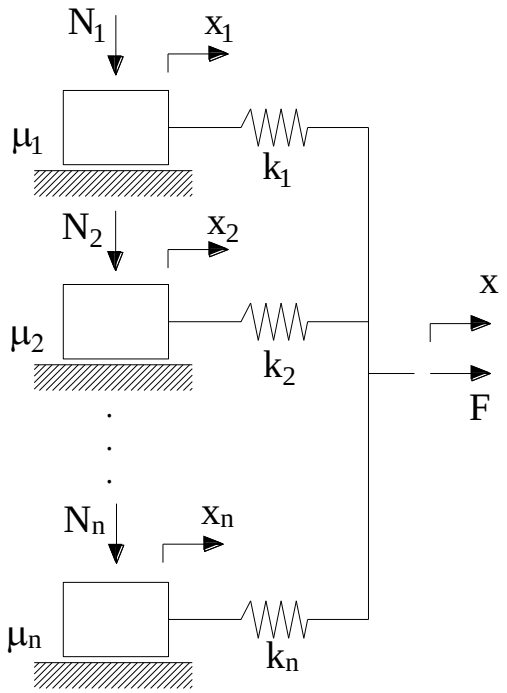

Fig. 1.6 The physical interpretation of the MRC hysteresis model

where x is the input displacement, F is the output force, k_i, x_i and $f_i = \mu_i N_i$ are the spring stiffness, block position, and breakaway force of the ith spring-slider element, respectively.

When the displacement increases or decreases continuously, the gain between the force and the displacement changes piecewise linearly, this is used to fit the nonlinear gain between the input and output in the hysteresis loop. The sliding elements come to stick when the

movement changes direction, which is used to characterize the sudden switch of the gain at the endpoint of the hysteresis loop.

1.3.4 Duhem Model

The generalized Duhem model is also a candidate for hysteresis. It can be described by

$$\begin{aligned} \dot{x}(t) &= f[x(t),u(t)]g[\dot{u}(t)], x(0) = x_0, t \geq 0 \\ y(t) &= h[x(t),u(t)] \end{aligned} \tag{1.13}$$

where x is the state, x_0 is the initial state, u and y are respectively the input and output of the hysteresis, f, g and h are continuous functions.

If the following parameters are given: $f[x(t),u(t)] = \left[-\gamma x(t) + \frac{d\phi[u(t)]}{du(t)}, \gamma x(t) + \frac{d\phi[u(t)]}{du(t)} \right]$;

$g[\dot{u}(t)] = [\dot{u}_+(t), \dot{u}_-(t)]^T$; $y(t) = x(t) + \mu u(t) + h_0[u(t)]$; where $\dot{u}_+(t) \triangleq \max\{0, \dot{u}\}$ and $\dot{u}_-(t) \triangleq \min\{0, \dot{u}\}$ then the Duhem model can be changed into the Bouc-Wen model [34].

1.3.5 Bouc-Wen Model

The Bouc-Wen model has received an increased interest in recent years. Due to its capability to form a range of shapes of hysteretic cycles which match the behavior of a wide class of hysteretic systems. It can be seen in Fig. 1.7 that a force F corresponding to the point $x = x_0$ is not unique, there are four values of F. Therefore, the force at the instant time t depends not only on the displacement at the time t but also on the past values of the displacement. Introducing an assumption:

A1*: Fig. 1.7 remains the same for all increasing functions* $x(.)$ *between 0 and* x_1*, for all decreasing functions* $x(.)$ *between the values* x_1 *and* x_2*, etc.*

The aforementioned assumption is called rate-independent property [17]. The form of the function F is described as

$$\frac{dF}{dt} = g\left(x, F, sign\left(\frac{dx}{dt} \right) \right) \frac{dx}{dt} \tag{1.14}$$

Consider the following equation

$$\frac{d^2 x}{dt} + F(t) = u(t) \tag{1.15}$$

for some given input $u(t)$ and initial conditions $\frac{dx}{dt}(t_0)$, $x(t_0)$ and $F(t_0)$ at the initial time instant t_0, Equations (1.14) and (1.15) can describe the hysteresis oscillator.

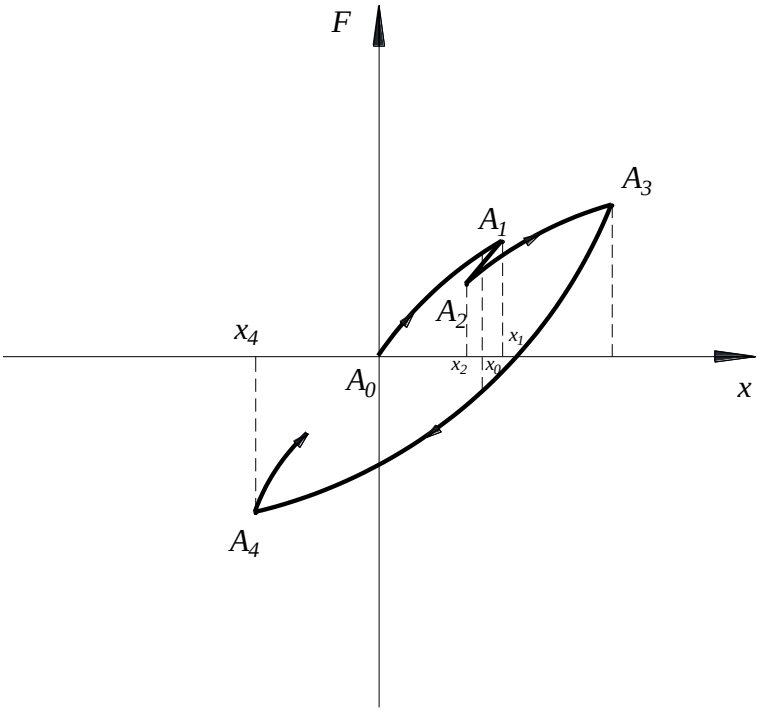

Fig. 1.7 Force and displacement for a hysteresis functional

However, due to the nonlinearity of the function g, it is difficult to give the explicit solutions of Equation (1.14) [35]. Applying a variant of the Stieltjes integral, the function F is defined as follow

$$F(t) = \mu^2 x(t) + \int_{t_1}^{t} F\left(V_s^t\right) dx(s) \tag{1.16}$$

where $t_1 \in [-\infty,+\infty)$ is the time instant, which is given after the force and the displacement is defined. V_s^t is the total variation of x in the time interval $[s,t]$. The function F can be chosen manually such that it satisfies some mathematical properties of the hysteresis properties. An example of F is as follow

$$F(u) = \sum_{i=1}^{N} A_i e^{-\alpha_i u} \tag{1.17}$$

where A_i are shown in Fig. 1.7 and $\alpha_i > 0$. Equations (1.15)-(1.17) can be written in the form

$$\frac{d^2x}{dt} + \mu^2 x + \sum_{i=1}^{N} Z_i = u(t) \tag{1.18}$$

$$\frac{dZ_i}{dt} + \alpha_i \left|\frac{dx}{dt}\right| Z_i - A_i \frac{dx}{dt} = 0,\ i = 1,\ldots,N \tag{1.19}$$

Equations (1.18) and (1.19) are known as the Bouc model. Later, Wen [16] extended the Equation (1.19) to describe the restoring forces with hysteresis as follow:

$$\dot{z} = \alpha\dot{x} - \beta|\dot{x}||z^{n-1}|z - \gamma\dot{x}|z^n| \tag{1.20}$$

1.3.6 Bashash and Jalili Model

Bashash and Jalili [36] introduced an intelligence rule for representing piecewise hysteresis. They used an exponential expression to describe the hysteresis curve between two extreme points in the voltage-displacement plane

$$x(v) = F(v, v_1, x_1, v_2, x_2) = k\left(1 + \alpha e^{-\tau(v-v_1)}\right)(v - v_1) + x_1 \tag{1.21}$$

where $k = \dfrac{x_2 - x_1}{v_2 - v_1}\left(1 + \alpha e^{-\tau(v-v_1)}\right)^{-1}$, and (v_1, x_1) and (v_1, x_1) are the two arbitrary extreme points. The predicted ascending hysteresis path can be represented by:

$$x_A(v) = F(v, v_{L1}, x_{L1}, v_{U1}, x_{U1})H(v, v_{L1}, v_{U1}) + \sum_{i=1}^{A} F_{Ai}(v)H(v, v_{U_i}, v_{U_{i+1}}) \tag{1.22}$$

where H is the Heaviside function. The same equation predicts the descending hysteresis path. When the intelligence rule is applied to feedforward control, determining the inverse of the intelligence hysteresis model is not difficult. Bashash and Jalili reduced the nonlinearity of hysteresis from 14 to 1%. However, all of the extreme points must be considered in predicting the hysteresis path. Therefore, its implementation is difficult.

1.4 Displacement Control

Piezo electric actuators are widely used in applications requiring high resolution and accuracy. However, hysteresis reduces the open-loop positioning accuracy. If high accuracy is required, these nonlinearities need to be compensated. The compensation is usually accomplished by means of two control method: feedforward control, where nonlinear hysteresis models are typically used [37], [1], [10]; feedback control, where various displacement sensors are used [38], [39], [40], [41], [42], and [43].

1.4.1 Feedforward Control

The basic idea of feedforward control is the inverse compensation. The approximate inverse hysteresis model is used to cancel the effects of hysteresis. Assume an actuator with an approximate mathematical model H. The inverse model H^{-1} is calculated based on identified model H. In no load condition the open-loop feedforward compensation has been shown effective in [1], [44-48].

However, one major disadvantage of the open-loop feedforward is that their positioning performances are highly sensitive to disturbances and modelling errors. In practice, feedforward control is commonly combined with feedback control, as shown in Fig. 1.8.

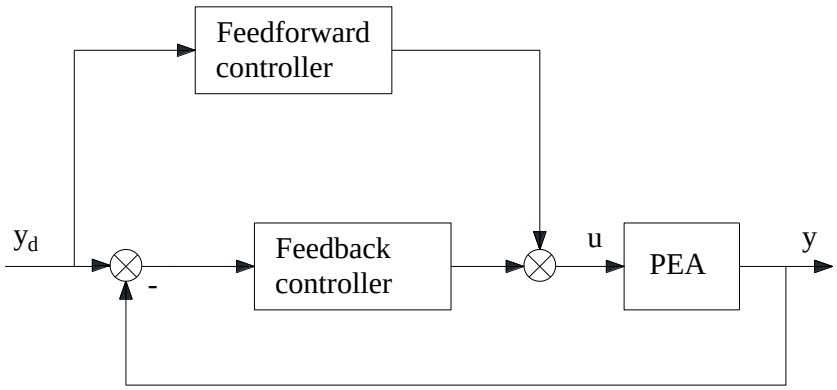

Fig. 1.8 Inverse feedforward based feedback control

1.4.2 Iterative Learning Control

Iterative learning control (ILC) does not require accurate hysteresis models. An iterative controller generates the control action at present based on the tracking error and the control action of the previous iteration, as shown in Fig. 1.9.

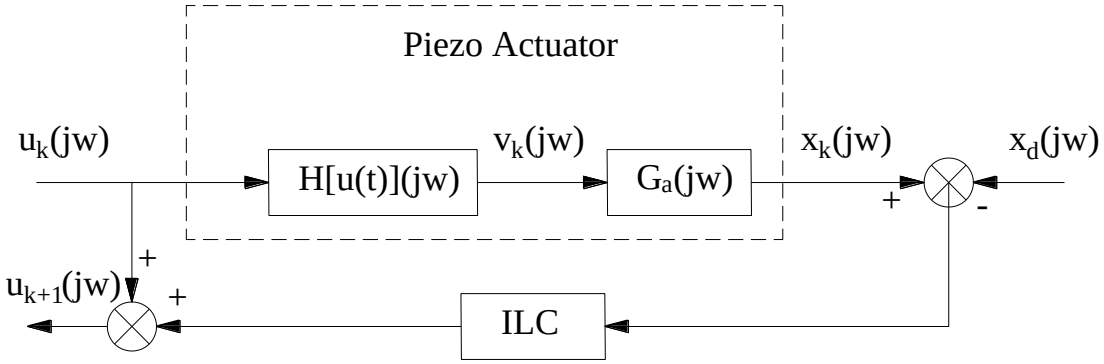

Fig. 1.9 Iterative learning control

The control action of ILC is given by

$$u_0(jw)=0, u_{k+1}(jw)=u_k(jw)+\rho(jw)G_{a.m}^{-1}(jw)\times[x_d(jw)-x_k(jw)] \quad (1.23)$$

where $G_{a.m}^{-1}(jw)$ is the frequency response model of the system, $\rho(jw)$ is the frequency-dependent iterative coefficient, $u_k(jw)$ and $x_k(jw)$ are the Fourier transform of the input and output at the k^{th} iteration respectively. The goal of ILC is to generate a feedforward control that tracks a specific reference signal and rejects the repeating disturbance. As such, the control performance is highly robust for system uncertainties. Moreover, it can significantly increase the manipulation bandwidth without reducing the positioning precision. However, ILC is an open-loop control. For non-repeating disturbance or system uncertainties, a

feedback controller is required as well. In spite of this, ILC has been widely used in nanopositioning, such as in the control of automated teller machine (ATM), because a plant model is not required, it has self-learning adaptability, and it is robust.

1.4.3 Feedback Control

Feedback control schemes as shown in Fig. 1.10 can lead to strong suppression of unknown effects including disturbances, modelling errors, as well as improvement in position control performance hence they are widely used.

A classical control technique such as PID control is widely used because of its simplicity [49], [50], [51], [52]. However, because PID control is limited in bandwidth while dealing with strong uncertainties [53], advance control techniques, such as sliding model control [54-58], adaptive control [59-65], model predictive control [66], [67] are required.

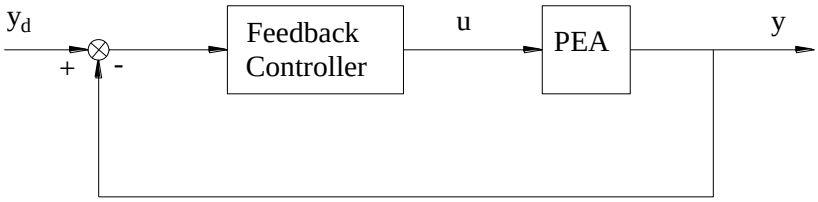

Fig. 1.10 A feedback control scheme for PEAs

1.4.3.1 Sliding Mode Control

Sliding mode control (SMC), which is sometimes known as variable structure control (VSC), is characterized by a discontinuous control action which changes structure upon reaching a set of predetermined switching surfaces. This kind of control may result in a very robust system and thus provides a possibility for achieving the goals of high-precision and fast response. Some promising features of SMC are listed below:

• The order of the motion can be reduced

• The motion equation of the sliding mode can be designed linear and homogenous, despite that the original system may be governed by non-linear equations.

• The sliding mode does not depend on the process dynamics, but is determined by parameters selected by the designer.

• Once the sliding motion occurs, the system has invariant properties which make the motion independent of certain system parameter variations and disturbances. Thus the system performance can be completely determined by the dynamics of the sliding manifold.

Consider the system defined below

$$\dot{x} = f(x,t) + B(x,t)u(x,t),\ x \in R^n,\ u \in R^m \tag{1.24}$$

where $f(x,t)$ and $B(x,t)$ are assumed continuous and bounded and the rank of $B(x,t)$ is m.

The discontinuous control is given by

$$u = \begin{cases} u^+(x,t) & if\ \sigma(x) > 0 \\ u^-(x,t) & if\ \sigma(x) < 0 \end{cases} \tag{1.25}$$

where $u^+(x,t)$, $u^-(x,t)$ and $\sigma(x)$ are continuous functions. Since $u(x,t)$ undergoes discontinuity on the surfaces $\sigma_i(x) = 0$, $\sigma_i(x) = 0$ is called the switching surface or the switching hyperplane.

Let $S = x\big|_{\sigma(x)=0}$ be a switching surface that includes the origin $x = 0$. If, for any x_0 in S , $x(t)$ is in S for all $t > t_0$, then $x(t)$ is a sliding mode of the system and the switching surface S is called a sliding surface or sliding manifold. A sliding mode exists, if in the vicinity of the switching surface S, the tangent or the velocity vectors of the state trajectory always point towards the switching surface.

Existence of a sliding mode requires stability of the state trajectory towards the sliding surface $S = x\big|_{\sigma(x)=0}$ at least in the neighborhood of S , i.e., the representative point must approach the sliding surface at least asymptotically. This sufficient condition for sliding mode is called reaching condition and state trajectory under the reaching condition is called the reaching mode or reaching phase. The largest neighborhood of S for which the reaching condition is satisfied is called the region of attraction.

In order to guarantee desired behavior of the closed-loop system, the sliding mode controller requires infinitely fast switching mechanism. However, due to physical limitations

in real-world systems, directly applying the above control will always lead to some oscillations in some vicinity of the sliding surface, i.e., the so called chattering problem. The main limitations come from the implementation of controllers in digital computers which work on discrete-time principles and cannot allow infinitely fast switching.

1.4.3.2 Adaptive Control

The modelling error, parameter uncertainty and the changes to the system's environment will result in differences between the desired and real situations. An effective way to solve this problem is to use adaptive control. Adaptive Control covers a set of techniques which provide a systematic approach for automatic adjustment of controllers in real time, in order to achieve a desired performance when the parameters of the plant dynamic model are unknown and/or change in time. The foundation of adaptive control is parameter estimation. Common methods of estimation are recursive least squares and gradient descent. Lyapunov stability is used to derive these update laws and show convergence criterion. Fig. 1.11 shows an adaptive control system, where u and y are system input and output, respectively.

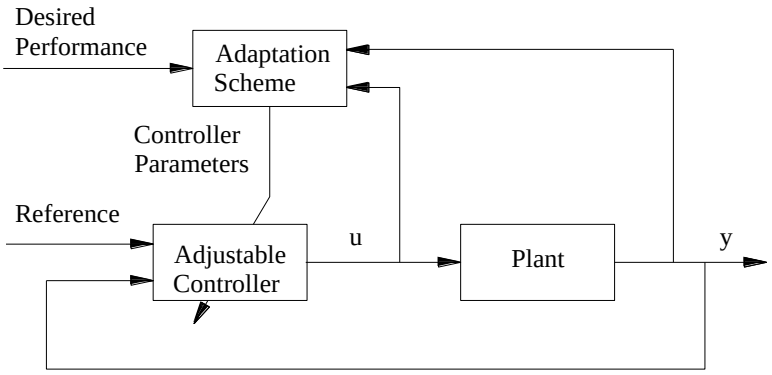

Fig. 1.11 Adaptive control system

1.4.3.3 Intelligent Control

Essentially, two main types of intelligent control have been widely used, i.e., fuzzy logic control and neural network control. Researchers have encountered significant challenges in active vibration suppression using the traditional control method. Therefore, intelligent control attracts great attention. The characteristics of fuzzy control are that it can use

subjective experience and intuition. It provides a new idea in solving complicated system control problems. In addition, the neural network which has learning and adaptive abilities can approximate the continuous function in arbitrary precision. It is able to conduct a large number of operations quickly. So, the neural network control has a great potential in the identification and control of nonlinear and uncertain systems, especially in piezo-positioning mechanism.

1.4.4 Charge Control

In 1981, a patent was granted for the use of charge control to reduce the hysteresis effect of PEAs [68]. Many researchers combined the use of charge control with other feedback control methods to reduce hysteresis nonlinearity [69], [70], [71], [72]. A grounded load charge amplifier is illustrated in Fig. 1.12, where R_s and R_L are resistances C_s and C_L are capacitors, v_{ref} is the applied reference voltage, q_L and q_{L_C} represents the load charge and actual charge respectively.

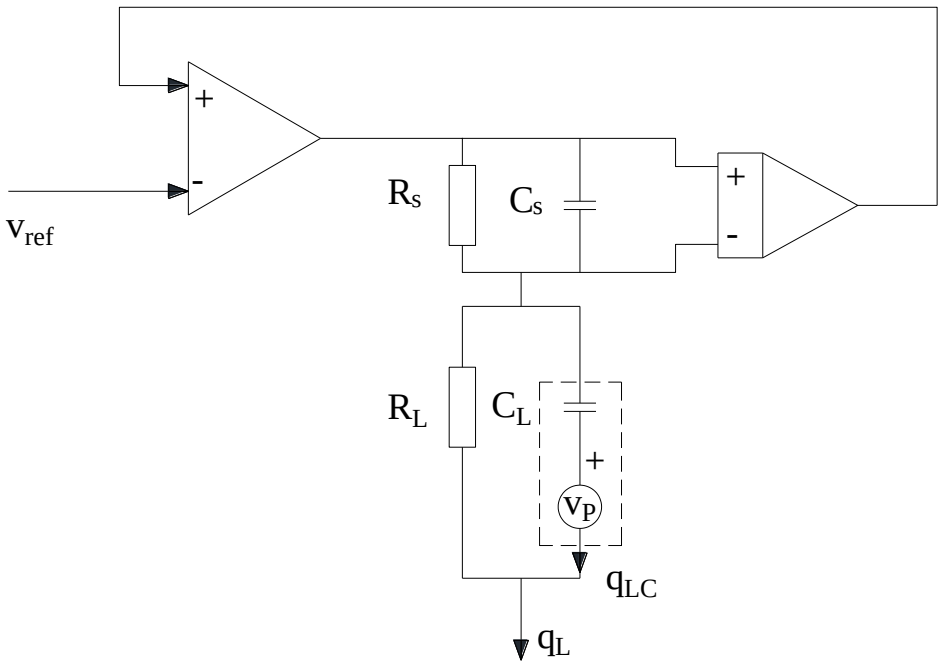

Fig. 1.12 Grounded load charge amplifier

The transfer function between the load charge and the reference voltage is:

$$\frac{q_L(s)}{v_{ref}(s)} = C_s \frac{s + \dfrac{1}{C_s R_s}}{s} \tag{1.26}$$

Thus, $\dfrac{q_{L_C}(s)}{v_{ref}(s)} = \dfrac{q_L(s)}{v_{ref}(s)} \dfrac{q_{L_C}(s)}{q_L(s)} = C_s \dfrac{s + \dfrac{1}{C_s R_s}}{s} \dfrac{s}{s + \dfrac{1}{C_L R_L}}$. Setting $C_s R_s = C_L R_L$, $\dfrac{q_{L_C}(s)}{v_{ref}(s)} = C_s$.

At frequencies above $1/RC$, the charge of the amplifier can be used to reduce the hysteresis effect. The results show an 89% reduction in the hysteresis. However, charge control requires hardware support which increases the difficulty and cost in applications.

1.5 Objectives

From these backgrounds, this dissertation aims at developing control techniques to improve the PEAs performance and implementing them digitally. To fulfill this requirement, the following objectives are set.

1. Model the PEAs to describe their behavior.

Hysteresis is an important nonlinear effect in PEAs. To develop the control scheme for the PEA, it is necessary to introduce the appropriate models.

Linear system identification method, which is based on the relationship between inputs (voltage) and outputs (displacement), is applied to obtain the nominal linear PEAs model. Hysteresis nonlinearities in PEAs are neglected.

To describe the hysteresis in PEAs, two hysteresis models are proposed which are classical PI model and pseudo discrete-time Bouc-Wen model. The PI model is validated by experimental results; also the explicit inverse model can be generated.

In comparison with classical PI model, the pseudo Bouc-Wen model has less parameters, the model structure is simple and can be used directly for model based control.

2. Controller design

In order to compensate for the hysteresis and improve the performance of PEA, an output tracking feedforward compensation approach will be developed. The inverse classical PI model is adopted. The performance of this method is shown by experimental results.

Also, this thesis considers applications of PID control, model predictive control and adaptive model predictive control on PEAs with the proposed linear system identification model. To demonstrate the effectiveness of the developed methods, experiments will be carried out on a PEA with varying sampling rates.

To have a further look into model based control, this thesis introduces adaptive control based on pseudo discrete-time Bouc-Wen model. The stability and zero steady state error of the proposed method will be theoretically proven. The experimental results show the effectiveness of the proposed method.

1.6 Hardware for Experiments

The PEA using for experiments is PFT-1110 (Nihon Ceratec Corporation) as shown in Fig. 1.13. Table 1.1 shows the actuator specifications. The displacement is measured by the noncontact capacitive displacement sensor (PS-1A Nanotex Corporation) which has 2-nm resolution. Specifications of the sensor are shown in table 1.2. Fig. 1.14 shows the experimental schemes. Input/output data are handled by an interface board AIO-163202F-PE installed on PCI-Express bus. The board includes high precision 16-bits analog inputs (32 channels) and 16-bits analog outputs (2 channels) with sampling rate up to 500kHz. The control program is implemented on computer in C language.

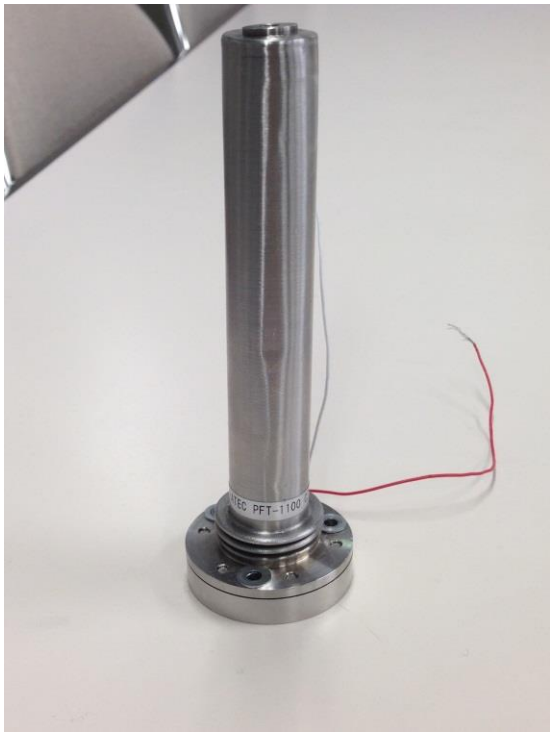

Fig. 1.13 Piezo electric actuator PFT-1110

Table 1.1 Piezo electric actuator PFT-1100 specifications

Specifications	PFT 1110
Operating temperature range	-20~85 ^{o}C
Maximum operating voltage	150V
Maximum displacement	≥ 83 μm
Hysteresis	15 ± 3%
Maximum generated force	≥ 800N
Resonance frequency	5 ± 3kHz
Capacitance	10.8μF ± 20%
Dielectric loss	≤ 3.0%
Insulation resistance	≥ 100 MQ

Dimension: L x ϕ (mm)	125.9 x ϕ40
High stiffness	

Table 1.2 Sensor PS-IA specifications

Specifications	PS-IA
Basic output voltage range	0~10 V
Frequency characteristic	DC~1 kHz
Operating temperature limit	10~40^{o}C
Resolution	2 nm
External Dimension	110W x 30H x 162D mm
Weight	335 gr

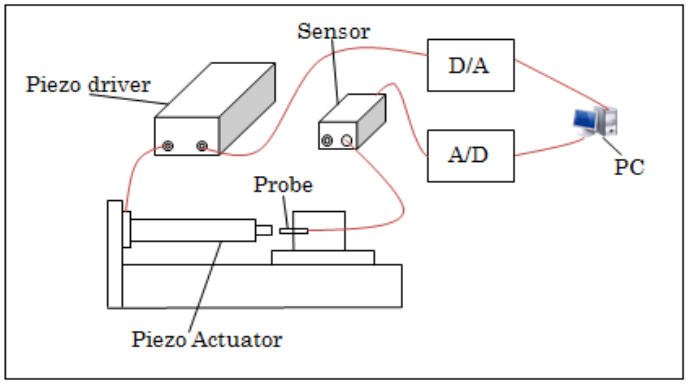

Fig. 1.14 Experimental schemes

1.7 Composition of The Dissertation

This dissertation is structured as follows:

Chapter 2 discusses a simple open-loop control known as feedforward compensation. First, the classical PI hysteresis model is adopted and identified. Then, an inversion of Prandlt-Ishlinskii model is calculated to design the controller. The tracking performance is verified by experiments at different reference signal frequencies and magnitudes.

In Chapter 3, a conventional PI controller is designed base on linear system identification. The strength and weakness of the method is also discussed.

To utilize the linear system identification model, model predictive control and adaptive model predictive control are proposed in Chapter 4. These methods are proved to have a better tracking performance comparing to simple PI control.

In Chapter 5, a model reference control base on pseudo discrete-time Bouc-Wen model is proposed. The control law is simple and easy to be implemented. The control algorithm ensures the stability of the closed-loop system. Experimental results show the effectiveness of the proposed method.

Chapter 6 concludes this thesis and discusses the future works.

Chapter 2: Feedforward Compensation

2.1 Introduction

This chapter concerns with controller design based on feedforward compensation technique using classical PI hysteresis model in discrete-time formulation [73].

Feedforward compensation (open-loop) schemes are usually employed in application in which position feedback is difficult to implement due to mechanical constraints such as atomic force microscopes [1-3]. In such schemes, the inverse model of the PEA to be control is calculated and implemented to PEA. The inverse model generates an input voltage to PEA according to desired displacement, such that the PEA produces an output that tracks the reference output. Usually, the inverse of the transfer function is cascaded with the plant. In this thesis, a feedforward controller which is based on Prandlt-Ishlinskii hysteresis model is designed.

One major disadvantage of the open-loop control schemes is that their positioning performances are highly sensitive to unknown effects such as model errors and disturbances.

2.2 Identified PI Model Parameters

The threshold of play operator (1.10) is applied in the Prandlt-Ishlinskii model as $r_1 < r_2 < ... < r_N$ and N is chosen as 16. The constant A and the weighted coefficients are identified off-line by curve fitting toolbox in MATLAB using experimental data. This tool

box uses Levenberh-Marquardt algorithm, which will be discussed in Appendix, to identify model parameters. The input $u(k) = 20*(-0.06*k*0.001+1.1)\sin(2*\pi*k*0.001+3*\pi/2)$ $+1.1$ is applied to the PEA for identification, the sampling time period is chosen as 0.001 s. Table 2.1 shows the identified parameters.

Table 2.1 Identified parameter Prandlt Ishlinskii model

Number	Threshold r_i	Parameter $\mu(r_i)$	A
1	1	0.3209	0.5
2	2	0.0011	
3	3	0.0172	
4	4	0.0205	
5	5	0.0173	
6	6	0.0158	
7	7	0.0158	
8	8	0.0188	
9	9	0.0111	
10	10	0.0010	
11	11	0.1161	
12	12	0.5591	
13	13	0.0010	
14	14	0.0010	
15	15	0.0010	
16	16	0.0010	

Fig. 2.1 shows comparison of the experimental and simulation results. The difference between measure output and calculated output is shown in Fig. 2.2.

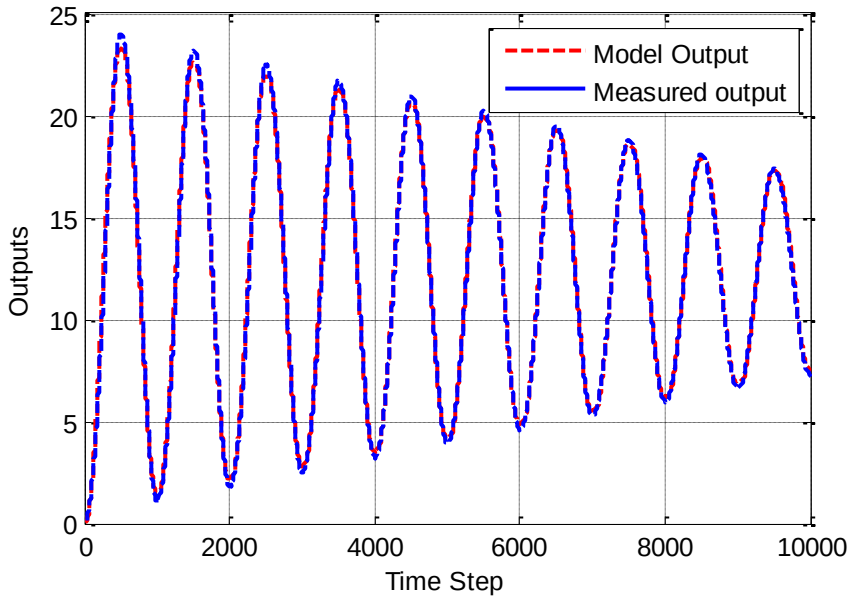

Fig. 2.1 Comparison of measured output and model output

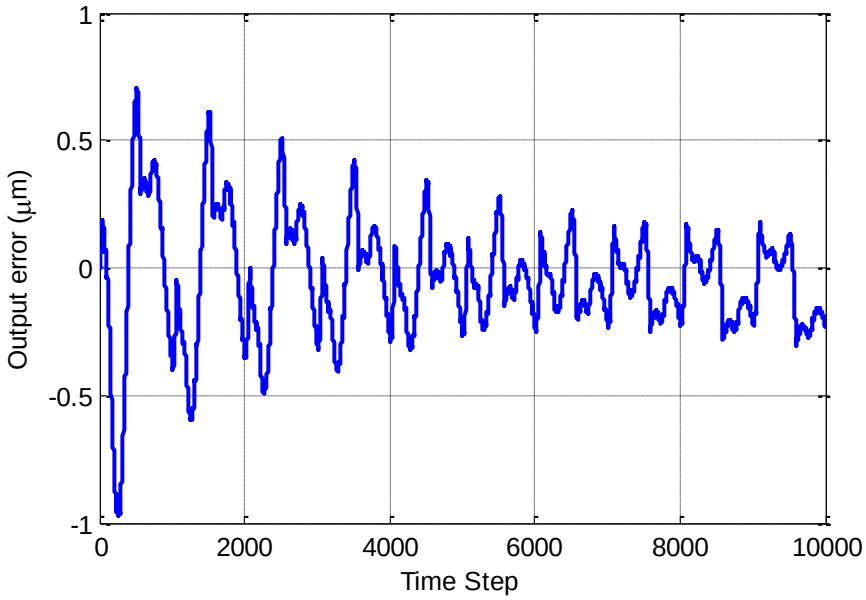

Fig. 2.2 Difference between measured output and calculated PI model output

It should be mentioned that, the identified parameters are not unique; they depend upon the nature of hysteresis of PEAs. Furthermore, the relationship between input and modelling error is still some kinds of hysteresis (as in Fig. 2.3). Thus, the compensation is difficult.

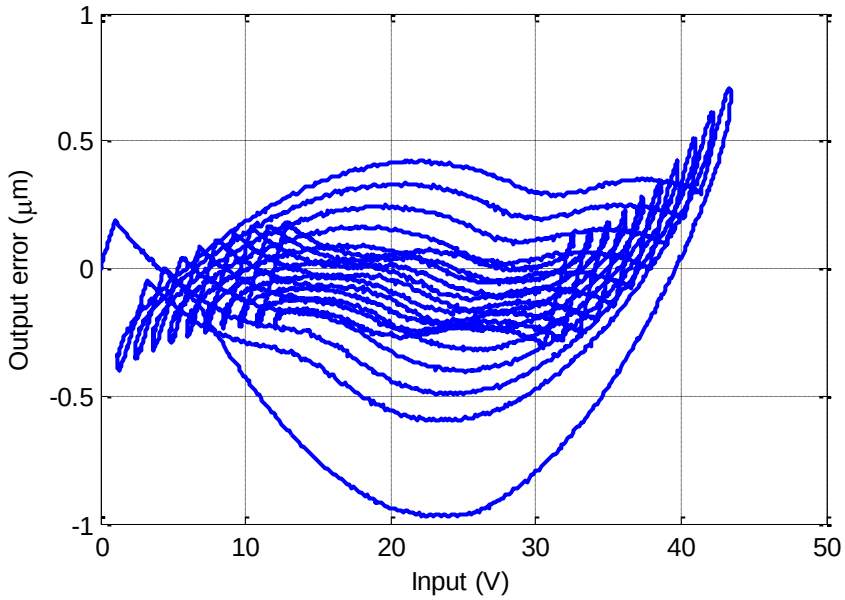

Fig. 2.3 Input and output error

The validity of the Prandlt-Ishlinskii model employing play operators are examined by comparing the model output with the measured data, as shown in Fig. 2.4. The results clearly suggest that the model can describe the hysteresis properties of PEAs.

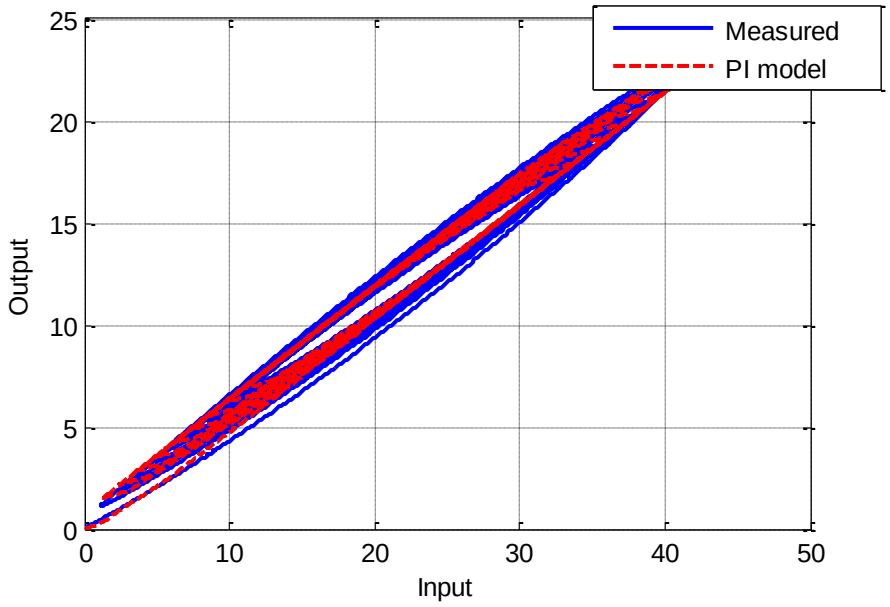

Fig. 2.4 Comparison of hysteresis loop

2.3 Open-Loops Control Scheme

Open-loop control schemes are a conventional control for PEA. Fig. 2.5 depicts block diagram of open-loop controller. The object here is to find an appropriate inversion from the identified model.

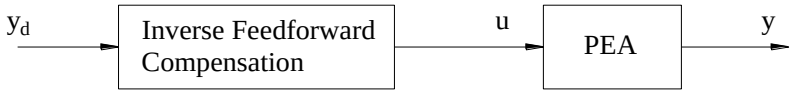

Fig. 2.5 Block diagram of open-loop control schemes

In this section, the inverse Prandlt-Ishlinskii model is introduced as a feed forward compensator for purpose of control PEA.

From the identified data in Table 2.1, an explicit inverse of the Prandlt-Ishlinskii can be formulated analytically.

According to [74], the control input is calculated as follow

$$u(k) = \hat{A} y_d(k) + \sum_{i=1}^{N} \hat{\mu}(\hat{r}_i) F_{\hat{r}_i}[y_d](k) \tag{2.1}$$

where $u(k)$ is the control input, $y_d(k)$ is the reference signal, $\hat{A}$ is a constant; $\hat{\mu}(\hat{r}_i)$ are the coefficients of the inverse operator; N is the number of operators, $\hat{r}_i$ are the thresholds of inverse operators. All these parameters will be calculated based on identified parameters from Prandlt-Ishlinskii hysteresis model as follows

$$\hat{r}_j = A r_j + \sum_{i=1}^{j} \mu(r_i)(r_j - r_i) \tag{2.2}$$

$$\hat{A} = \frac{1}{A} \tag{2.3}$$

$$\hat{\mu}(\hat{r}_j) = -\frac{\mu(r_j)}{\left(A + \sum_{i=1}^{j} \mu(r_i)\right)\left(A + \sum_{i=1}^{j-1} \mu(r_i)\right)} \tag{2.4}$$

Table 2.2 shows the calculated results.

Table 2.2 Inverse Prandlt-Ishlinskii model parameters

Number	Threshold $\hat{r}_i$	Parameter $\hat{\mu}(\hat{r}_i)$	$\hat{A}$
1	0.5	0.4762	2
2	1.0011	0.0016	
3	1.5183	0.0395	
4	2.0388	0.0443	
5	2.5561	0.0355	
6	3.0719	0.0309	
7	3.5877	0.0296	
8	4.1065	0.0334	
9	4.6176	0.0192	
10	5.1186	0.0017	
11	5.7347	0.1497	
12	6.7938	0.2676	
13	7.2948	0.0005	
14	7.7958	0.0005	
15	8.2968	0.0005	
16	8.7978	0.0005	

2.4 Experiment of Open-Loop Schemes

This section shows the experimental results of open-loop control. The experiments are conducted with four reference outputs which are $y_{d1}(k)=10\sin(2\pi*k*0.0005)\mu m$, $y_{d2}(k)=10\sin(2\pi*10*k*0.0005)\mu m$, $y_{d3}=10\sin(2\pi*30*k*0.0005)\mu m$ and $y_{d4}(k)=$

$7\sin(2\pi*5*k*0.0005)+3\cos(2\pi*0.5*k*0.0005)\mu m$. The sampling period is chosen as 0.0005s. The offset voltage of the driver is set to 30V.

Fig. 2.6 shows the control input for the first experiment which is 1Hz. The tracking result is shown in Fig. 2.7.

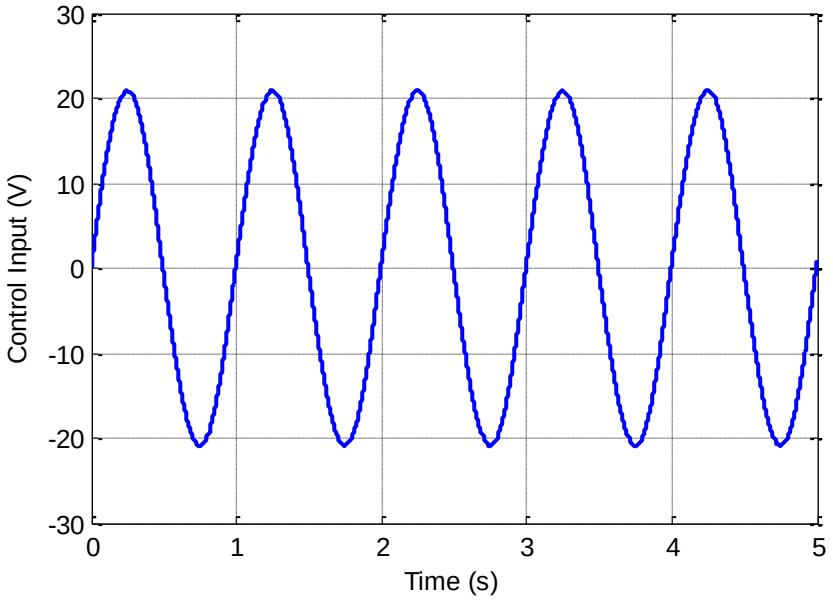

Fig. 2.6 Control input of feedforward compensation (1Hz)

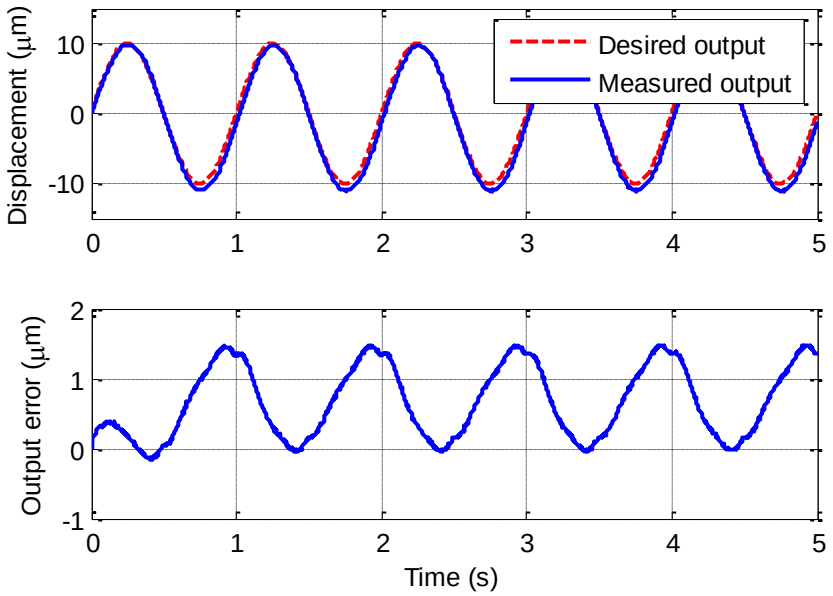

Fig. 2.7 Tracking error of feedforward compensation (1Hz)

Fig. 2.8 shows the control input for the experiment with $y_{d2}(k)$ which is 10 Hz. The tracking result is shown in Fig. 2.9.

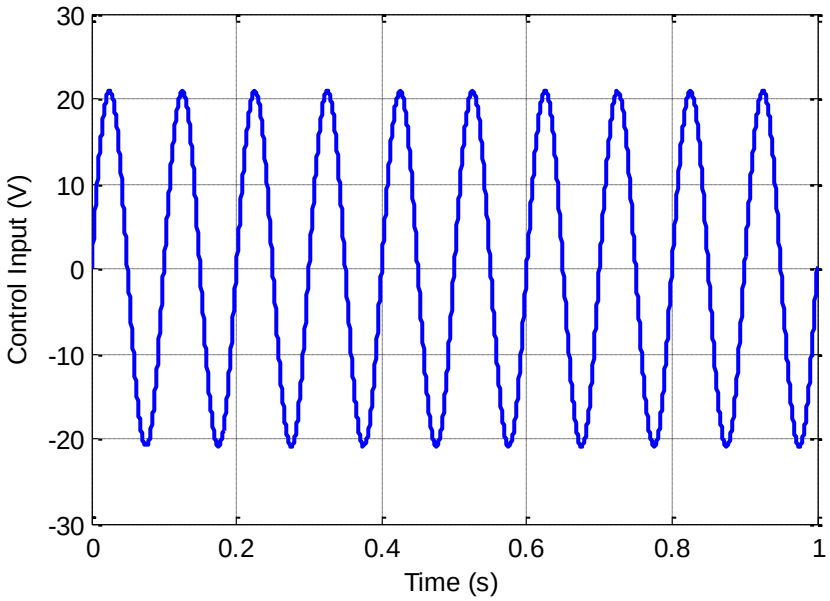

Fig. 2.8 Control input of feedforward compensation (10Hz)

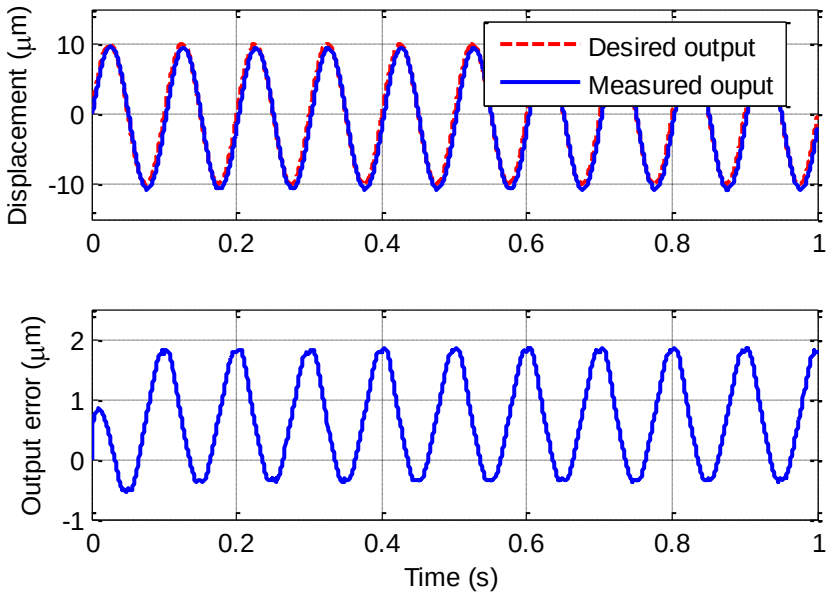

Fig. 2.9 Tracking error of feedforward compensation (10Hz)

Fig. 2.10 shows the control input for the experiment with $y_{d3}(k)$ which is 30Hz. The tracking result is shown in Fig. 2.11.

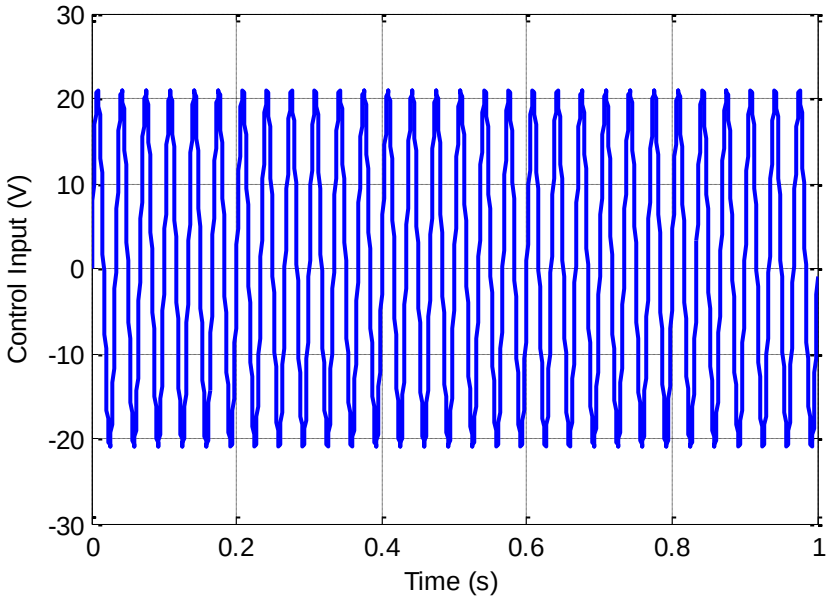

Fig. 2.10 Control input of feedforward compensation (30Hz)

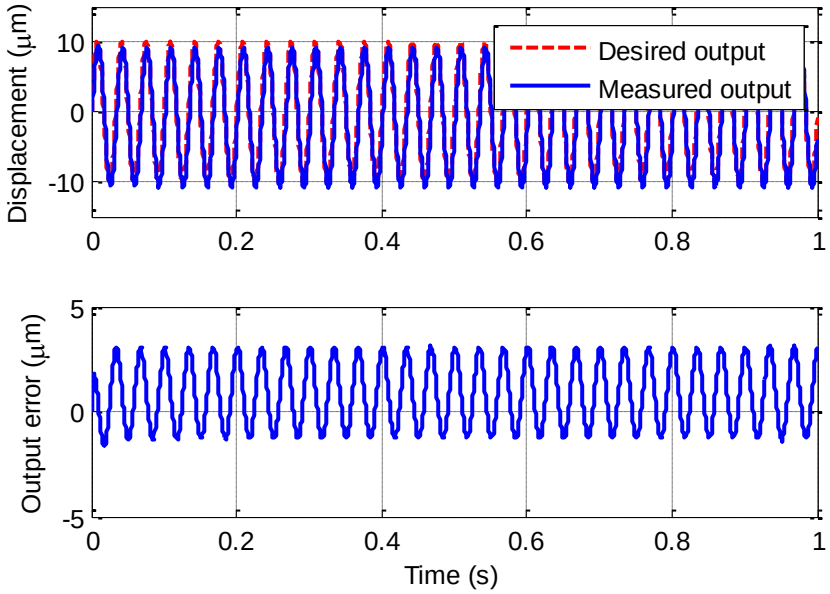

Fig. 2.11 Tracking error of feedforward compensation (30Hz)

Fig. 2.12 shows the control input for the experiment with $y_{d4}(k)$. The tracking result is shown in Fig. 2.13.

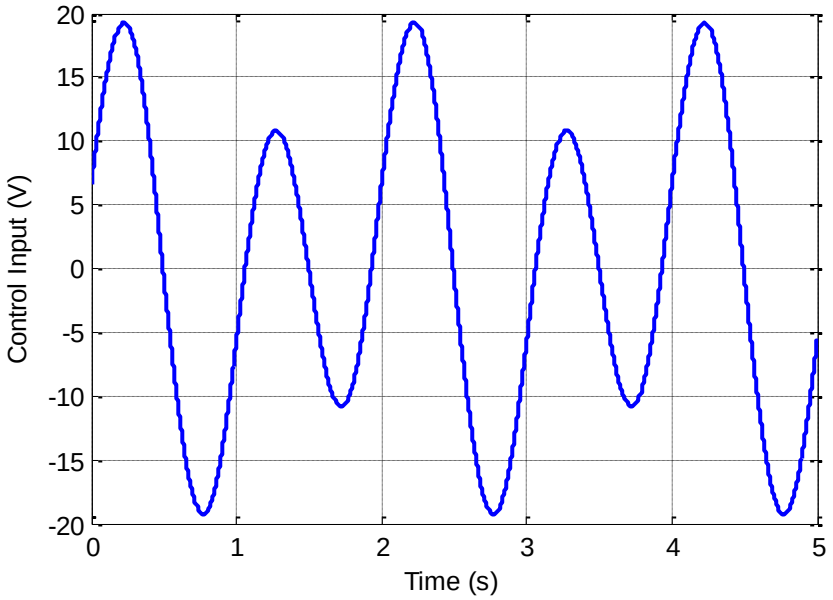

Fig. 2.12 Control input of feedforward compensation with multiple frequencies signal

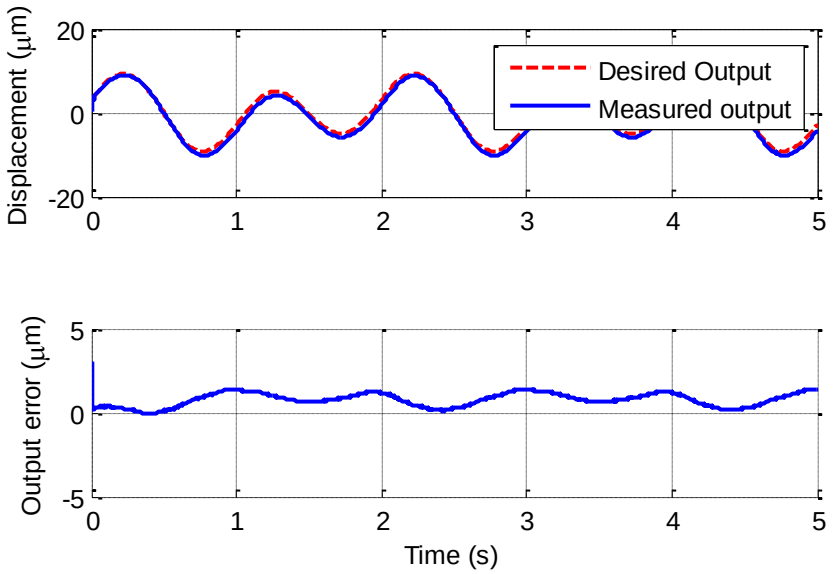

Fig. 2.13 Tracking error of feedforward compensation with multiple frequencies signal

2.5 Discussion

Experimental results shows that the feedforward controller based on inverse PI model can compensate the hysteresis nonlinearities in PEAs. Moreover, the identification procedure and the inverse calculation are simple. However, the accuracy is low. When the frequency is 30

Hz, the error even exceeds 20%. To improve the performance of PEAs, a combination of feedback control and feedforward compensation is desired.

Chapter 3: Conventional PI control

3.1 Introduction

One major disadvantage of the open-loop control schemes is that their positioning performances are highly sensitive to unknown effects such as model errors and disturbances. Due to this disadvantage, it is necessary to develop more effective control strategies to improve PEA performances. This chapter considers a conventional PID control method for PEAs. The advantage of PID control is that it is easy to be implemented.

3.2 PEAs Model Based on Linear System Identification

This section proposes a PEA model derived by linear system identification method [75]. System identification is based on statistical method and assumes that objectives are black-boxes. The obtained model is simple and can be used as a nominal model of model-based control methods. It should be noted that nonlinearities of PEAs is neglected because this is only the linear system identification method. A structure of the identified model should be selected. In this identification, Auto-regressive exogenous (ARX) model is applied because ARX model is suitable for least square method and is usually used for system identification. The identified PEA model $G(z)$ has second-order denominator and first-order numerator polynomials, and is expressed as follows:

$$G(z)=\frac{Y(z)}{U(z)}=\frac{b_1 z^{-1}+b_2 z^{-2}}{1+a_1 z^{-1}+a_2 z^{-2}} \tag{3.1}$$

where $Y(z)$ is z-transformation of PEA displacement; $U(z)$ is z-transformation of applied voltage; and b_1, b_2, a_1, a_2 are plant parameters.

Equation (2.1) can be rewritten as

$$y(k) = b_1 u(k-1) + b_2 u(k-2) - a_1 y(k-1) - a_2 y(k-2)$$

$$= \phi^T \theta \tag{3.2}$$

where $\phi(k)^T = [u(k-1), u(k-2), y(k-1), y(k-2)]$, $\theta = [b_1, b_2, -a_1, -a_2]^T$ is the parameter vector which is to be identified; Equation (3.2) is linear, so the vector of θ can be readily identified by using the least squares method as follows

Let N be the number of sampling cycles for input and output data. Define

$$A = \begin{bmatrix} \phi(N)^T \\ \phi(N-1)^T \\ \vdots \\ \phi(1)^T \\ \phi(0)^T \end{bmatrix} \text{ and } Y = \begin{bmatrix} y(N) \\ y(N-1) \\ \vdots \\ y(1) \\ y(0) \end{bmatrix}, \tag{3.4}$$

they give:

$$\theta = \left(A^T A\right)^{-1} A^T Y \tag{3.5}$$

The input $u(k) = 20*(-0.06*k*0.0005+1.1)\sin(2*\pi*k*0.0005+3*\pi/2)+1.1$ is applied to the PEA for identification, the sampling time period is chosen as 0.0005 s. Fig. 3.1 shows the input signal and measured output signal.

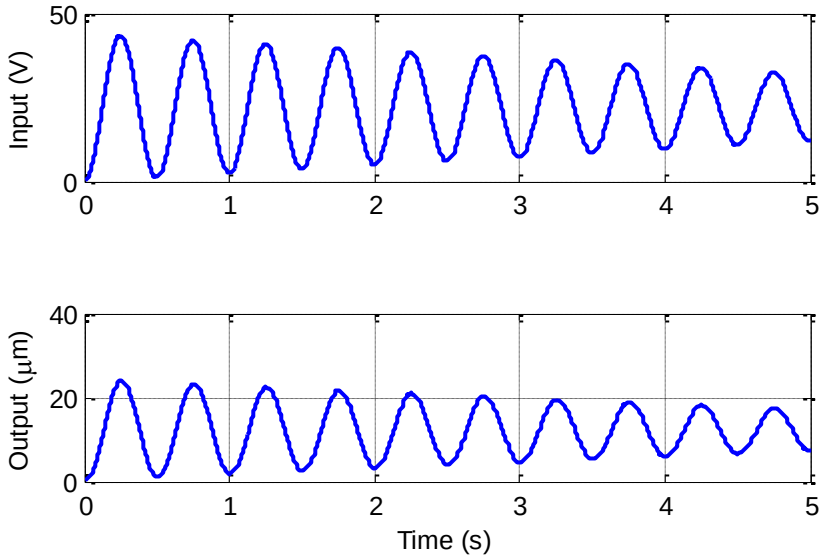

Fig. 3.1 Input and output signal for identification

First, by using least square method, the values of b_1, b_2, a_1, and a_2 are approximated. Afterwards, the identified parameters are validated by comparing the input-output relationship of the model and of the PEA. During this step, the parameters can be manually refined if required.

As the result, the identified parameters are shown in table 3.1.

Table 3.1 Identification results of linear PEA model using least square method.

Parameters	b_1	b_2	a_1	a_2
Value	0.02623	0.007647	-0.9549	0.01666

Fig. 3.2 shows the difference between the measured output and the model output. It should be mentioned that the hysteresis nonlinearities of PEA is neglected because the introduced model is only the linear model.

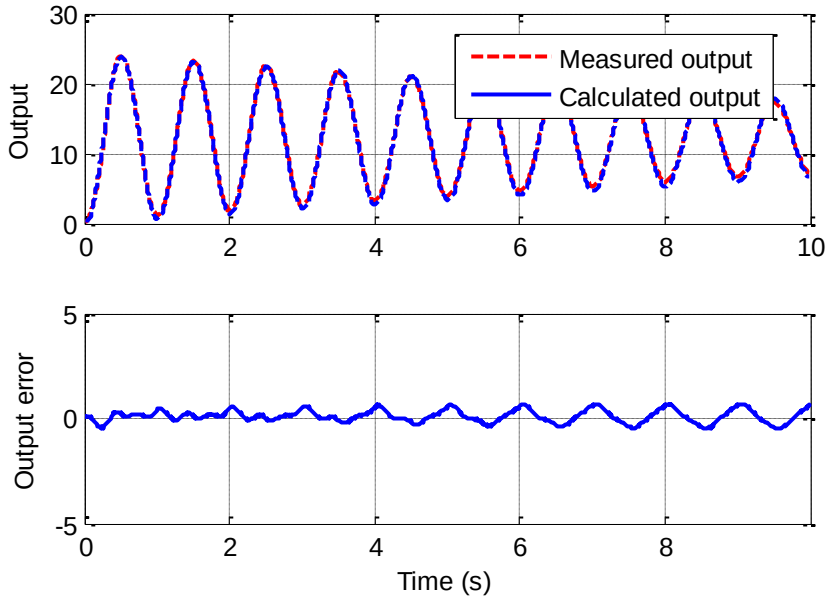

Fig. 3.2 Comparison of measured output and identified output

3.3 Conventional PI Control

PID control is a traditional control technique for many kinds of mechanical systems. In this thesis, only PI control is used. Fig. 3.3 shows the block diagram of a PI controller.

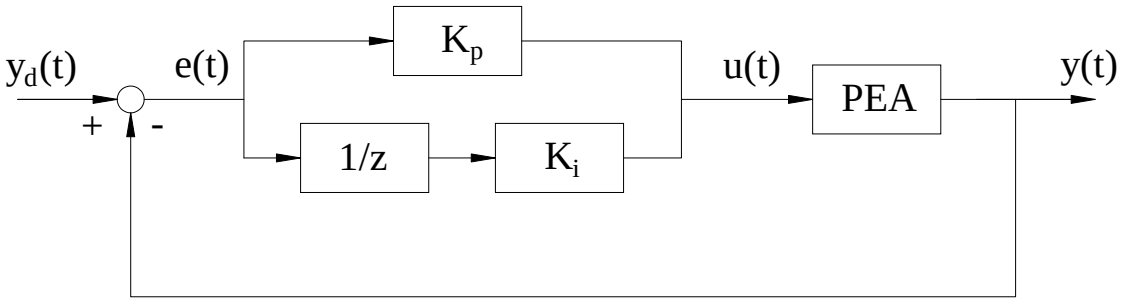

Fig. 3.3 Block diagram of PI control

3.4 Experiment of PI Control

The experiments of PI control are also conducted with the same four reference trajectories $y_{d1}(k)$, $y_{d2}(k)$, $y_{d3}(k)$, and $y_{d4}(k)$ as in Chapter 2. The proportional and integral gains K_p and K_i are chosen by Ziegler–Nichols method, and by trial and error; K_p and K_i are 0.926 and 1819, respectively. The sampling time in these experiments is 0.0005 s.

Fig. 3.4 shows the control input for the experiment with $y_{d1}(k)$ which is 1 Hz. The tracking result is shown in Fig. 3.5.

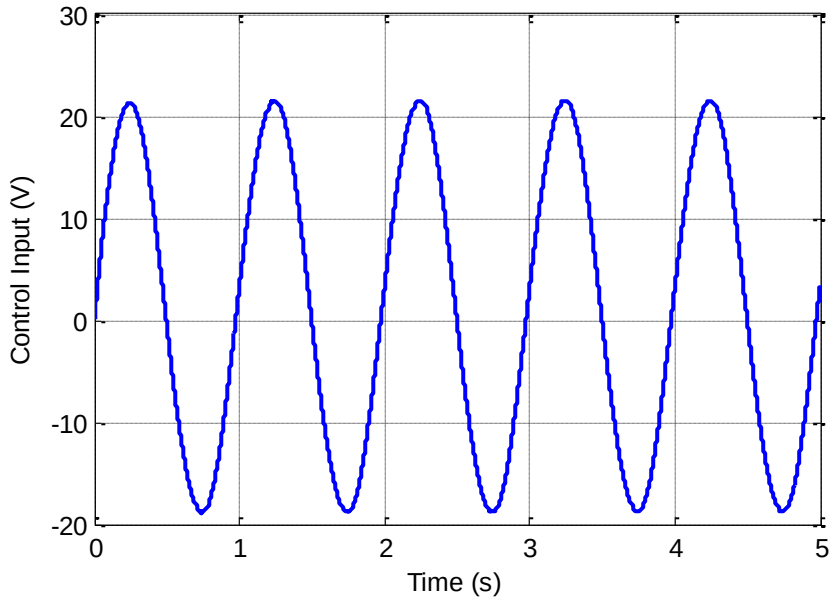

Fig. 3.4 Control input for $y_{d1}(k)$ (1 Hz) in PI control

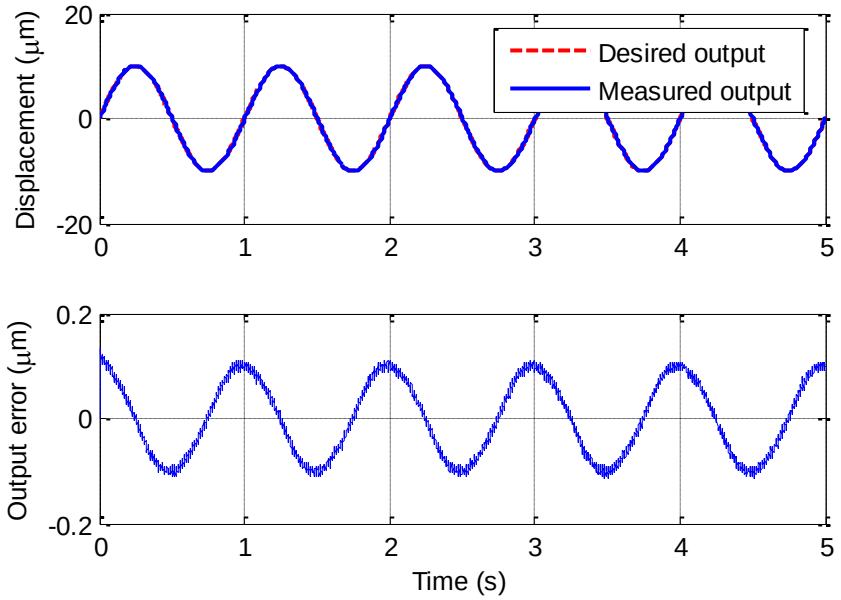

Fig. 3.5 Tracking result for $y_{d1}(k)$ (1 Hz) in PI control

Fig. 3.6 shows the control input for the experiment with $y_{d2}(k)$ which is 10 Hz. The tracking result is shown in Fig. 3.7.

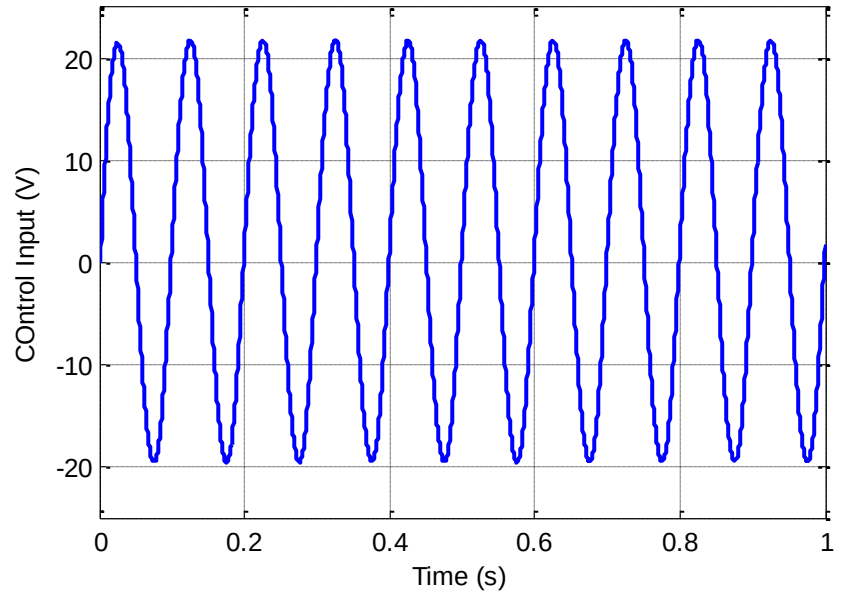

Fig. 3.6 Control input for $y_{d2}(k)$ (10 Hz) in PI control

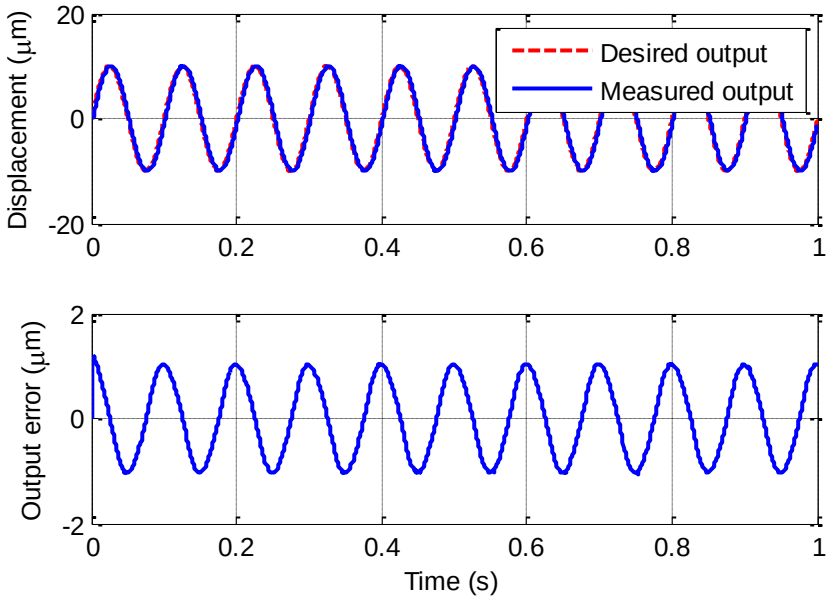

Fig. 3.7 Tracking result for $y_{d2}(k)$ (10 Hz) in PI control

Fig. 3.8 shows the control input for the experiment with $y_{d3}(k)$ which is 30 Hz. The tracking result is shown in Fig. 3.9.

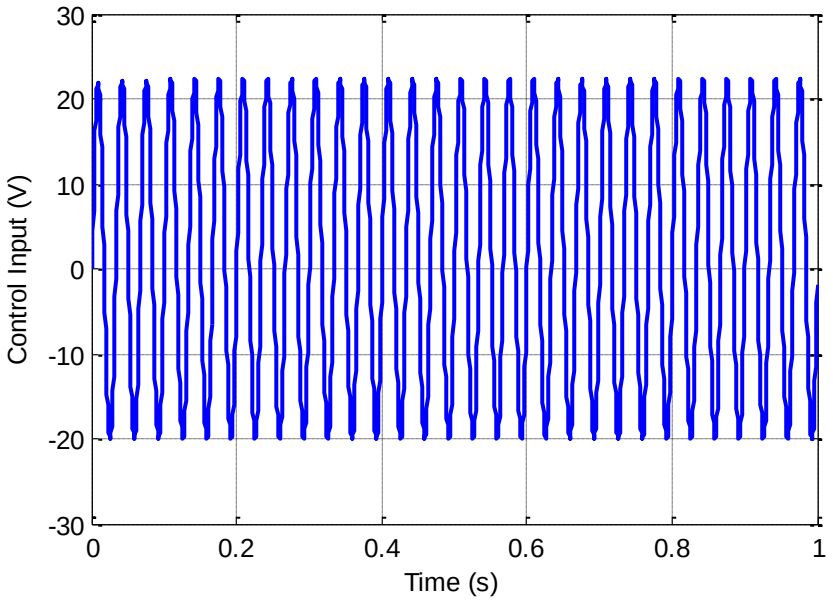

Fig. 3.8 Control input for $y_{d3}(k)$ (30 Hz) in PI control

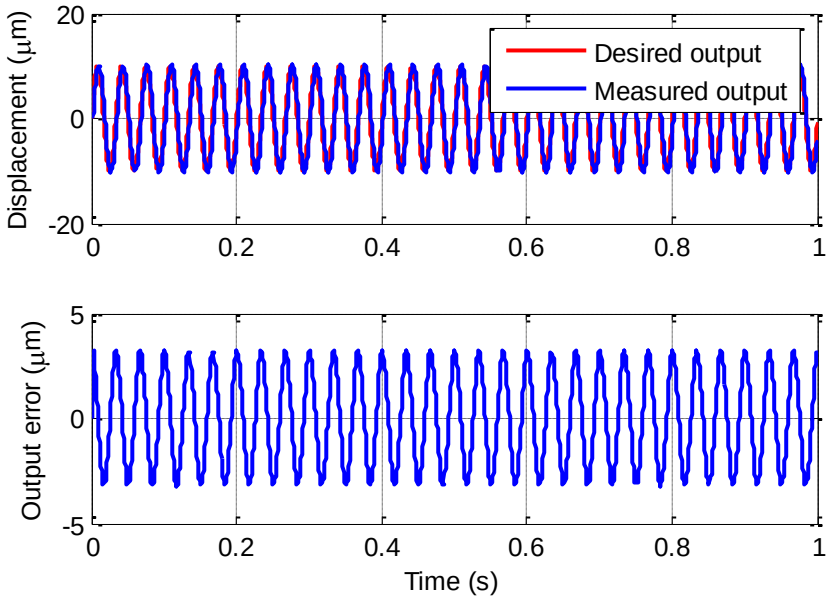

Fig. 3.9 Tracking result for $y_{d3}(k)$ (30 Hz) in PI control

Fig. 3.10 shows the control input for the experiment with $y_{d4}(k)$ which is a multiple frequencies signal. The tracking result is shown in Fig. 3.11.

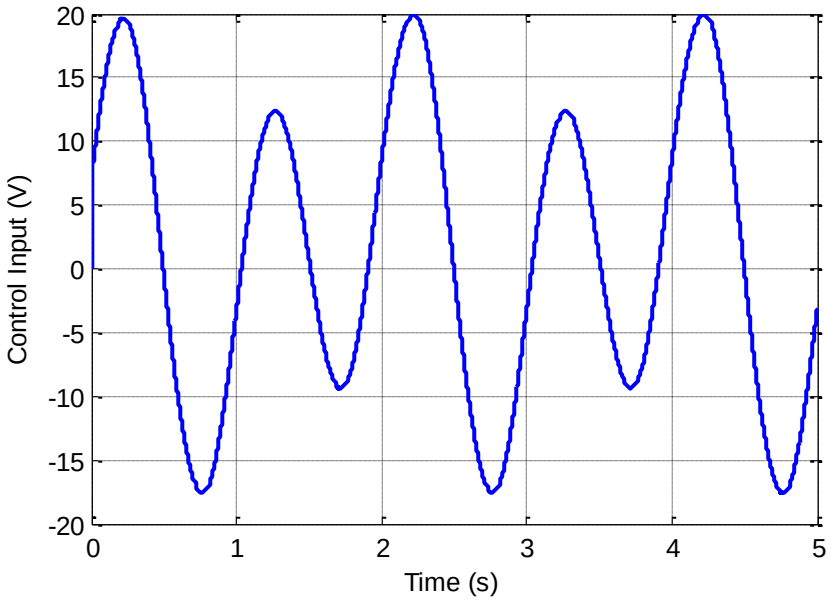

Fig. 3.10 Control input for multiple frequencies signal in PI control

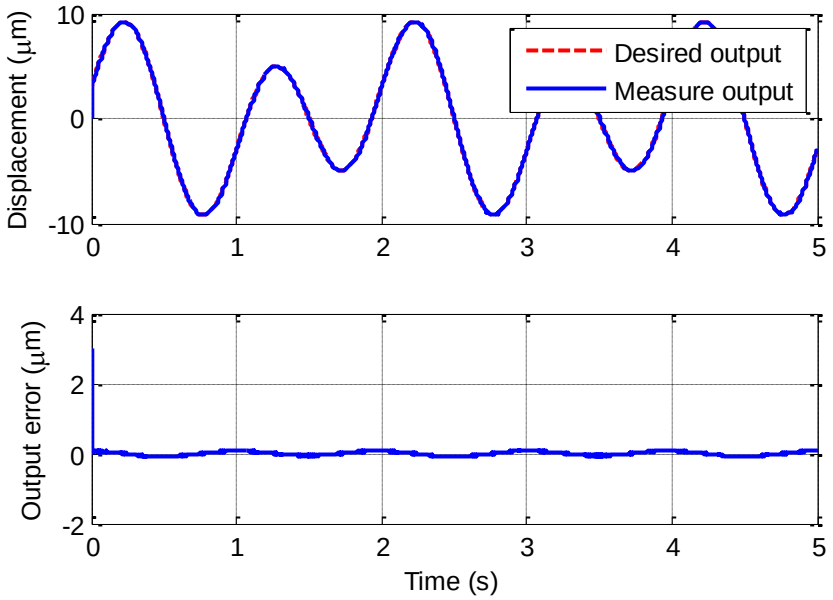

Fig. 3.11 Tracking result for multiple frequencies signal in PI control

4.1 Discussion

It can be seen that PI control has better performance than feedforward compensation using inverse PI model. At low frequency, the PI control works well. At high frequencies, conventional PI control can no longer provide accuracy. As can be seen in Fig. 3.9, at 30 Hz, the tracking error is more than 20%.

Chapter 4: Model Predictive Control and Adaptive Model Predictive Control

4.1 Introduction

In Chapter 3, a conventional PI control is adopted to the control of PEAs. At low frequency reference signals, conventional PI control shows its effectiveness. However, conventional PI control performance is poor because it is based on linear system identification model. Thus, it cannot get a good tracking performance when the hysteresis nonlinearities are strong.

To utilize the linear PEA model, this chapter introduces model predictive control method. Once the linear model parameters are identified, the control law is easy to be implemented. Due to the modelling error, MPC tracking performance is not so high. Thus, this chapter also proposes adaptive model predictive control to control the PEAs.

4.2 Model Predict Control

4.2.1 Methodology

Model predictive control (MPC) is an advanced method of process control [76]. Model predictive controllers rely on dynamic models of the process; most often are linear empirical models obtained by system identification. The main advantage of MPC is the fact that it allows the current time step to be optimized, while keeping future time steps in

account. This is achieved by optimizing a finite time-horizon, and then only the current time step is implemented. Fig. 4.1 shows the basic structure of MPC.

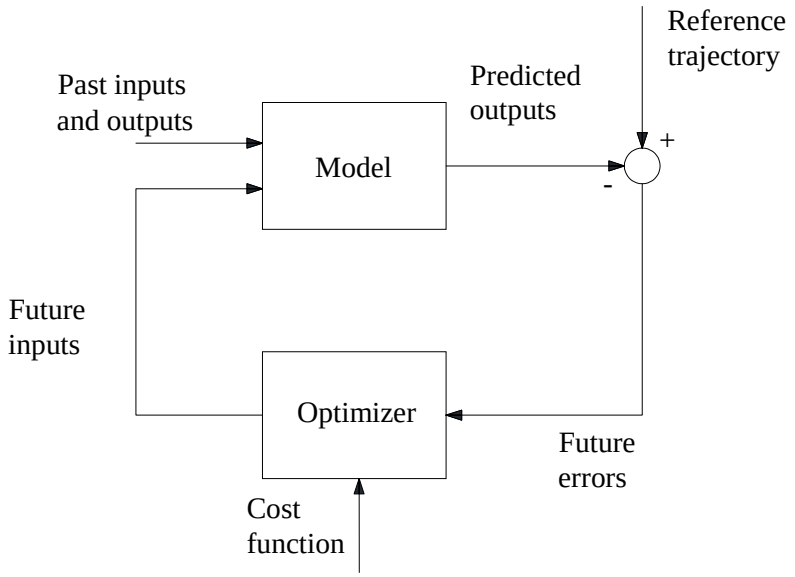

Fig. 4.1 Basic structure of MPC

Model Predictive Control (MPC) is a multivariable control algorithm that needs the following information:

(I1) Internal dynamic model of the process.

(I2) History of past inputs and outputs.

(I3) Optimization cost function P over the receding prediction horizon, to calculate the optimum control inputs.

The optimization cost function is given by:

$$P = \sum_{i=1}^{N_p} \omega(i)\left(\hat{y}(k+i \mid k) - y_d(k+i \mid k)\right)^2 + \sum_{i=1}^{N_p} \rho(i)\left(\Delta\hat{u}(k+i \mid k)\right)^2 \tag{4.1}$$

where $\hat{y}(k \mid i)$ is the ith step predicted output from time k, $y_d(k \mid i)$ is the ith step reference signal from time k, $\Delta\hat{u}(k \mid i)$ is the difference between ith step predicted input from time k and control input at time k, N_p is the number of predicted steps; ω and ρ are weighting coefficients.

Consider dynamic system

$$x(k+1) = Ax(k) + Bu(k)$$

$$y(k) = Cx(k) \tag{4.2}$$

where $y(k)$ is the system output; $u(k)$ is the system input; $x(k)$ is the state vector; A, B, and C are known system matrices.

An incremental state space model can also be used if the model input is the control increment $\Delta u(k)$. This model can be written in the general state space form by taking into account that $\Delta u(k) = u(k) - u(k-1)$. The following representation is obtained by combining this expression with (4.2):

$$\begin{bmatrix} x(k+1) \\ u(k) \end{bmatrix} = \begin{bmatrix} A & B \\ 0 & I \end{bmatrix} \begin{bmatrix} x(k) \\ u(k-1) \end{bmatrix} + \begin{bmatrix} B \\ I \end{bmatrix} \Delta u(k)$$

$$y(k) = \begin{bmatrix} C & 0 \end{bmatrix} \begin{bmatrix} x(k) \\ u(k-1) \end{bmatrix} \tag{4.3}$$

Defining a new state vector as $\bar{x}(k) = \begin{bmatrix} x(k) & u(k-1) \end{bmatrix}^T$, the incremental model takes the general form:

$$\bar{x}(k+1) = M\bar{x}(k) + N\Delta u(k)$$

$$y(k) = Q\bar{x}(k) \tag{4.4}$$

where the relationship between (M, N, Q) and (A, B, C) can easily be obtained by comparing (4.2) and (4.4).

In order to minimize the cost function (4.1), output predictions over the horizon must be computed. Predictive outputs can be obtained by using (4.4) recursively, resulting in:

$$\hat{y}(k+j) = QM^{j}\hat{x}(k) + \sum_{i=0}^{j-1} QM^{j-i-1}N\Delta u(t+i) \tag{4.5}$$

Now, the predictions along the horizon are given by

$$\hat{y}(k)=\begin{bmatrix}\hat{y}(k+1\mid k)\\ \hat{y}(k+2\mid k)\\ \vdots\\ \hat{y}(k+N_p\mid k)\end{bmatrix}=\begin{bmatrix}QM\hat{x}(k)+QN\Delta u(k)\\ QM^2\hat{x}(k)+\sum_{i=0}^{1}QM^{1-i}N\Delta u(k+i)\\ \vdots\\ QM^{N_p}\hat{x}(k)+\sum_{i=0}^{N_p-1}QM^{N_p-1-i}N\Delta u(k+i)\end{bmatrix} \tag{4.6}$$

For simplicity, denote

$$\hat{Y}(k)=F\hat{x}(k)+H\Delta U \tag{4.7}$$

Where $\hat{Y}=\begin{bmatrix}\hat{y}(k+1\mid k) & \hat{y}(k+2\mid k) & \dots & \hat{y}(k+N_p\mid k)\end{bmatrix}^T$ is the predicted future output, $\Delta U=\begin{bmatrix}\Delta u(k) & \Delta u(k+1) & \dots & \Delta u(k+N_p-1)\end{bmatrix}^T$ is the vector of future control increments, the matrix H defined as $H=\begin{bmatrix}QN & 0 & \cdots & \cdots & 0\\ QMN & QN & \ddots & \ddots & \vdots\\ \vdots & \ddots & \ddots & \ddots & \vdots\\ QM^{N_p-2}N & \ddots & \ddots & QN & 0\\ QM^{N_p-1}N & QM^{N_p-2}N & \cdots & QMN & QN\end{bmatrix}$, and matrix F is defined as $F=\begin{bmatrix}QM & QM^2 & \dots & QM^{N_p}\end{bmatrix}^T$.

Consider the case where $\omega(i)=1$ and $\rho(i)=\rho$. The control sequence Δu is calculated minimizing the cost function (4.1), that can be written as:

$$P=(H\Delta U+F\hat{x}(k)-Y_d)^T(H\Delta U+F\hat{x}(k)-Y_d)+\rho(\Delta U)^T(\Delta U) \tag{4.8}$$

An analytical solution exists that can be calculated as follows

$$\Delta U=\left(H^TH+\rho I\right)^{-1}H^T(y_d-F\hat{x}(k)) \tag{4.9}$$

It should be note that only $\Delta u(k)$ is sent to the plant and all the computation is repeated at the next sampling time.

4.2.2 Experiment of MPC

In this thesis the nominal model used for MPC has the form as in Section 3.2.

The transfer function (3.1) is changed into state space as follow:

$$y(k) = -a_1 y(k-1) - a_2 y(k-2) + b_1 u(k-1) + b_2 u(k-2) \tag{4.10}$$

Denote $x_1(k+1) = x_2(k) = y(k)$, it gives

$$\begin{cases} x_1(k+1) = x_2(k) \\ x_2(k+1) = -a_1 x_2(k) - a_2 x_1(k) + b_1 u(k) + b_2 u(k-1) \end{cases} \tag{4.11}$$

Introduce new state $u(k) = u(k-1) + \Delta u(k)$, Equation (4.11) becomes

$$\begin{bmatrix} x_1(k+1) \\ x_2(k+1) \\ u(k) \end{bmatrix} = \begin{bmatrix} 0 & 1 & 0 \\ -a_2 & -a_1 & b_1 + b_2 \\ 0 & 0 & 1 \end{bmatrix} \begin{bmatrix} x_1(k) \\ x_2(k) \\ u(k-1) \end{bmatrix} + \begin{bmatrix} 0 \\ b_1 \\ 0 \end{bmatrix} \Delta u(k)$$

$$y(k) = \begin{bmatrix} 0 & 1 & 0 \end{bmatrix} \begin{bmatrix} x_1(k) \\ x_2(k) \\ u(k-1) \end{bmatrix} \tag{4.12}$$

For simplicity denote $M = \begin{bmatrix} 0 & 1 & 0 \\ -a_2 & -a_1 & b_1 + b_2 \\ 0 & 0 & 1 \end{bmatrix}$, $N = \begin{bmatrix} 0 \\ b_1 \\ 0 \end{bmatrix}$ and $Q = \begin{bmatrix} 0 & 1 & 0 \end{bmatrix}$.

In this thesis, 3 steps ahead are predicted. It means $N_p = 3$.

Now, the predictions along the horizon are given by

$$\begin{bmatrix} \hat{y}(k+1) \\ \hat{y}(k+2) \\ \hat{y}(k+3) \end{bmatrix} = \begin{bmatrix} QM\hat{x}(k) + QN\Delta u(k) \\ QM^2\hat{x}(k) + QMN\Delta u(k) + QN\Delta u(k+1) \\ QM^3\hat{x}(k) + QM^2N\Delta u(k) + QMN\Delta u(k+1) + QN\Delta u(k+2) \end{bmatrix}$$

$$= \begin{bmatrix} QM \\ QM^2 \\ QM^3 \end{bmatrix} \hat{x}(k) + \begin{bmatrix} QN & 0 & 0 \\ QMN & QN & 0 \\ QM^2N & QMN & QN \end{bmatrix} \begin{bmatrix} \Delta u(k) \\ \Delta u(k+1) \\ \Delta u(k+2) \end{bmatrix} \tag{4.13}$$

Denote $H = \begin{bmatrix} QN & 0 & 0 \\ QMN & QN & 0 \\ QM^2N & QMN & QN \end{bmatrix}$; $F = \begin{bmatrix} QM \\ QM^2 \\ QM^3 \end{bmatrix}$, the solution that provides the optimum input difference as:

$$\begin{bmatrix} \Delta u(k) \\ \Delta u(k+1) \\ \Delta u(k+2) \end{bmatrix} = \left(H^T H + \rho I\right)^{-1} H^T \left(y_d - F\hat{x}(k)\right) \tag{4.14}$$

The matrices H and F can be easily calculated by a_1, a_2, b_1, b_2. From Section 3.2, $a_1 = -0.9549$, $a_2 = -0.01666$, $b_1 = 0.02623$, and $b_2 = 0.007647$. The weighting coefficients are chosen as $\omega(i) = 1$ and $\rho = 0.1$.

In order to have a good comparison between control methods, the experiments of MPC are also conducted with the same four reference trajectories $y_{d1}(k)$, $y_{d2}(k)$, $y_{d3}(k)$, and $y_{d4}(k)$ as in other control techniques. The sampling time in these experiments is 0.0005 s.

Fig. 4.2 shows the control input for the experiment with $y_{d1}(k)$ which is 1 Hz. The tracking result is shown in Fig. 4.3.

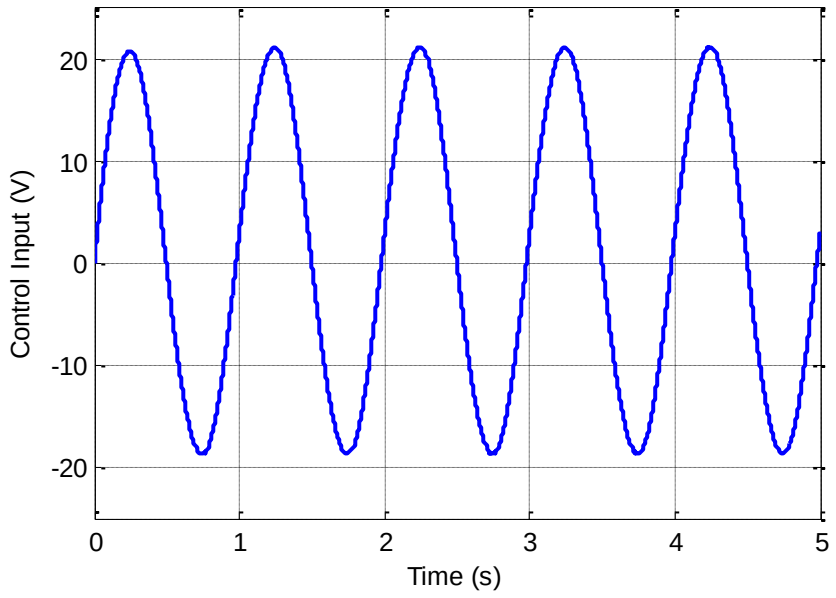

Fig. 4.2 Control input for in MPC (1 Hz) (3 predictive steps)

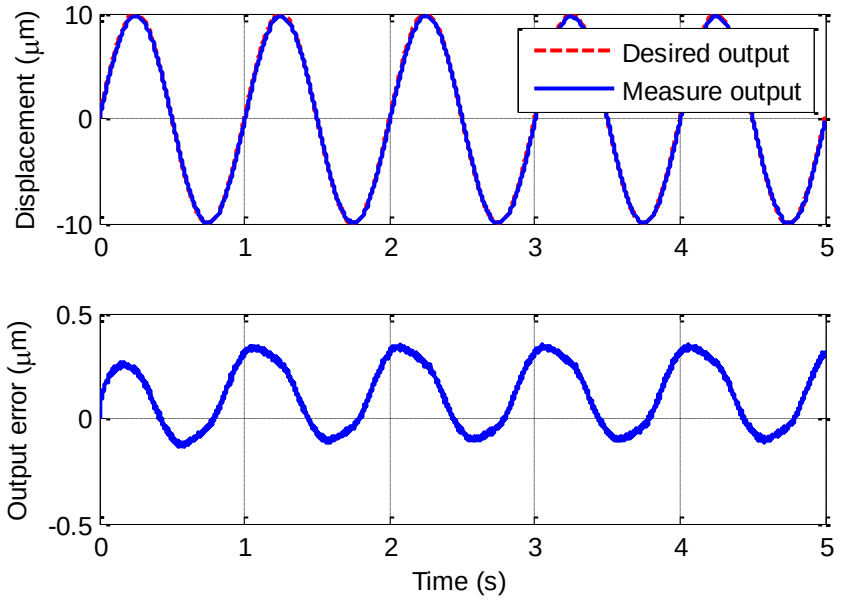

Fig. 4.3 Tracking result for MPC (1 Hz) (3 predictive steps)

Fig. 4.4 shows the control input for the experiment with $y_{d2}(k)$ which is 10 Hz. The tracking result is shown in Fig. 4.5.

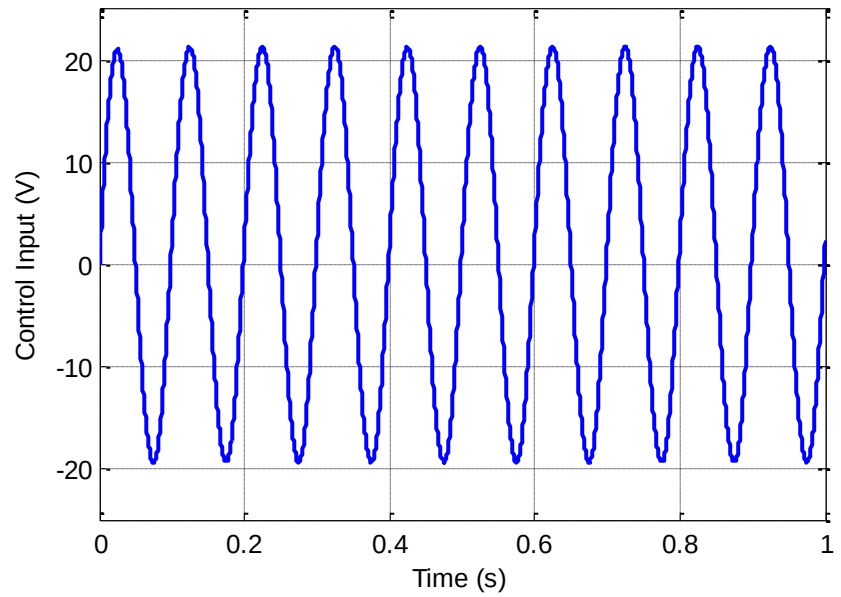

Fig. 4.4 Control input for MPC (10 Hz) (3 predictive steps)

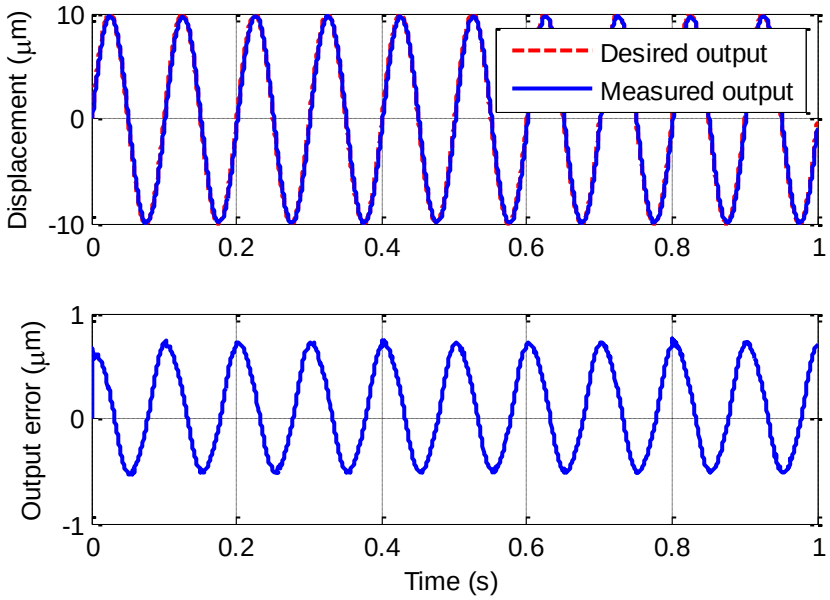

Fig. 4.5 Tracking result for MPC (10 Hz) (3 predictive steps)

Fig. 4.6 shows the control input for the experiment with $y_{d3}(k)$ which is 30 Hz. The tracking result is shown in Fig. 5.7.

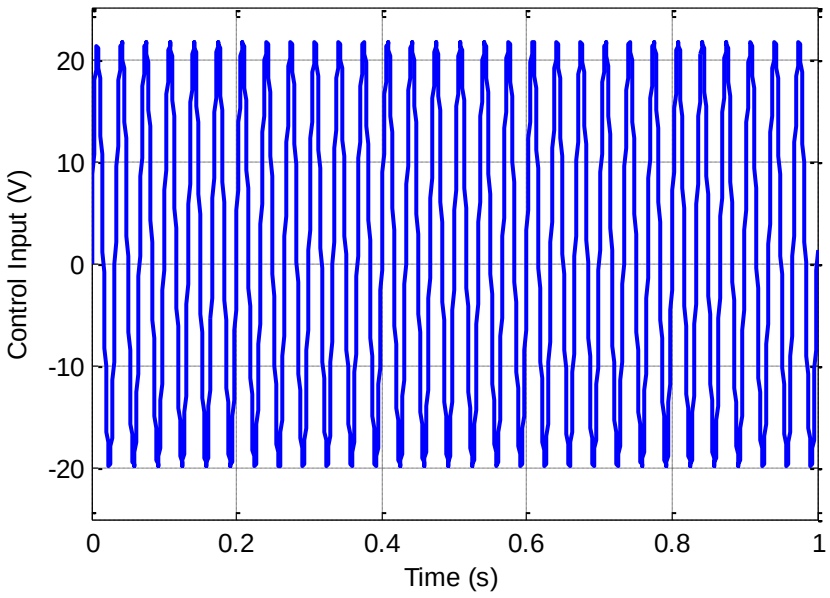

Fig. 4.6 Control input for MPC (30 Hz) (3 predictive steps)

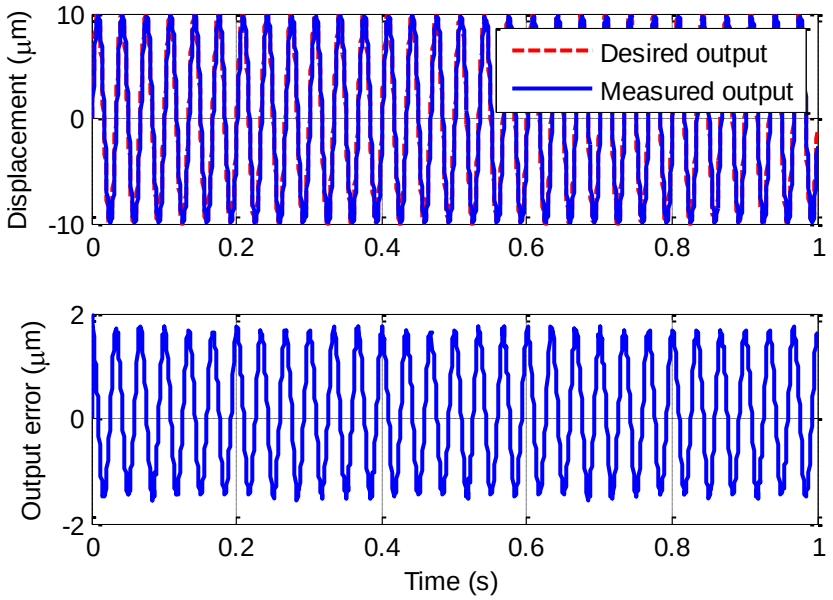

Fig. 4.7 Tracking result for MPC (30 Hz) (3 predictive steps)

Fig. 4.8 shows the control input for the experiment with $y_{d4}(k)$. The tracking result is shown in Fig. 4.9.

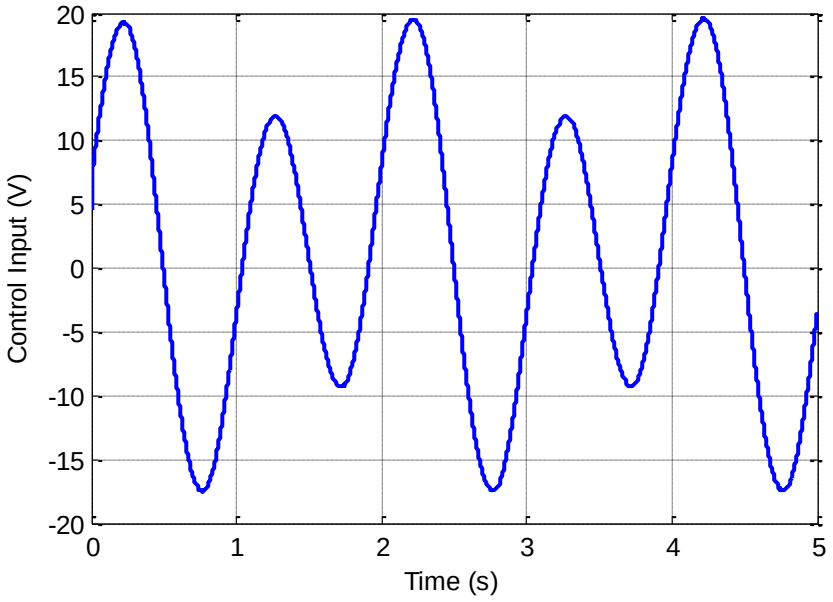

Fig. 4.8 Control input for MPC with multiple frequencies signal (3 predictive steps)

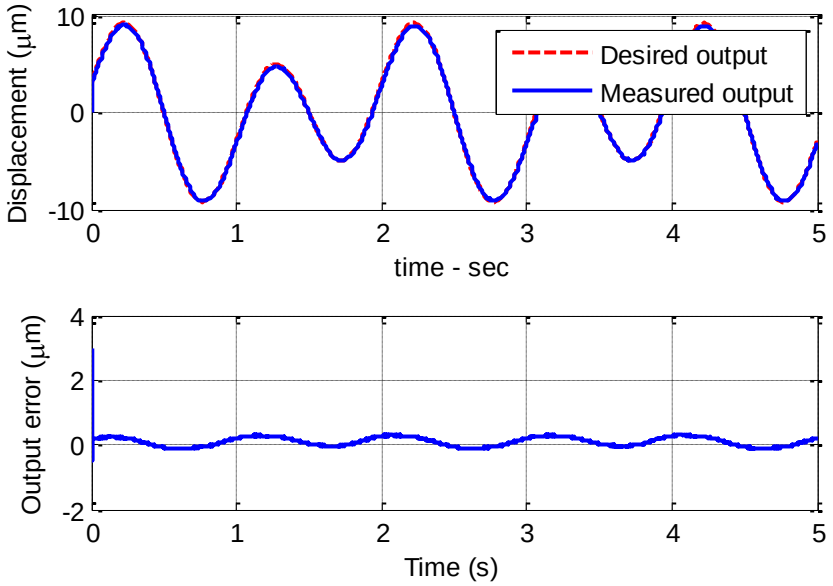

Fig. 4.9 Tracking result for MPC with multiple frequencies signal (3 predictive steps)

4.3 Adaptive Model Predictive Control

Since the modelling error exists, the performance of MPC is limited. In this section, an adaptive parameter estimation algorithm is applied to the MPC in order to compensate parameter changing of the PEAs linear model due to hysteresis nonlinearities. This updates the parameters of the nominal model (4.10) by using recursive least squares method. The experiments results show the effectiveness of proposed method.

4.3.1 Least Squares Algorithm

Consider the single-input single output system which can be describes as

$$y(k)=a(q^{-1})y(k-1)+b(q^{-1})u(k-1) \tag{4.17}$$

where

$$a(q^{-1})=a_0+a_1q^{-1}+\ldots+a_nq^{-n+1}$$

$b(q^{-1})=b_0+b_1q^{-1}+\ldots+b_mq^{-m+1}$, m and n are known.

In this section the least squares algorithm is adopted to estimate system parameters online.

Let θ be the vector of unknown system parameters

$$\theta = [a_0, a_1, \ldots, a_n, b_0, b_1, \ldots, b_m]^T \tag{4.18}$$

Then Equation (4.17) can be written as

$$y(k) = \phi^T(k-1)\theta \tag{4.19}$$

where $\phi^T(k-1) = [y(k-1), y(k-2), \ldots, y(k-n+1), u(k-1), u(k-2), \ldots, u(k-m+1)]$

The least squares algorithm can be expressed as

$$\hat{\theta}(k) = \hat{\theta}(k-1) + \frac{P(k-1)\phi(k)}{1+\phi(k)^T P(k-1)\phi(k)}\left(y(k) - \phi(k-1)^T \hat{\theta}(k-1)\right) \tag{4.20}$$

$$P(k-1) = P(k-2) - \frac{P(k-2)\phi(k-1)\phi(k-1)^T P(k-2)}{1+\phi(k-1)^T P(k-2)\phi(k-1)} \tag{4.21}$$

where $\hat{\theta}(k)$ is the estimated parameter vector of θ with $\hat{\theta}(0)$ is given, $P(k)$ is the covariance matrix with $P(-1)$ is any positive define matrix P_0. Usually, P_0 is chosen as $P_0 = \lambda I$, where λ is a positive constant, I is the identity matrix.

Note that, the convergence of $\hat{\theta}(k)$ to θ is not proven or claimed.

4.3.2 Experiment of AMPC

This section shows the effectiveness of the AMPC. The nominal model is still chosen as in section 4.2.2.

Equation (4.10) can be written as

$$y(k) = \phi^T(k-1)\theta \tag{4.22}$$

where $\theta = [\theta_1, \theta_2, \theta_3, \theta_4]^T = [a_1, a_2, b_1, b_2]^T$; $\phi^T(k) = [y(k-1), y(k-2), u(k-1), u(k-2)]$

The estimated parameter vector $\hat{\theta}(k) = [\hat{\theta}_1(k), \hat{\theta}_2(k), \hat{\theta}_3(k), \hat{\theta}_4(k)]^T$ is updated by Equations (4.20) and (4.21) on real-time basis. Then, it is used for computing the future predictive input

difference as in Equation (4.16) by calculating matrix H and F . The weighting coefficients are chosen as $\omega(i)=1$ and $\rho=0.1$. The initial values of $\hat{\theta}(0)$ and $P(-1)$ are chosen as $[0.2 \quad 0.2 \quad 0.2 \quad 0.2]^T$ and $0.1I$, respectively.

The experimental conditions are same as those in the experiment of MPC. However, in order to have a better look at computation cost, this section conducts experiments with predictions of 3 steps and 5 steps ahead.

4.3.2.1 Experiment of AMPC with 3 Predictive Steps

Fig. 4.10 shows the control input for the experiment with 1Hz sinusoid reference signal. The estimated parameters are shown in Fig. 4.11.

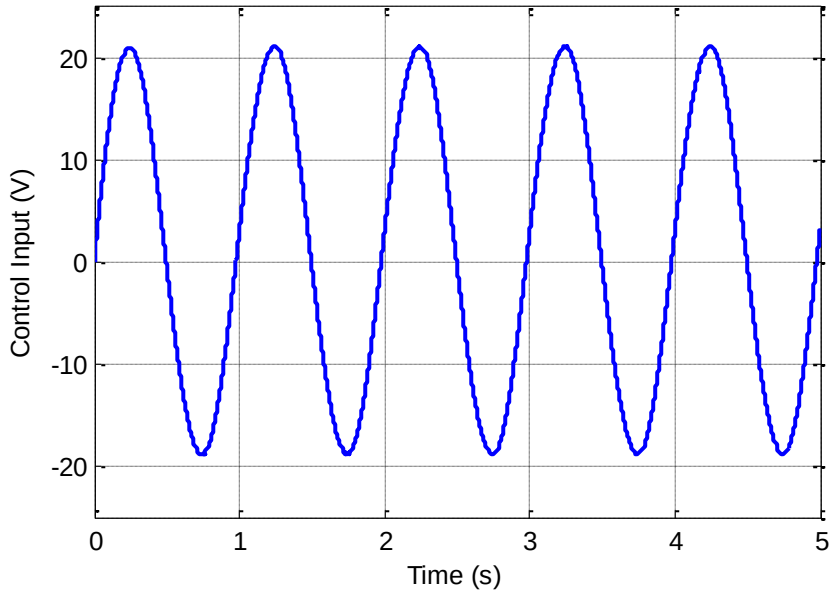

Fig. 4.10 Control input for AMPC (1 Hz) (3 predictive steps)

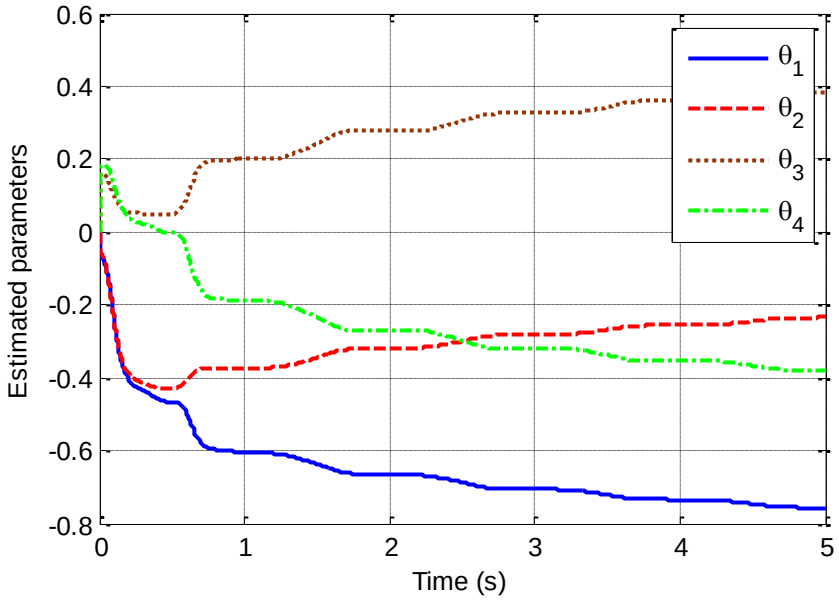

Fig. 4.11 Estimated parameters for AMPC (1 Hz) (3 predictive steps)

Fig. 4.12 shows the tracking result. The tracking error is shown in Fig. 4.13. It can be seen that the maximum error at steady state is about 0.4%.

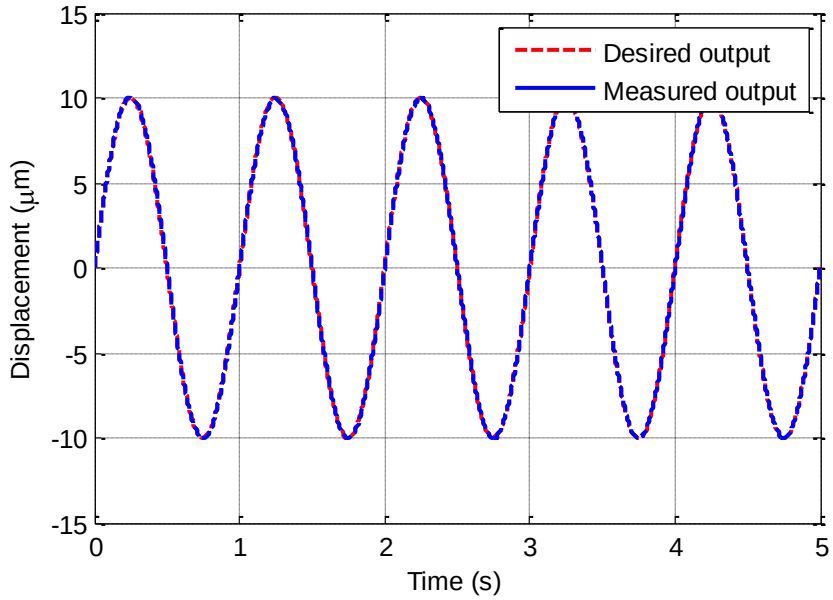

Fig. 4.12 Tracking results for AMPC (1 Hz) (3 predictive steps)

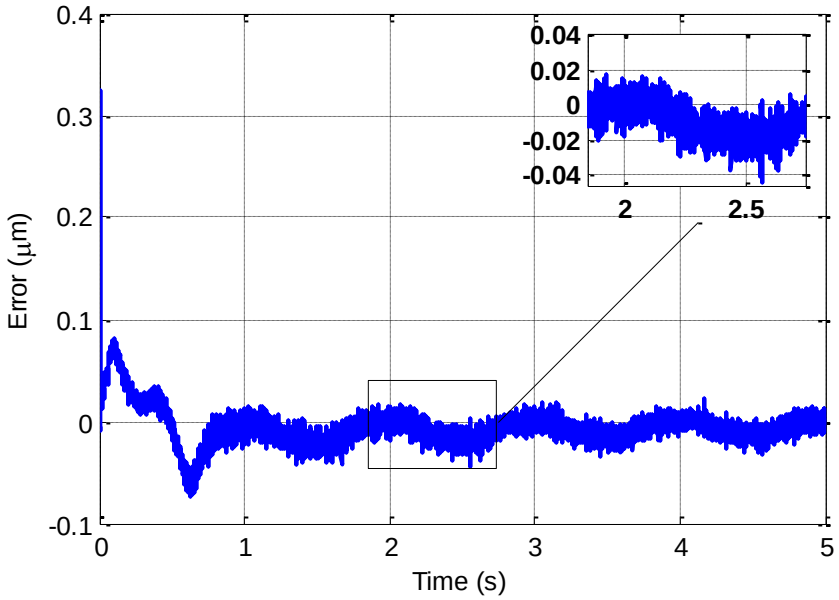

Fig. 4.13 Tracking results for AMPC (1 Hz) (3 predictive steps)

Fig. 4.14 shows the computation time of the first experiments.

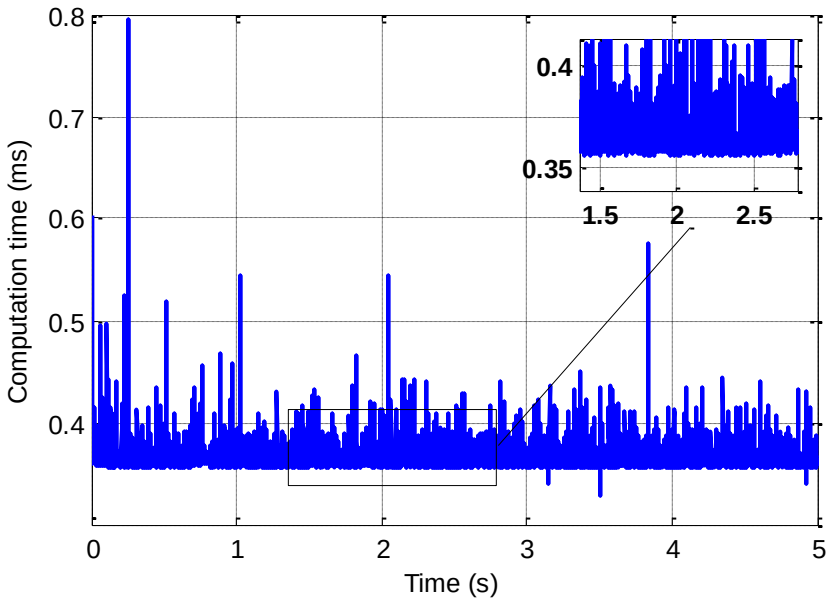

Fig. 4.14 Computation time for AMPC (1 Hz) (3 predictive steps)

The experiment is also conducted with higher frequency references, which are 10 Hz and 30 Hz.

Fig. 4.15 shows the control input for the experiment with 10Hz sinusoid reference signal. The estimated parameters are shown in Fig. 4.16.

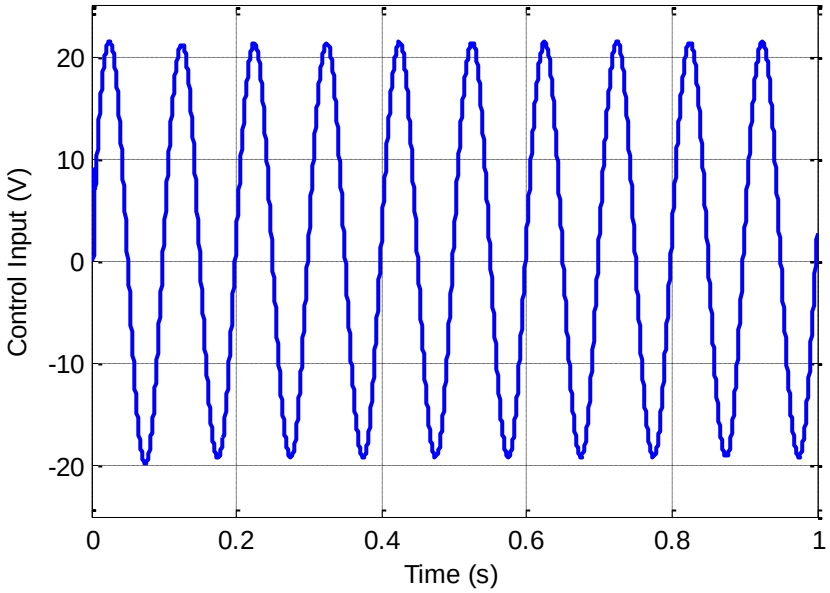

Fig. 4.15 Control input for AMPC (10 Hz) (3 predictive steps)

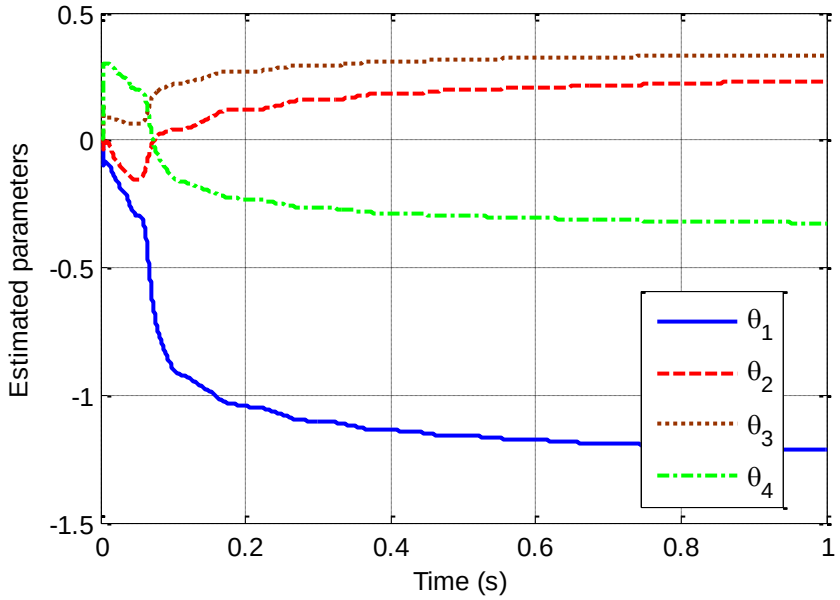

Fig. 4.16 Estimated parameters for AMPC (10 Hz) (3 predictive steps)

Fig. 4.17 shows the comparison between measured output and desired output. The tracking error is shown in Fig. 4.18. It can be seen that the maximum error at steady state is about 2%.

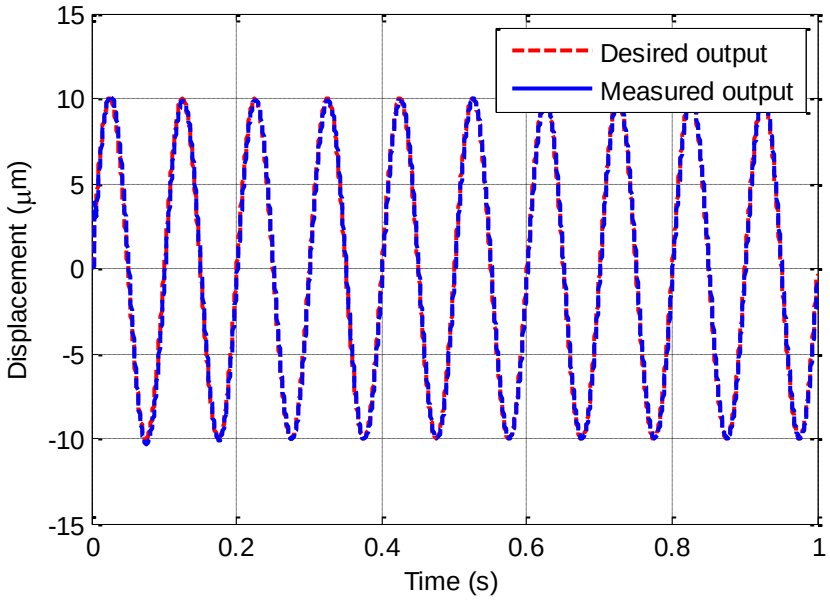

Fig. 4.17 Tracking results for AMPC (10 Hz) (3 predictive steps)

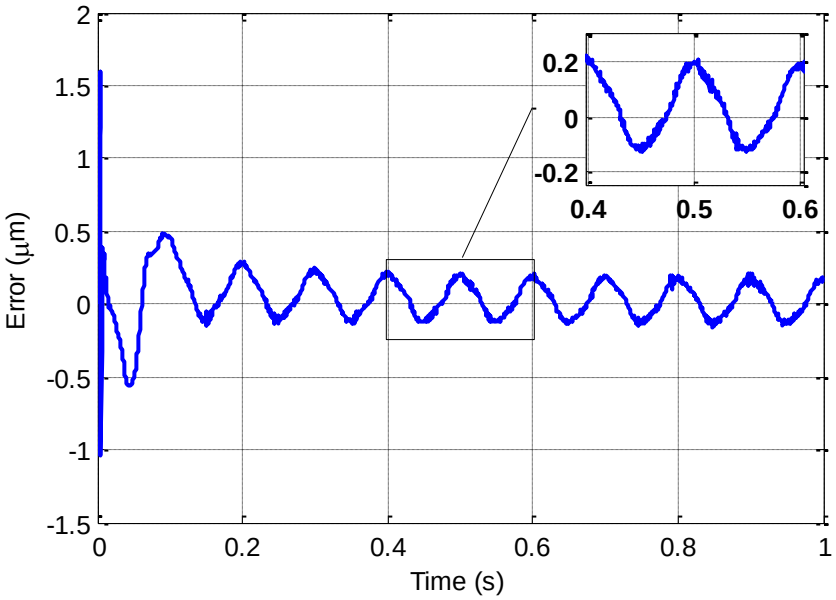

Fig. 4.18 Tracking error for AMPC (10 Hz) (3 predictive steps)

The computation time is shown in Fig. 4.19.

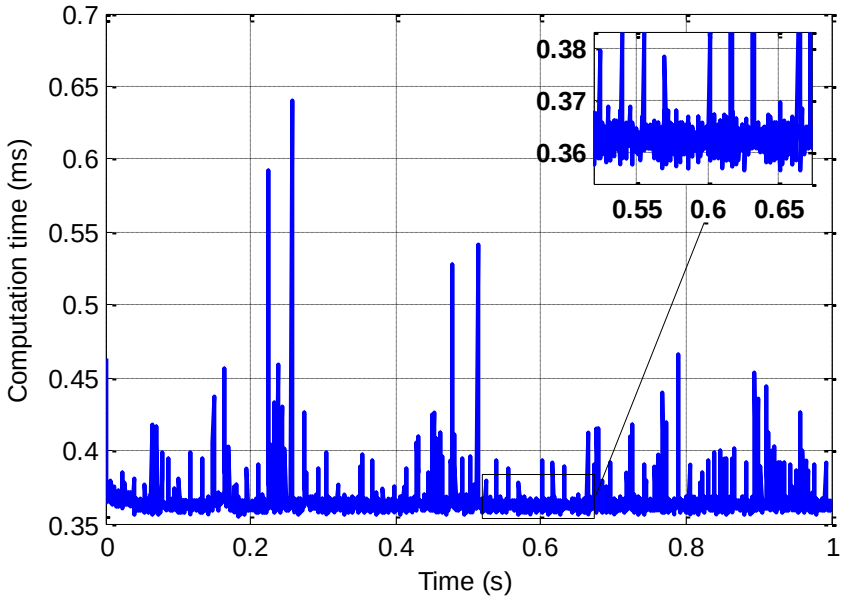

Fig. 4.19 Computation time for AMPC (10 Hz) (3 predictive steps)

Fig. 4.20 shows the control input for the experiment with 30Hz sinusoid reference signal. The estimated parameters are shown in Fig. 4.21.

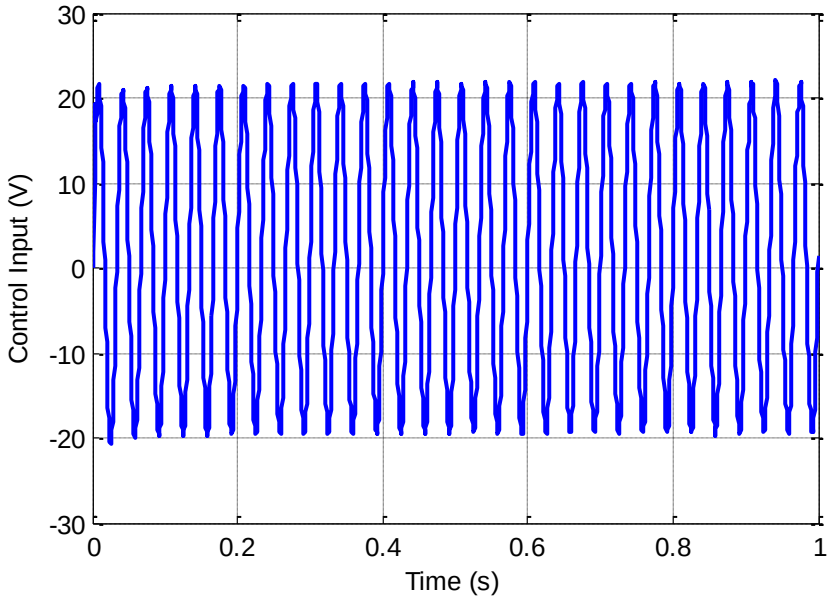

Fig. 4.20 Control input for AMPC (30 Hz) (3 predictive steps)

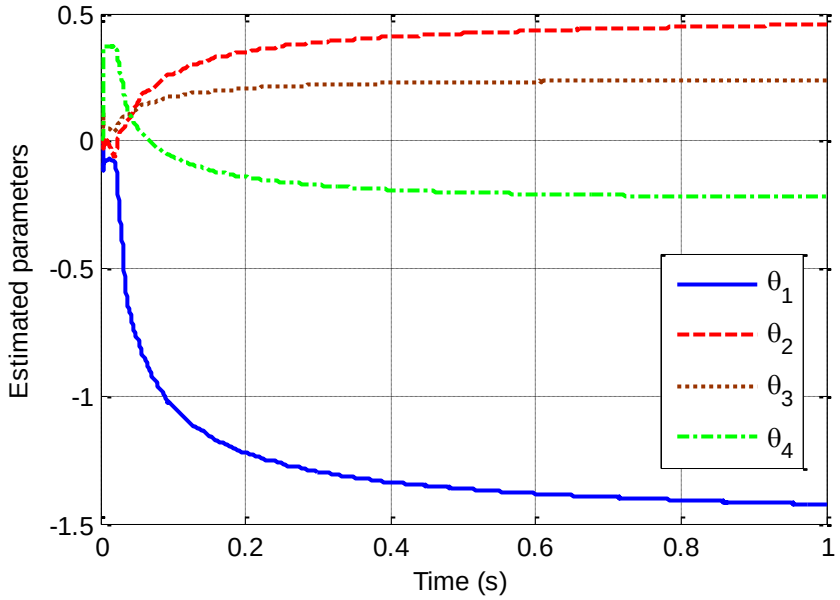

Fig. 4.21 Estimated parameters for AMPC (30 Hz) (3 predictive steps)

Fig. 4.22 shows the comparison between measured output and desired output. The tracking error is shown in Fig. 4.23. It can be seen that the maximum error at steady state is about 8%.

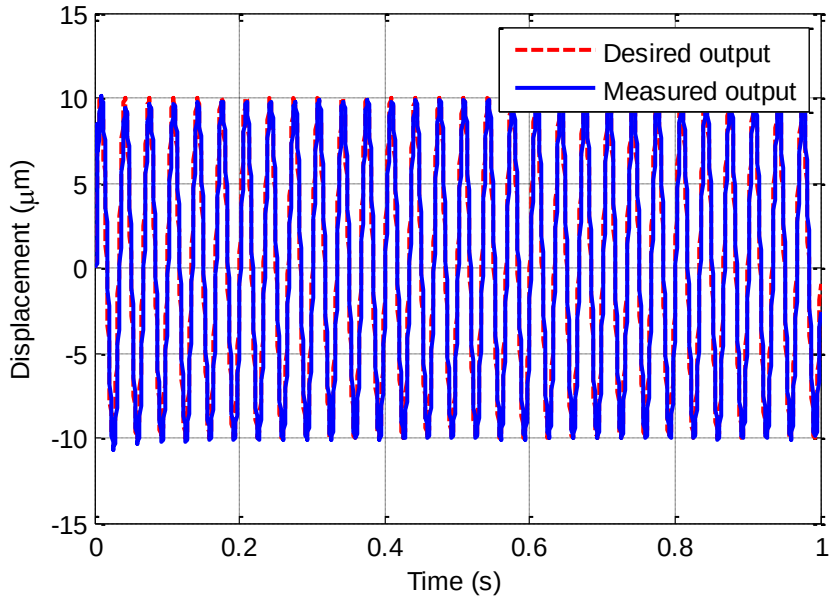

Fig. 4.22 Tracking results for AMPC (30 Hz) (3 predictive steps)

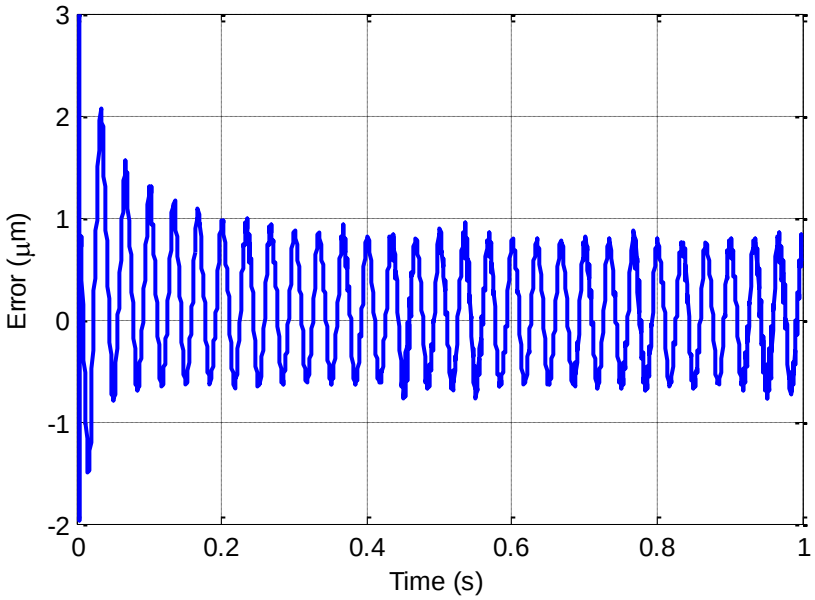

Fig. 4.23 Tracking error for AMPC (30 Hz) (3 predictive steps)

The computation time is shown in Fig. 4.24.

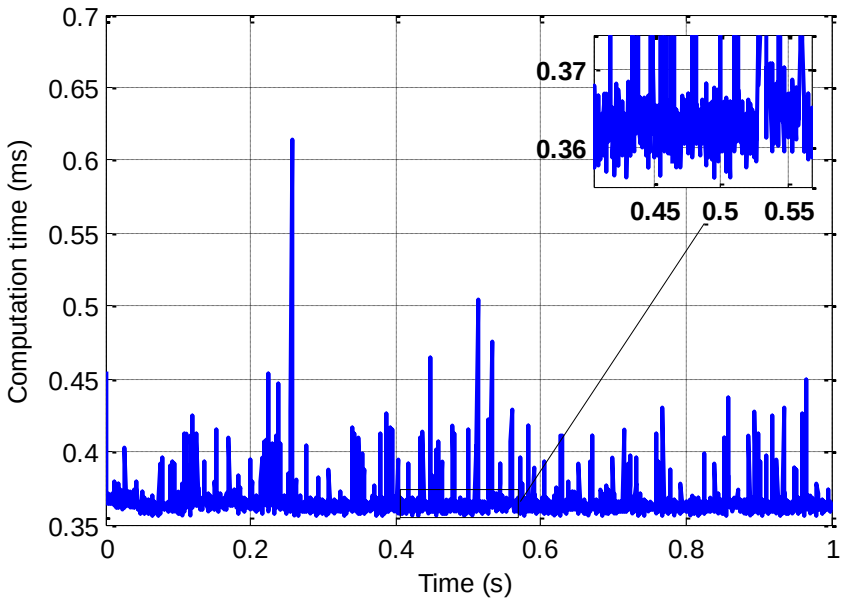

Fig. 4.24 Computation time for AMPC (30 Hz) (3 predictive steps)

The last experiment for 3 predictive steps is with multiple frequencies reference signal. Fig. 4.25 shows the control input for the experiment with complex reference reference signal. The estimated parameters are shown in Fig. 4.26.

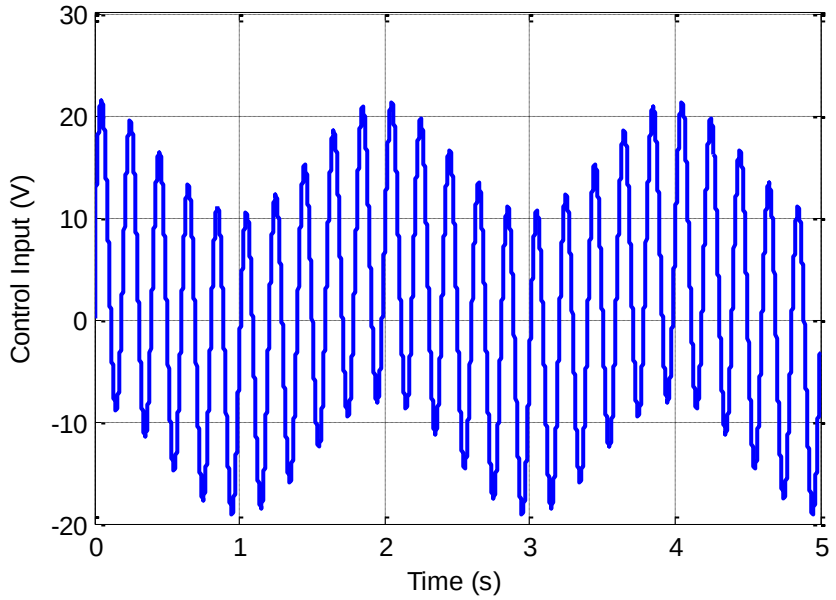

Fig. 4.25 Control input for AMPC with combinative sinusoid signal (3 predictive steps)

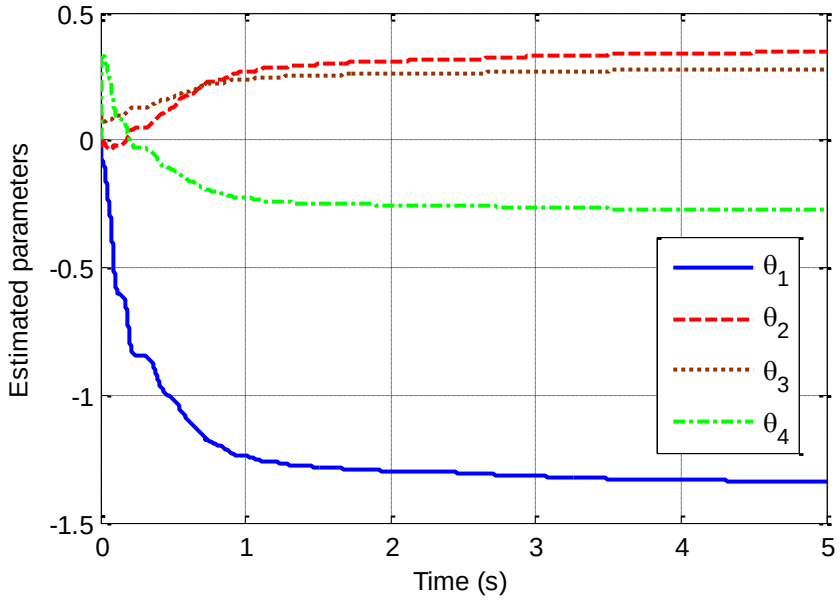

Fig. 4.26 Estimated parameters for AMPC with multiple frequencies signal (3 predictive steps)

Fig. 4.27 shows the comparison between measured output and desired output. The tracking error is shown in Fig. 4.28. It can be seen that the maximum error at steady state is about 0.8%.

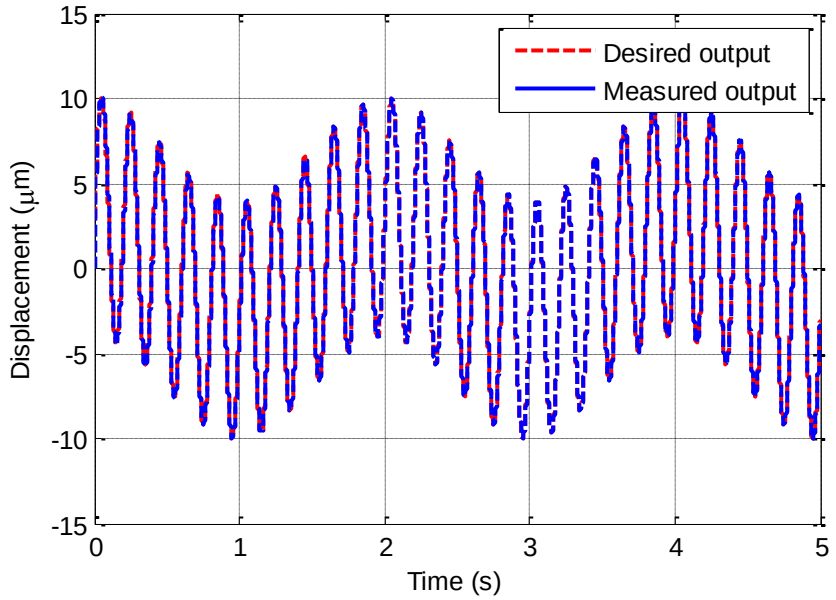

Fig. 4.27 Tracking results for AMPC with multiple frequencies signal (3 predictive steps)

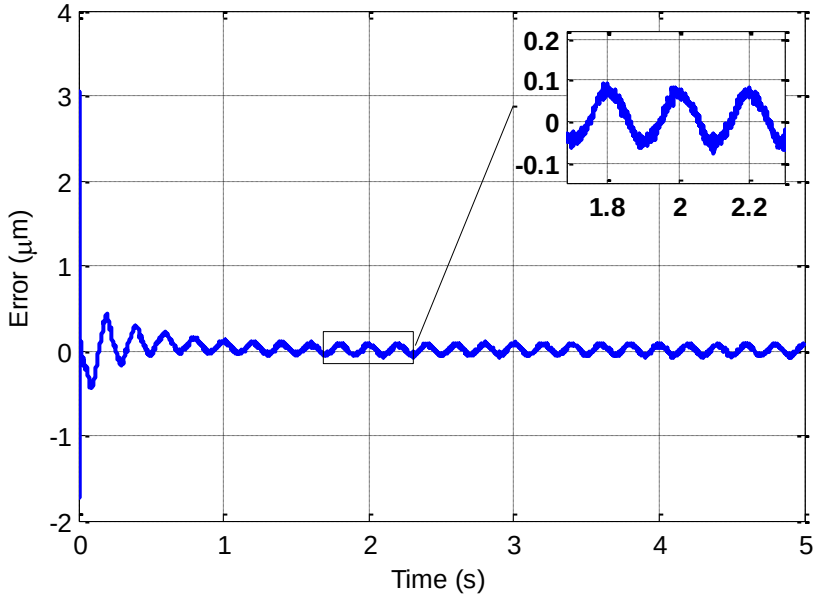

Fig. 4.28 Tracking error for AMPC with multiple frequencies signal (3 predictive steps)

The computation time is shown in Fig. 4.29.

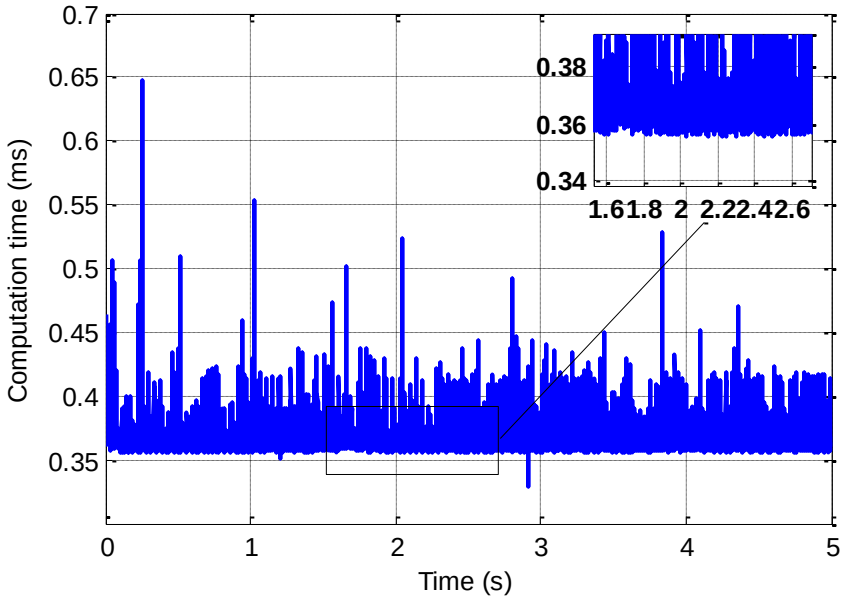

Fig. 4.29 Computation time for AMPC with multiple frequencies signal (3 predictive steps)

4.3.2.2 Experiment of AMPC with 5 Predictive Steps

In order to have a better look inside the performance of AMPC technique, another experiment is conducted with 5 predictive steps. For the purpose of comparison, it is only required the tracking error and the computation time of the experiment.

Fig. 4.30 shows the tracking error with experiment at 1Hz. The computation time is shown in Fig. 4.31.

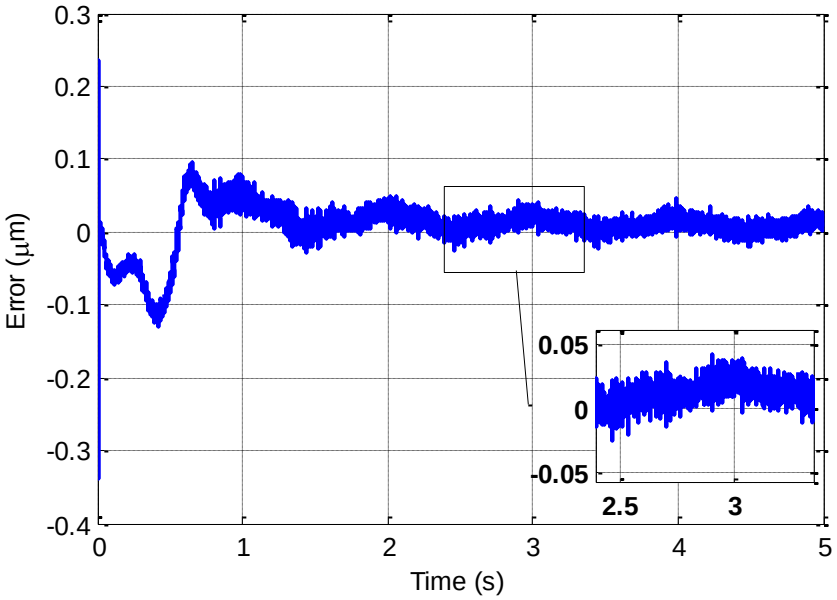

Fig. 4.30 Tracking error for AMPC (1HZ) (5 predictive steps)

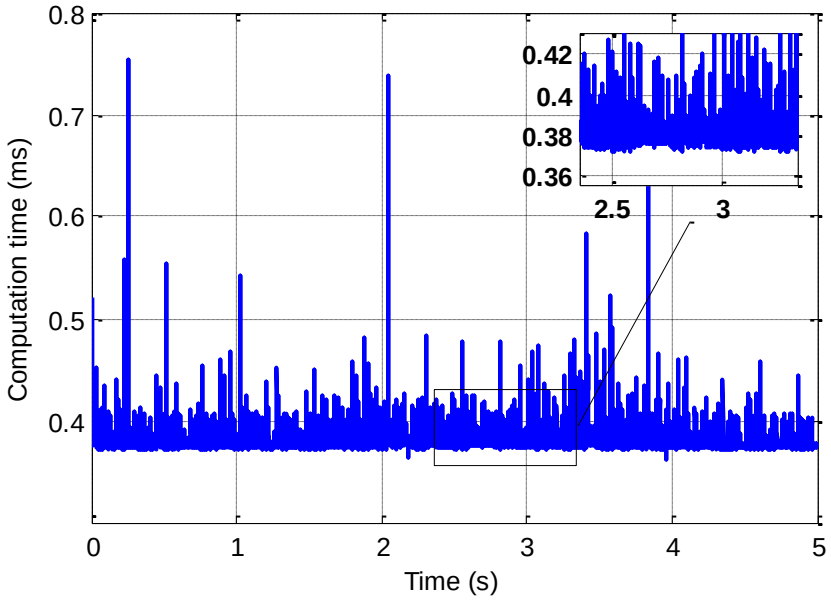

Fig. 4.31 Computation time for AMPC (1 Hz) (5 predictive steps)

Fig. 4.32 shows the tracking error with experiment at 10Hz. The computation time is shown in Fig. 4.33.

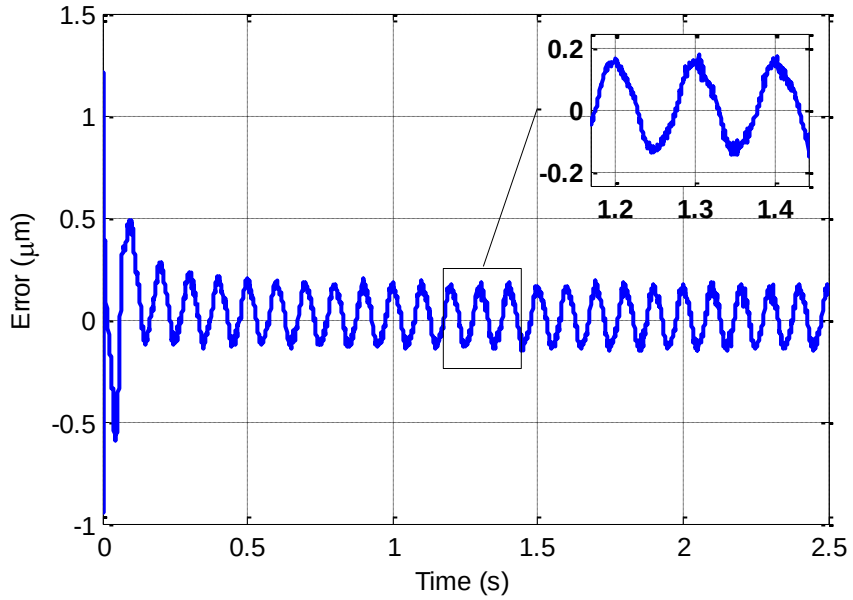

Fig. 4.32 Tracking error for AMPC (10HZ) (5 predictive steps)

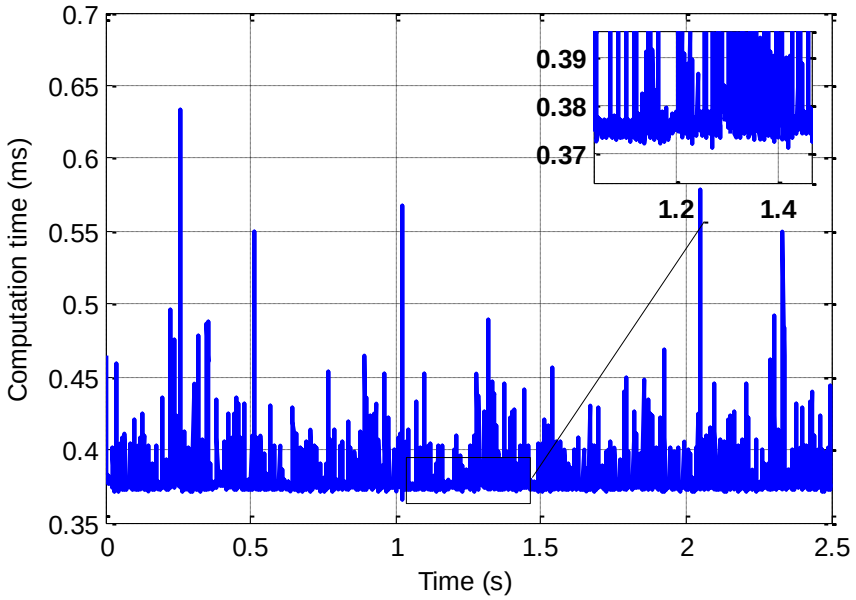

Fig. 4.33 Computation time for AMPC (10 Hz) (5 predictive steps)

The tracking error and computation time with 30 Hz frequency reference signal are shown in Fig. 4.34 and Fig. 4.35, respectively.

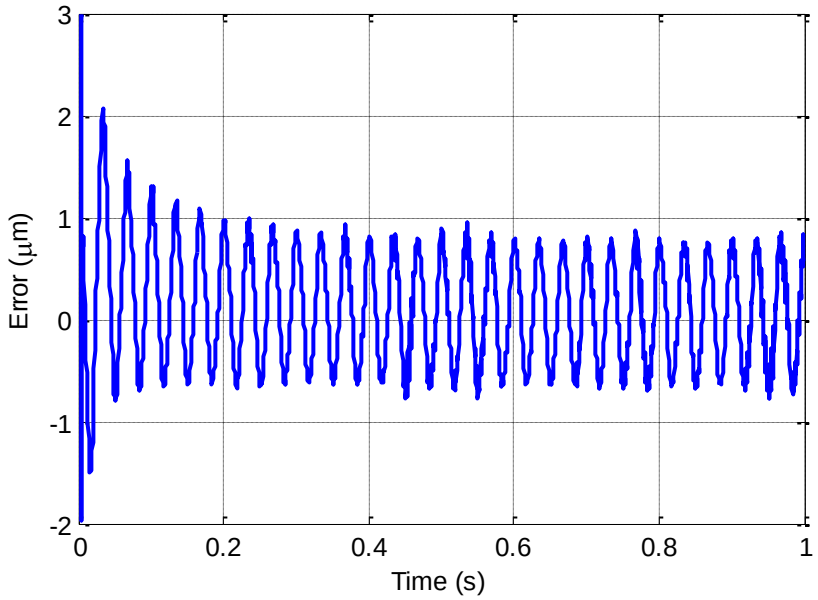

Fig. 4.34 Tracking error for AMPC (30HZ) (5 predictive steps)

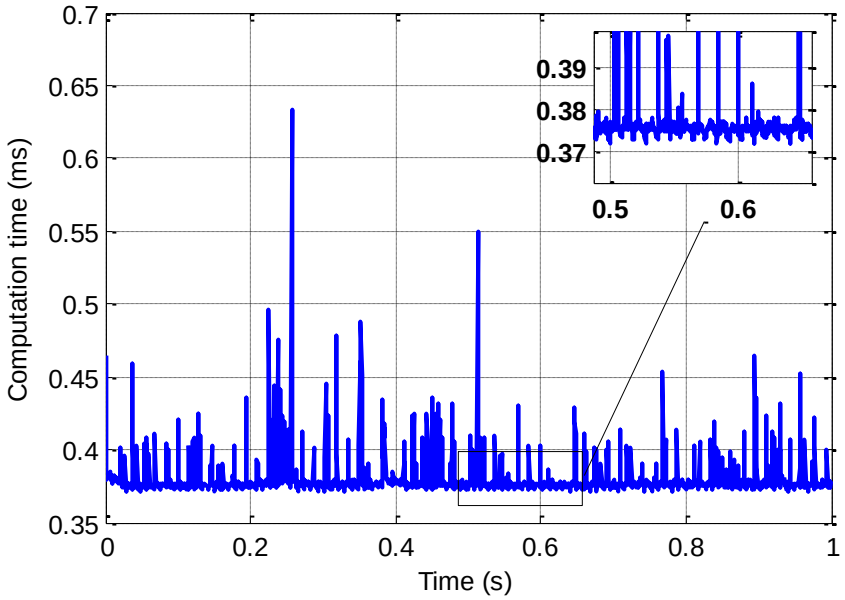

Fig. 4.35 Computation time for AMPC (30 Hz) (5 predictive steps)

Lastly, the experimental results with complex reference signal are shown in Fig. 4.36 and. 4.37.

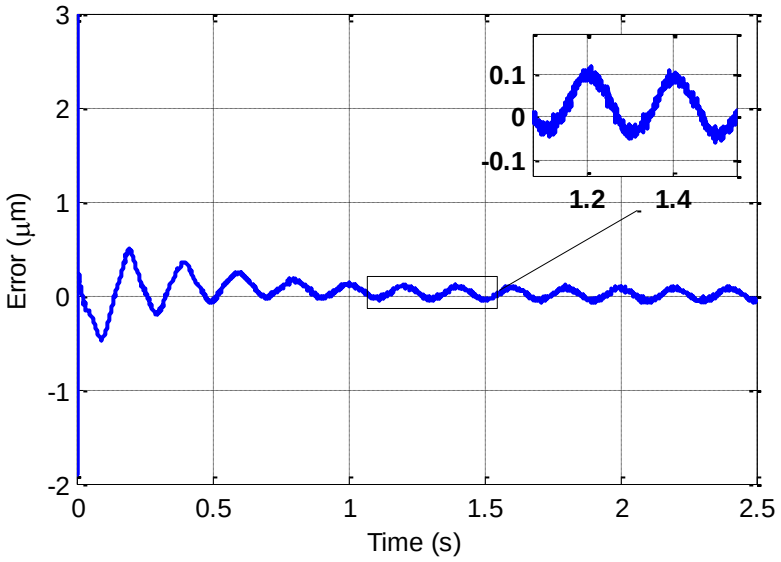

Fig. 4.36 Tracking error for AMPC with multiple frequencies signal (5 predictive steps)

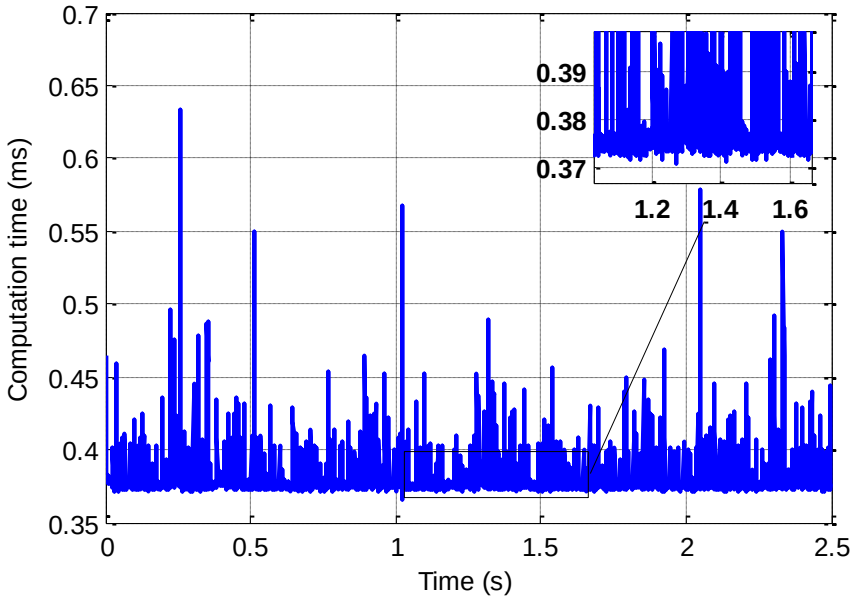

Fig. 4.37 Computation time for AMPC with multiple frequencies signal (5 predictive steps)

4.4 Discussion

Through the experiments of MPC and AMPC, it can be seen that the system have better performance comparing to PI control. Unlike the conventional PI control, MPC still works in high frequency. As it can be seen in Fig. 4.7, even at 30 Hz frequency, the maximum tracking

error of MPC is only 8%. The performance of AMPC at steady state is almost the same with MPC as can be seen in Fig. 4.13, Fig. 4.18 and Fig. 4.23 for frequencies at 1 Hz, 10 Hz, and 30 Hz, respectively. The advantage of AMPC is that the model parameters need not to be identified. However, one drawback of MPC and AMPC is the computation effort. The average computation time for AMPC 3 predictive steps experiment at 1 Hz, 10 Hz and 30 Hz are 0.3644 ms, 0.3661 ms and 0.3661 ms, respectively. The average computation time for AMPC 5 predictive steps experiment at 1 Hz, 10 Hz and 30 Hz are 0.3789 ms, 0.3791 ms and 0.3794 ms, respectively. Meanwhile the tracking errors in both 3 predictive steps and 5 predictive steps are almost the same. It can be seen that the computation cost increases when the number of predictive steps increase.

Chapter 5: Adaptive Control Based on Pseudo Discrete-time Bouc-Wen Model

5.1 Introduction

Controlling hysteresis systems using Bouc-Wen model has been reported in [77], [78], [79], [80], and [81]. In [77], a hysteresis observer based on Bouc-Wen model is proposed to describe hysteresis nonlinearity of the PEA. The model parameters are identified by root-mean-square method. In [11], the Bouc-Wen model is adopted to describe the behavior of base-isolation systems, and then an adaptive controller is designed to stabilize the close-loop system and to improve the system performance. It should be noted that the effect of the hysteresis is treated as a bounded disturbance in [78]. In [79], firstly the dynamic system with Bouc-Wen model is established and identified by using particles swarm optimization. Then a PID controller is employed to compensate the nonlinearity hysteresis of piezo-driven micromanipulator. In [80], a feedforward controller, which is formulated based on the identified Bouc-Wen model parameters, is used to compensate hysteresis nonlinearity in piezoelectric material. In [81], a new perfect inverse function of the hysteresis (which is described by Bouc-Wen model) is constructed and used to cancel the hysteresis effects in adaptive backstepping control design. All works mentioned above have to take the identification procedure which costs a lot of time and work.

This chapter proposes an adaptive controller based on Pseudo-Discrete-time Bouc-Wen model. It should be mentioned that the model is adapted directly in to controller design where real model parameters need not to be identified. The adaptive control law guarantees the closed-loop system stability. The proposed method is simple and easy to be implemented. Experimental results confirm the effectiveness of proposed method.

5.2 Discrete-Time Model Inspired by Bouc-Wen Model

The expression of Bouc-Wen model [82] is

$$y(t) = \mu k u(t) + (1-\mu) k z(t) \tag{5.1}$$

$$\dot{z}(t) = \alpha_m \dot{u}(t) - \beta_m |\dot{u}(t)||z(t)|^{n-1} z(t) - \gamma_m \dot{u}(t)|z(t)|^n,\ z(0) = z_0 \tag{5.2}$$

Consider the case $n = 1$ and focus on (5.2).

The hysteresis nonlinearity $z(t)$ is treated as output $y(t)$. The differential equation (5.2) is written as follows:

$$\dot{y}(t) = \alpha_m \dot{u}(t) - \beta_m |\dot{u}(t)| y(t) - \gamma_m \dot{u}(t) |y(t)|, y(0) = y_0 \tag{5.3}$$

Now, let us consider the discretization of Equation (5.3). Define

$$y'(t) = \frac{y(t+\Delta t) - (1-\Theta_1(\Delta t)) y(t)}{\Delta t}; u'(t) = \frac{u(t+\Delta t) - (1-\Theta_2(\Delta t)) u(t)}{\Delta t} \tag{5.4}$$

where Δt is sampling period, $t = k\Delta t$ is sampling instant, $\Theta_1(\Delta t)$ and $\Theta_2(\Delta t)$ are known high order functions of Δt .It can be observed that $\lim_{\Delta t \to 0} y'(t) = \dot{y}(t)$ and $\lim_{\Delta t \to 0} u'(t) = \dot{u}(t)$, i.e. $y'(t)$ and $u'(t)$ can be regarded as the approximations of $\dot{y}(t)$ and $\dot{u}(t)$, respectively.

For a chosen sampling period Δt , denote $(1-\Theta_1(\Delta t)) = \vartheta$ and $(1-\Theta_2(\Delta t)) = \lambda$ .Then, it gives

$$\dot{y}(t) \approx \frac{y(t+\Delta t) - \vartheta y(t)}{\Delta t}; \dot{u}(t) \approx \frac{u(t+\Delta t) - \lambda u(t)}{\Delta t} \tag{5.5}$$

where λ and ϑ are known parameters satisfying $0 < \lambda < 1, 0 < \vartheta < 1$ and their values are nearly equal to 1 when Δt is small.

From (5.4) and (5.5), Equation (5.3) will become

$$y(k\Delta t+\Delta t)=\Delta t\alpha_m\frac{u(k\Delta t+\Delta t)-\lambda u(k\Delta t)}{\Delta t}-\Delta t\beta_m\left|\frac{u(k\Delta t+\Delta t)-\lambda u(k\Delta t)}{\Delta t}\right|y(k\Delta t)$$
$$-\Delta t\gamma_m\frac{u(k\Delta t+\Delta t)-\lambda u(k\Delta t)}{\Delta t}|y(k\Delta t)|+\vartheta y(k\Delta t) \tag{5.6}$$

For simplicity, denote $k\Delta t$ as k. Then, it gives

$$y(k+1)=\Delta t\alpha_m\frac{u(k+1)-\lambda u(k)}{\Delta t}-\Delta t\beta_m\left|\frac{u(k+1)-\lambda u(k)}{\Delta t}\right|y(k)$$
$$-\Delta t\gamma_m\frac{u(k+1)-\lambda u(k)}{\Delta t}|y(k)|+\vartheta y(k) \tag{5.7}$$

Define $u_x(k+1)=\dfrac{u(k+1)-\lambda u(k)}{\Delta t}$. System (5.7) yields

$$y(k+1)=\Delta t\alpha_m u_x(k+1)-\Delta t\beta_m|u_x(k+1)|y(k)-\Delta t\gamma_m u_x(k+1)|y(k)|+\vartheta y(k) \tag{5.8}$$

i.e.

$$y(k)=\Delta t\alpha_m u_x(k)-\Delta t\beta_m|u_x(k)|y(k-1)-\Delta t\gamma_m u_x(k)|y(k-1)|+\vartheta y(k-1) \tag{5.9}$$

For simplicity, denote $\alpha=\Delta t\alpha_m$, $\beta=\Delta t\beta_m$ and $\gamma=\Delta t\gamma_m$. Equation (5.9) becomes

$$y(k)=\alpha u_x(k)-\beta|u_x(k)|y(k-1)-\gamma u_x(k)|y(k-1)|+\vartheta y(k-1) \tag{5.10}$$

In the following, it is assumed that $\alpha\geq\alpha_0>0$, where α_0 is a small constant.

Fig. 5.1 shows the hysteresis curve generated by model (5.10) where the parameters are set as $\alpha=0.0009$, $\beta=0.0005$, $\gamma=-0.0001$, $\lambda=0.9995$, $\vartheta=0.9995$, $u(k)=1.75*\sin(2\pi*5*0.001*k)/(1.0+1*k*0.001)$.

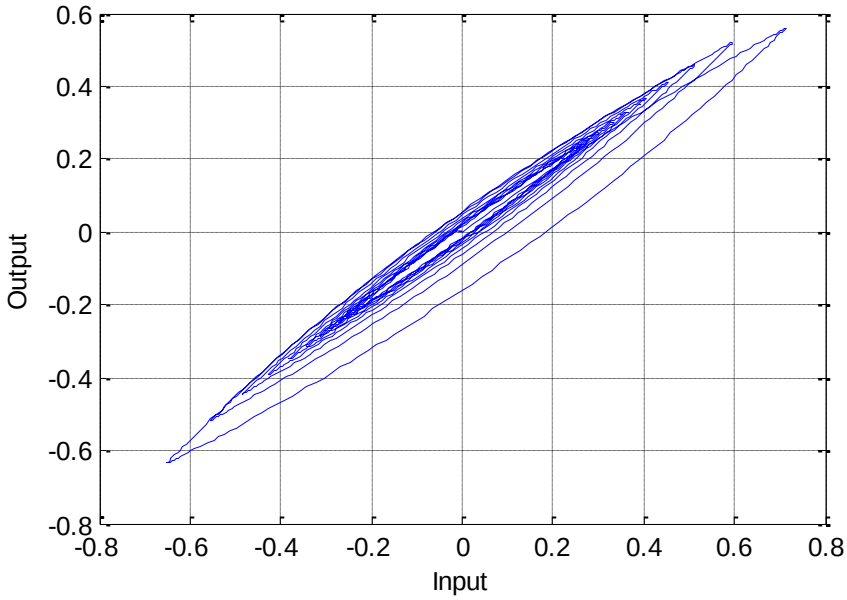

Fig. 5.1 Hysteresis curve by model (3.16)

It can be seen that the hysteresis curve by model (5.10) is similar to hysteresis curve in PEA as in Fig. 5.2.

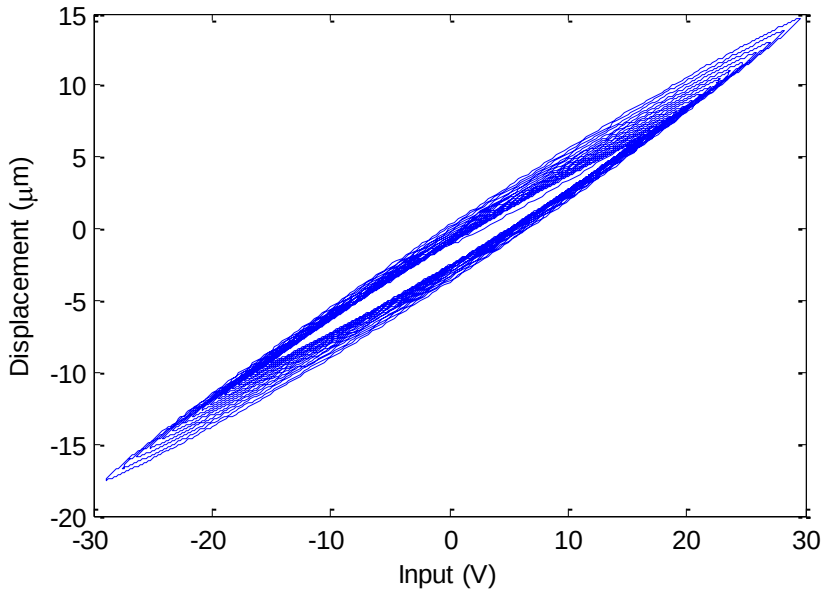

Fig. 5.2 Hysteresis curve by PEA

Since this model will be used for adaptive control later, the model parameters need not to be identified.

5.3 Model Reference Control Using Pseudo Bouc-Wen Model (MRAC)

5.3.1 System Description

This section considers the control problem of piezoelectric actuators which can be expressed by (5.10), where the parameters α, β and γ are unknown. Our control object is to find a feedback control input $u(k)$, such that all closed-loop signals are bounded, and the output $y(k)$ tracks the desired output $y_d(k)$ of a reference model.

$$y_d(k) = r(k) + a_m y_d(k-1) \tag{5.11}$$

where $|a_m| < 1$ and $r(k)$ is a bounded reference input.

5.3.2 Control Design and Stability Analysis

5.3.2.1 Parameter Estimation

Now rewrite (5.10) as

$$y(k) = \alpha u_x(k) - \beta|u_x(k)|y(k-1) - \gamma u_x(k)|y(k-1)| + a_m y(k-1) + (\vartheta - a_m)y(k-1) \tag{5.12}$$

and define the tracking error

$$e(k) = y(k) - y_d(k) \tag{5.13}$$

From (5.11) and (5.12), it yields

$$\begin{aligned} e(k) = {} & \alpha u_x(k) - \beta|u_x(k)|y(k-1) - \gamma u_x(k)|y(k-1)| \\ & + (\vartheta - a_m)y(k-1) - r(k) + a_m e(k-1) \end{aligned} \tag{5.14}$$

If the control input $u(k)$ satisfies

$$\alpha u_x(k) - \beta|u_x(k)|y(k-1) - \gamma u_x(k)|y(k-1)| + (\vartheta - a_m)y(k-1) = r(k) \tag{5.15}$$

it can be concluded that the tracking error will go to zero when k approaches to infinity.

Since the parameters α , β and γ are unknown, the control in (5.15) cannot be implemented. In the following, the adaptive method will be used to estimate these parameters. Let $\hat{\alpha}(k)$, $\hat{\beta}(k)$ and $\hat{\gamma}(k)$ be their adaptive estimates, respectively.

Now, define the estimated output $\hat{y}(k)$ as

$$\hat{y}(k) = \hat{\alpha}(k)u_x(k) - \hat{\beta}(k)|u_x(k)|y(k-1) - \hat{\gamma}(k)u_x(k)|y(k-1)| + \vartheta y(k-1) \tag{5.16}$$

and the estimation error as

$$\varepsilon(k) = \hat{y}(k) - y(k) \tag{5.17}$$

It follows from (5.16) and (5.17) that

$$\varepsilon(k) = \hat{\alpha}(k)u_x(k) - \hat{\beta}(k)|u_x(k)|y(k-1) - \hat{\gamma}(k)u_x(k)|y(k-1)| + \vartheta y(k-1) - y(k) \tag{5.18}$$

Define

$$\tilde{\alpha}(k) = \hat{\alpha}(k) - \alpha\,,\ \tilde{\beta}(k) = \hat{\beta}(k) - \beta\,,\ \tilde{\gamma}(k) = \hat{\gamma}(k) - \gamma\,. \tag{5.19}$$

Then, (5.18) becomes

$$\varepsilon(k) = \tilde{\alpha}(k)u_x(k) - \tilde{\beta}(k)|u_x(k)|y(k-1) - \tilde{\gamma}(k)u_x(k)|y(k-1)| \tag{5.20}$$

For simplicity, define

$$D(k) = \sqrt{1 + (u_x(k))^2 + 2(\,u_x(k)y(k-1))^2} \tag{5.21}$$

The adaptive laws for $\hat{\alpha}(k)$, $\hat{\beta}(k)$ and $\hat{\gamma}(k)$ are formulated as

$$\hat{\alpha}'(k) = \left| \hat{\alpha}'(k-1) - \Gamma \frac{\varepsilon(k-1)u_x(k-1)}{D^2(k-1)} \right| \tag{5.22a}$$

$$\hat{\alpha}(k) = \begin{cases} \hat{\alpha}'(k) & \text{if } \hat{\alpha}'(k) > \alpha_0 \\ \alpha_0 & \text{otherwise} \end{cases} \tag{5.22b}$$

$$\hat{\beta}(k) = \hat{\beta}(k-1) + \Gamma \frac{\varepsilon(k-1)|u_x(k-1)|y(k-2)}{D^2(k-1)} \tag{5.23}$$

$$\hat{\gamma}'(k) = \hat{\gamma}'(k-1) + \Gamma \frac{\varepsilon(k-1)u_x(k-1)|y(k-2)|}{D^2(k-1)} \tag{5.24a}$$

$$\hat{\gamma}(k) = \begin{cases} \hat{\gamma}'(k) & \text{if } \hat{\gamma}'(k) < -|\hat{\beta}(k)| \\ -|\hat{\beta}(k)| & \text{otherwise} \end{cases} \tag{5.24b}$$

where the parameter adaptation gain Γ $(0 < \Gamma < 2)$ adjusts the adaptation speed.

Lemma 1: For the adaptation law in (5.22)-(5.24), the following properties are held:

(P1) $\hat{\alpha}(k)$, $\hat{\beta}(k)$ and $\hat{\gamma}(k)$ are bounded for all $k > 0$.

(P2) $\sum_{k=1}^{\infty} \left(\frac{\varepsilon^2(k)}{D^2(k)} \right) < \infty$.

(P3) $\lim_{k\to\infty} \frac{|\varepsilon(k)|}{D(k)} = 0$.

(P4) For any positive integer p

$$\sum_{k=p}^{\infty} \|\hat{\alpha}(k) - \hat{\alpha}(k-p)\|_2^2 < \infty$$

$$\sum_{k=p}^{\infty} \|\hat{\beta}(k) - \hat{\beta}(k-p)\|_2^2 < \infty$$

$$\sum_{k=p}^{\infty} \|\hat{\gamma}(k) - \hat{\gamma}(k-p)\|_2^2 < \infty$$

Proof: Introduce the Lyapunov function

$$L(k) = \tilde{\alpha}^2(k) + \tilde{\beta}^2(k) + \tilde{\gamma}^2(k) \tag{5.25}$$

Taking the difference of $L(k)$ along the trajectories of (5.22)-(5.24) gives

$$
\begin{aligned}
L(k)-L(k-1) &= \tilde{\alpha}^2(k)-\tilde{\alpha}^2(k-1)+\tilde{\beta}^2(k)-\tilde{\beta}^2(k-1)+\tilde{\gamma}^2(k)-\tilde{\gamma}^2(k-1) \\
&\le -2\Gamma\frac{\varepsilon(k-1)\tilde{\alpha}(k-1)u_x(k-1)}{D^2(k-1)}+2\Gamma\frac{\varepsilon(k-1)\tilde{\beta}(k-1)|u_x(k-1)|y(k-2)}{D^2(k-1)} \\
&\quad +2\Gamma\frac{\varepsilon(k-1)\tilde{\gamma}(k-1)u_x(k-1)|y(k-2)|}{D^2(k-1)} \\
&\quad +\Gamma^2\frac{\varepsilon^2(k-1)\left(u_x{}^2(k-1)+2(u_x(k-1)y(k-2))^2\right)}{D^4(k-1)}
\end{aligned}
$$

$$
\le -2\Gamma\frac{\varepsilon^2(k-1)}{D^2(k-1)}+\Gamma^2\frac{\varepsilon^2(k-1)D^2(k-1)}{D^4(k-1)}
$$

$$
=-\frac{\Gamma(2-\Gamma)\varepsilon^2(k-1)}{D^2(k-1)} \tag{5.26}
$$

Because $L(k)$ is a positive function, the properties of Lemma 1 can be proved by referring to projection algorithm in [83] (Appendix B).

5.3.2.2 Control Input Design and Stability Analysis

The adaptive nonlinear controller is determined as

$$
u(k)=\lambda u(k-1)+u_x(k)\cdot\Delta t \tag{5.27}
$$

where $u_x(k)$ should satisfy

$$
u_x(k)=\frac{r(k)-(\vartheta-a_m)y(k-1)}{\left(\hat{\alpha}(k)-\hat{\beta}(k)sign\,(u_x(k))y(k-1)-\hat{\gamma}(k)|y(k-1)|\right)} \tag{5.28}
$$

It can be seen that

$$
\hat{\alpha}(k)-\hat{\beta}(k)sign(u_x(k))y(k-1)-\hat{\gamma}(k)|y(k-1)|\ge\alpha_0>0 \tag{5.29}
$$

By observing (5.28), it can be concluded that $u_x(k)$ must have the same sign with $r(k)-(\vartheta-a_m)y(k-1)$. Thus, $u_x(k)$ can be determined as follows.

If $r(k)-(\vartheta-a_m)y(k-1)\geq 0$, $u_x(k)$ is calculated by

$$u_x(k)=\frac{r(k)-(\vartheta-a_m)y(k-1)}{\hat{\alpha}(k)-\hat{\beta}(k)y(k-1)-\hat{\gamma}(k)|y(k-1)|} \tag{5.30}$$

If $r(k)-(\vartheta-a_m)y(k-1)<0$, $u_x(k)$ is calculated by

$$u_x(k)=\frac{r(k)-(\vartheta-a_m)y(k-1)}{\hat{\alpha}(k)+\hat{\beta}(k)y(k-1)-\hat{\gamma}(k)|y(k-1)|} \tag{5.31}$$

Theorem 1: For the system (5.10) controlled by (5.28), all the signals in the closed-loop system are bounded and the output tracking error $e(k)$ approaches zero as k approaches infinity.

Proof: Equation (5.28) can be expressed as

$$\hat{\alpha}(k)u_x(k)-\hat{\beta}(k)|u_x(k)|y(k-1)-\hat{\gamma}(k)u_x(k)|y(k-1)|+\vartheta y(k-1)=r(k)+a_m y(k-1) \tag{5.32}$$

Substituting (5.32) into (5.18) yields

$$\varepsilon(k)=r(k)+a_m y(k-1)-y(k) \tag{5.33}$$

From the definition of $D(k)$ in (5.21), it gives

$$\begin{aligned} D(k) &\leq 1+|u_x(k)|+\sqrt{2}|u_x(k)y(k-1)| \\ &\leq 1+|u_x(k)|+\sqrt{2}|u_x(k)||y(k-1)| \end{aligned} \tag{5.34}$$

Because the reference input $r(k)$ is bounded, from (5.28), there exist positive constants B_1 and B_2 such that.

$$u_x(k)\leq B_1+B_2|y(k-1)| \tag{5.35}$$

where (5.29) is employed.

From (5.33), (5.34) and (5.35), it gives

$$
\begin{aligned}
|y(k)| &= |-\varepsilon(k) + a_m y(k-1) + r(k)| \\
&\le \frac{|\varepsilon(k)|}{D(k)} D(k) + a_m |y(k-1)| + |r(k)| \\
&\le \frac{|\varepsilon(k)|}{D(k)} \left(1 + |u_x(k)| + \sqrt{2}|u_x(k)||y(k-1)|\right) + a_m |y(k-1)| + |r(k)| \\
&\le \frac{|\varepsilon(k)|}{D(k)} \left(1 + B_1 + B_2 |y(k-1)| + \sqrt{2}\left(B_1 + B_2 |y(k-1)|\right)|y(k-1)|\right) \\
&\quad + a_m |y(k-1)| + |r(k)| \\
&\le \frac{|\varepsilon(k)|}{D(k)} (1 + B_1) + \frac{|\varepsilon(k)|}{D(k)} \left(B_2 + \sqrt{2}B_1\right) y(k-1)| + \frac{|\varepsilon(k)|}{D(k)} \sqrt{2} B_2 |y(k-1)|^2 \\
&\quad + a_m |y(k-1)| + |r(k)|
\end{aligned}
\tag{5.36}
$$

Since $\lim_{k\to\infty} \frac{|\varepsilon(k)|}{D(k)} = 0$, and $|a_m| < 1$ there exist an instant K and positive constants C_1, C_2 and C_3 such that

$$
|y(k)| \le C_1 + C_2 |y(k-1)| + C_3 |y(k-1)|^2 \tag{5.37}
$$

for all $k > K$, where $C_2 < 1$, and C_3 is a very small positive constant satisfying

$$
\left(\sum_{i=K}^{k} C_1 C_2^k + C_2^{k+1} |y(K)| \right)^{-1} + (-1) C_3 \sum_{i=K}^{k-1} C_2^{k-i} > 0 \tag{5.38}
$$

At step $k - i$, multiplying both sides of (5.37) with C_2^i gives

$$
C_2^i y(k-i) \le C_1 C_2^i + C_2^{i+1} |y(k-i-1)| + C_3 C_2^i |y(k-i)|^2 \tag{5.39}
$$

where $k - i > K$.

Summing both sides of (5.39) from $i = 0$ to $i = k - K - 1$ gives

$$
|y(k)| \le \sum_{i=K}^{k} C_1 C_2^{k-i} + C_2^{k+1-K} |y(K)| + C_3 \sum_{i=K}^{k-1} C_2^{k-i} |y(i)|^2 \tag{5.40}
$$

By applying the results in [84] (Page 193, Chapter 4) with

$$p(k)=1$$

$$q=\sum_{i=K}^{k} C_1 C_2^{k-i} + C_2^{k+1-K}\left|y(K)\right|$$

$$H(k,y)=C_3\sum_{i=K}^{k-1} C_2^{k-i}\left|y(i)\right|^2$$

$$\alpha^{*}=2$$

it can be concluded that the closed-loop output $y(k)$ is bounded and the upper bound is estimated as

$$\left|y(k)\right| \le \left(\left(\sum_{i=K}^{k} C_1 C_2^{k-i} + C_2^{k+1-K}\left|y(K)\right|\right)^{-1} - C_3\sum_{i=K}^{k-1} C_2^{k-i}\right)^{-1} \tag{5.41}$$

From (5.35), the input variable $u_x(k)$ is also bounded, which means that the input $u(k)$ is also bounded by observing (5.27). Then, from (5.34), it can be seen that $D(k)$ is bounded. Thus, property (P3) in Lemma 1 means $\lim_{k\to\infty}\varepsilon(k)=0$. Since $r(k)=y_d(k)-a_m y_d(k-1)$, as from (5.33), it means $\varepsilon(k)=y_d(k)-a_m y_d(k-1)+a_m y(k-1)-y(k)=e(k)-a_m e(k-1)$, which means $\lim_{k\to\infty} e(k)=0$. It can be concluded that the tracking error will approach to zero asymptotically as k goes to infinity.

5.4 Simulation of MRAC

In this section, the above methodology is illustrated on a hysteresis system as in (5.10). The actual parameters are chosen as $\alpha=0.007$ $\beta=0.001$, $\gamma=-0.0015$, $\lambda=0.9995$, $\vartheta=0.9995$. The objective is to control the system output y to follow a desired trajectory $y(k)=4*sin(2\pi*0.001*k)$. The control design in Section 5.3.2.2 is applied with the initial value of parameters are chosen as $\hat{\alpha}(0)=0.5$, $\hat{\beta}(0)=0.5$ and $\hat{\gamma}(0)=-0.55$. The initial state is chosen as $y(0)=1.2$.

The simulation results presented in Fig. 5.3 are tracking error and controller input.

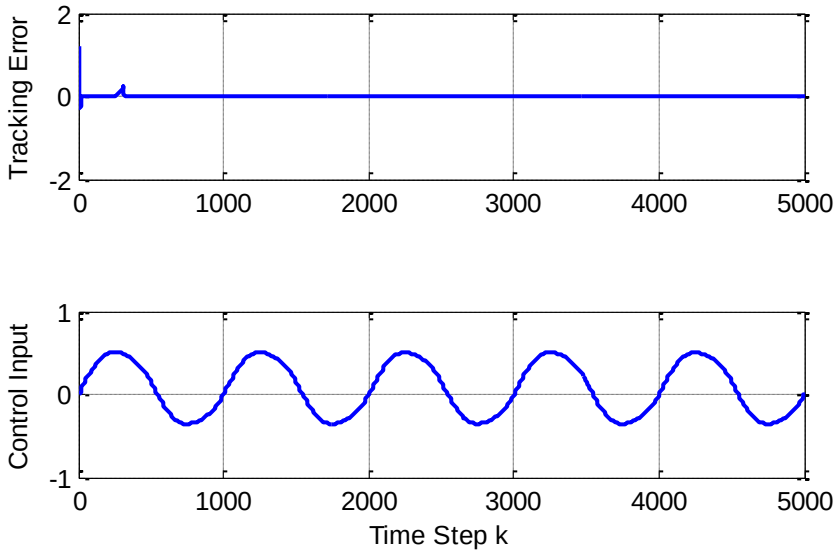

Fig. 5.3 Tracking error and input for simulation

5.5 Experiment of MRAC

The experiments of MRAC are conducted with the same four reference trajectories $y_{d1}(k)$, $y_{d2}(k)$, $y_{d3}(k)$, and $y_{d4}(k)$ as in other control techniques. The sampling time is chosen as 0.0005 s. λ and ϑ are chosen as 0.9995 and 0.9995, respectively. Table 5.1 shows the experimental setting.

Table 5.1 Experimental setting for MRAC

	$y_{d1}(k)$	$y_{d2}(k)$	$y_{d3}(k)$	$y_{d4}(k)$
$\hat{\alpha}(0)$	0.5	0.5	0.5	0.5
$\hat{\beta}(0)$	0.5	0.5	0.5	0.5
$\hat{\gamma}(0)$	-0.7	-0.7	-0.7	-0.7

Sampling time (s)	0.0005	0.0005	0.005	0.005
Adaptive gain	0.05	0.015	0.01	0.02
λ	0.9995	0.9995	0.9995	0.9995
ϑ	0.9995	0.9995	0.9995	0.9995

In the first experiment with $y_{d1}(k)$, the initial condition of $\hat{\alpha}(k)$, $\hat{\beta}(k)$ and $\hat{\gamma}(k)$ are set to 0.5, 0.5, -0.7, respectively. The initial value of output $y(k)$ is assumed as 0. The adaptive gain Γ is chosen as 0.05.

Fig. 5.4 shows the control input $u(k)$. The estimates of parameters $\hat{\alpha}(k), \hat{\beta}(k)$ and $\hat{\gamma}(k)$ are shown in Fig. 5.5. Fig. 5.6 shows the tracking result between reference and actual displacement. The tracking error for $y_{d1}(k)$ is shown in Fig. 5.7. The computation time is shown in Fig. 5.8.

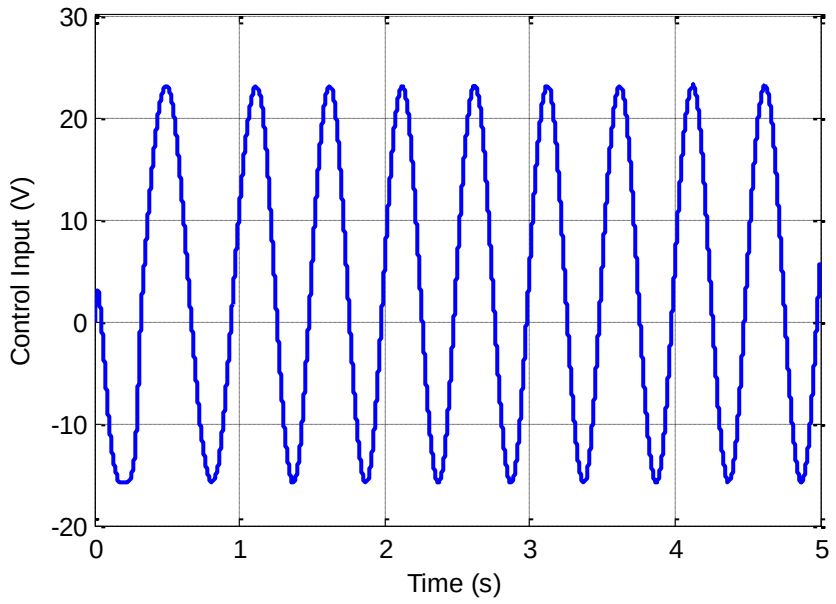

Fig. 5.4 Control input for experiment at 1 Hz in MRAC

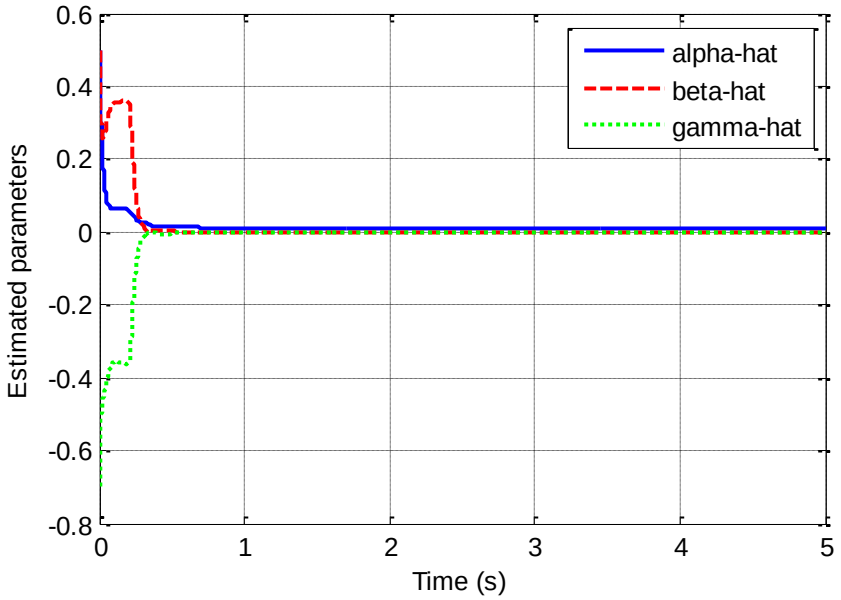

Fig. 5.5 Estimated parameters at 1 Hz in MRAC

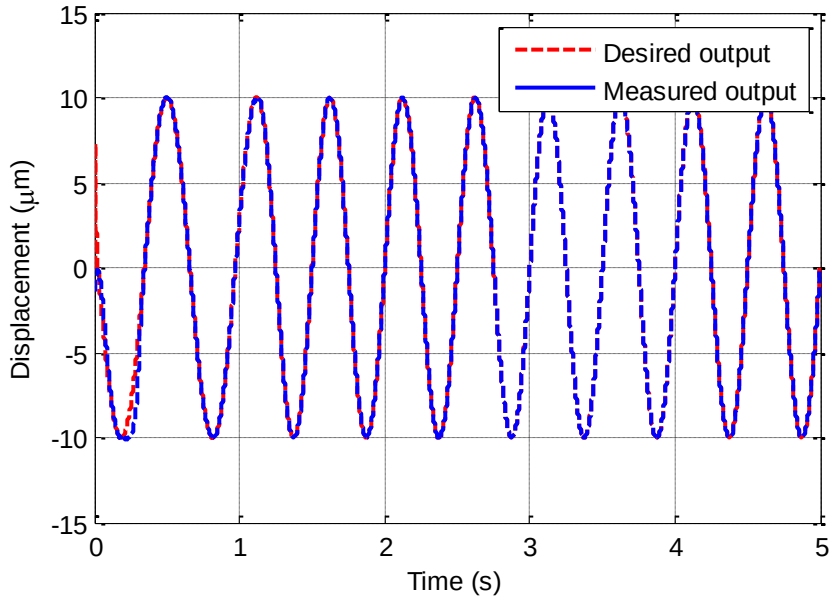

Fig. 5.6 Measured output and reference output at 1 Hz in MRAC

It is observed that the maximum error is within $\pm 0.02 \mu m$ when the system is at steady state.

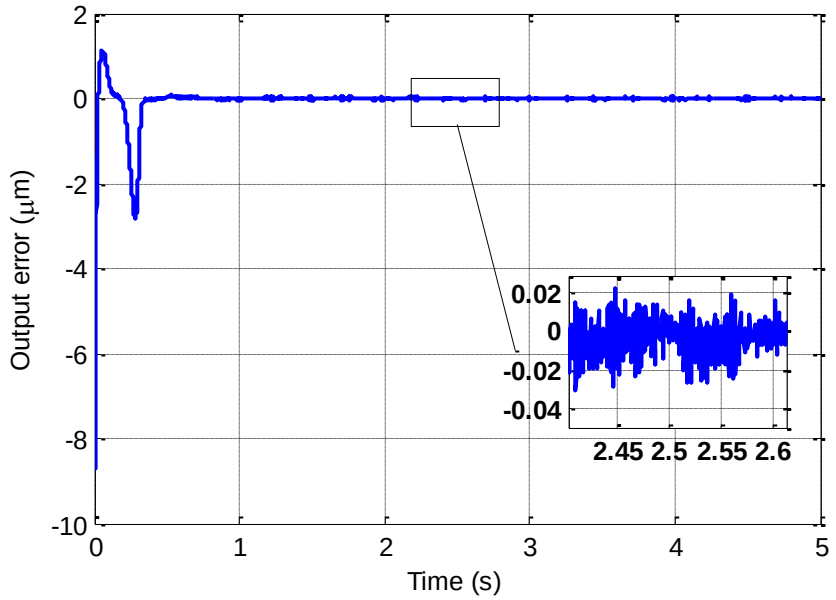

Fig. 5.7 Tracking error at 1 Hz in MRAC

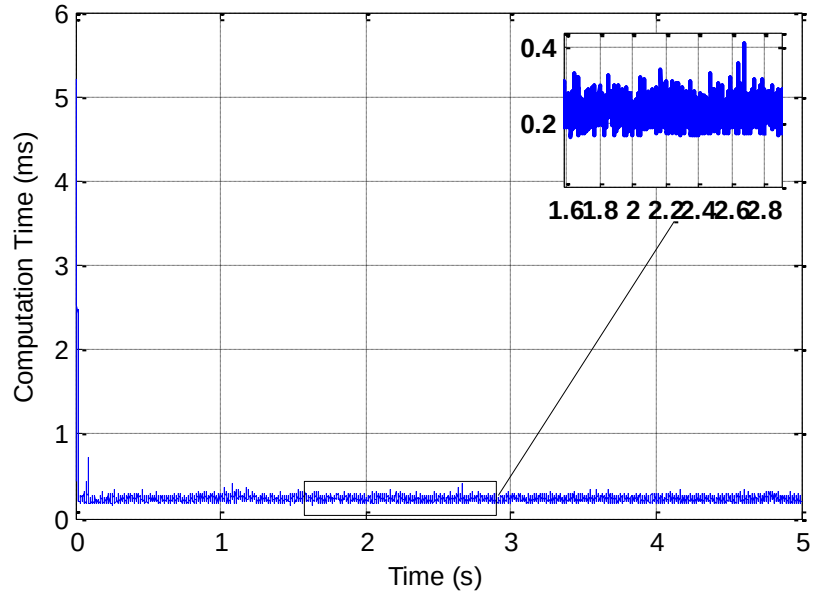

Fig. 5.8 Computation time in MRAC

In the experiment with $y_{d2}(k)$, the initial conditions of $\hat{\alpha}(k)$, $\hat{\beta}(k)$ and $\hat{\gamma}(k)$ are set to 0.5, 0.5, -0.7, respectively. The initial value of output $y(k)$ is assumed as 0. The adaptive gain Γ is chosen as 0.015.

Fig. 5.9 shows the control input $u(k)$. The estimates of parameters $\hat{\alpha}(k)$, $\hat{\beta}(k)$ and $\hat{\gamma}(k)$ are shown in Fig. 5.10. Fig. 5.11 shows the tracking result between reference and actual

displacement. The tracking error for $y_{d2}(k)$ is shown in Fig. 5.12. It is observed that the maximum error is within $\pm 0.1\mu m$ when the system is at steady state.

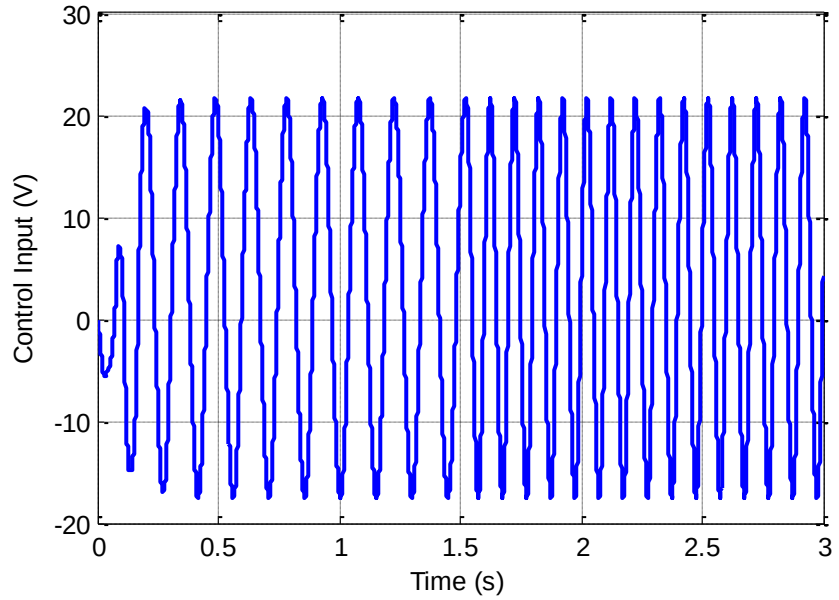

Fig. 5.9 Control input for experiment at 10 Hz in MRAC

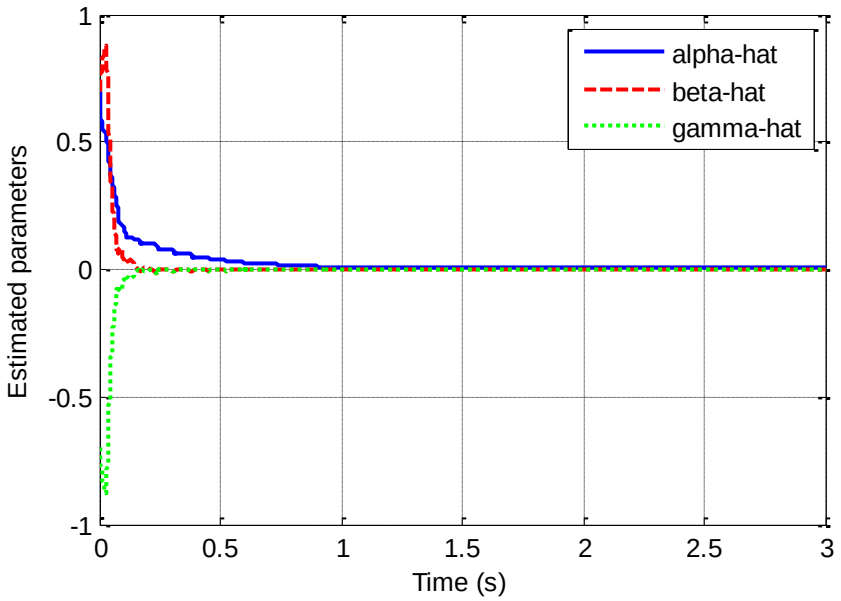

Fig. 5.10 Estimated parameters at 10 Hz in MRAC

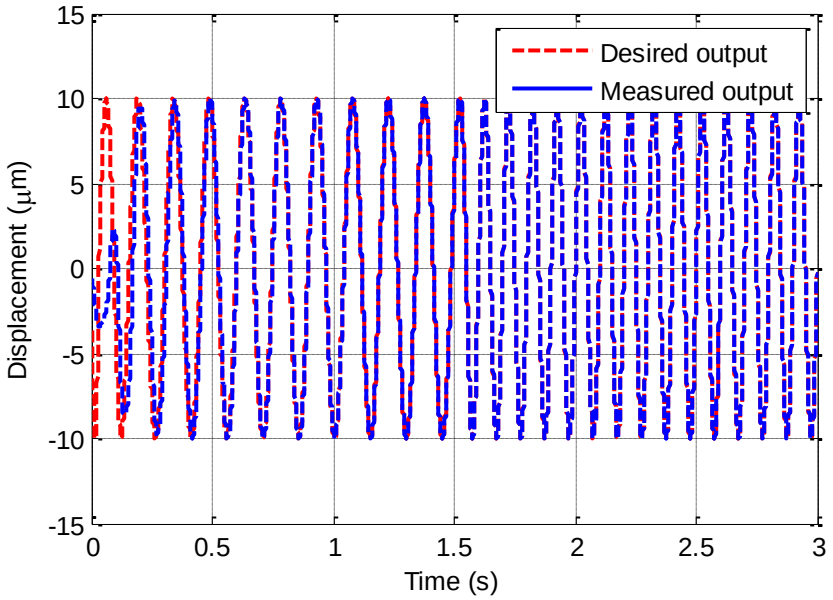

Fig. 5.11 Measured output and reference output at 10 Hz in MRAC

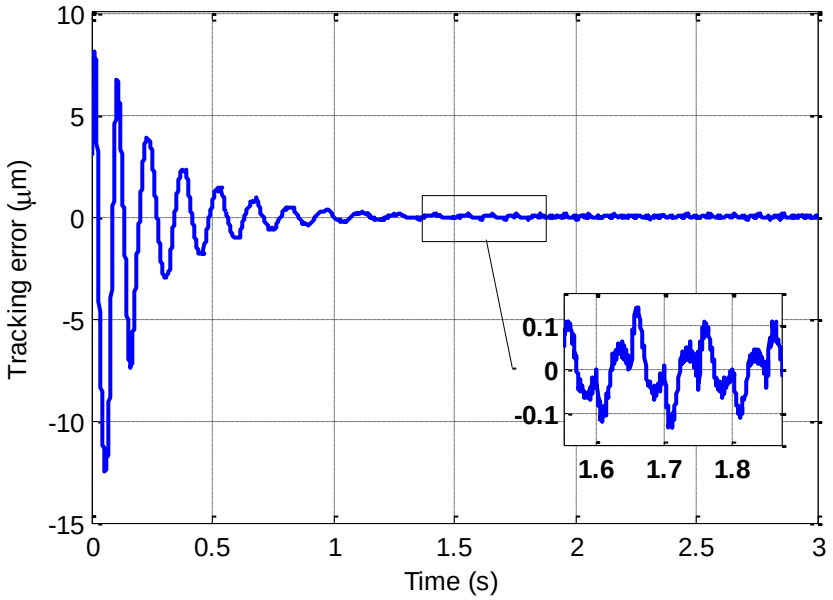

Fig. 5.12 Tracking error at 10 Hz in MRAC

In the experiment with $y_{d3}(k)$, the initial conditions of $\hat{\alpha}(k)$, $\hat{\beta}(k)$ and $\hat{\gamma}(k)$ are set to 0.5, 0.5, -0.7, respectively. The initial value of output $y(k)$ is assumed as 0. The adaptive gain Γ is chosen as 0.01.

Fig. 5.13 shows the control input $u(k)$. The estimates of parameters $\hat{\alpha}(k)$, $\hat{\beta}(k)$ and $\hat{\gamma}(k)$ are shown in Fig. 5.14. Fig. 5.15 shows the tracking result between reference and actual displacement. The tracking error for $y_{d3}(k)$ is shown in Fig. 5.16. It is observed that the maximum error is within $\pm 0.2\mu m$ when the system is at steady state.

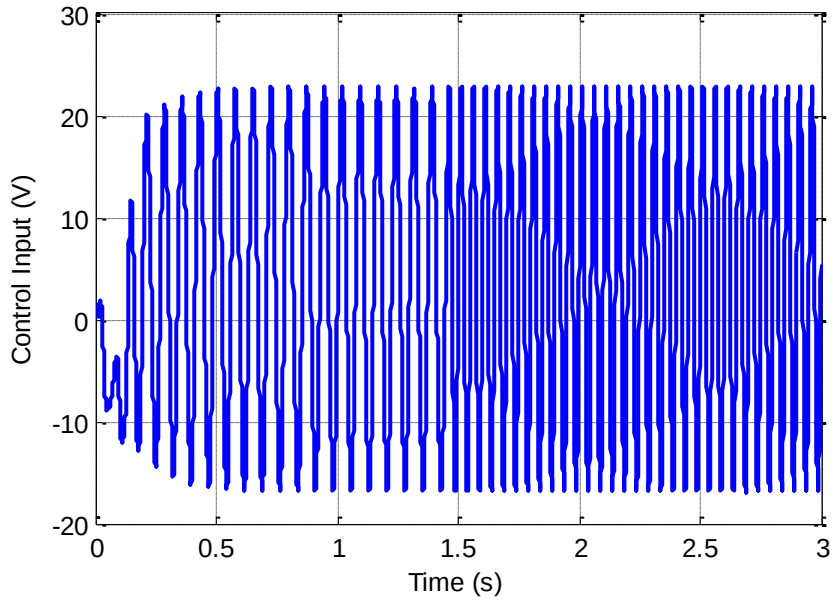

Fig. 5.13 Control input for experiment at 30 Hz in MRAC

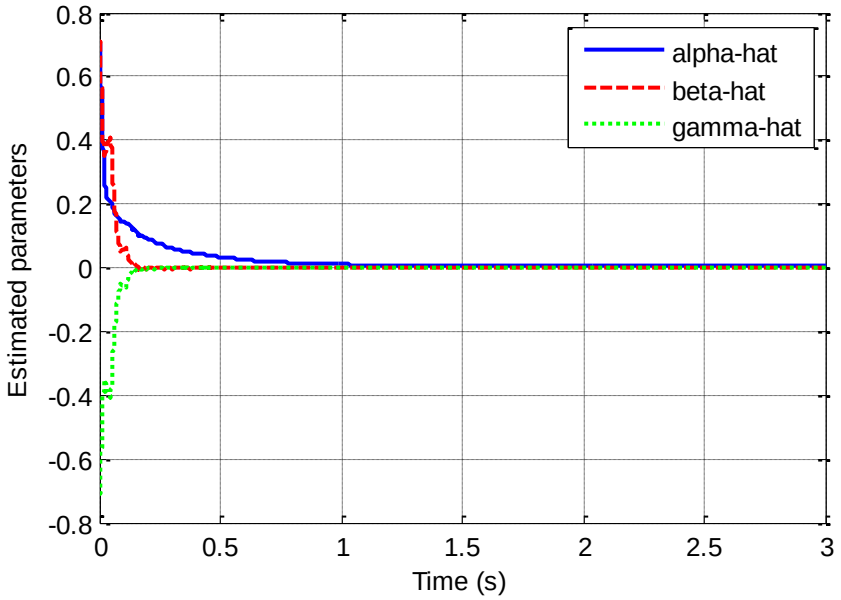

Fig. 5.14 Estimated parameters at 30 Hz in MRAC

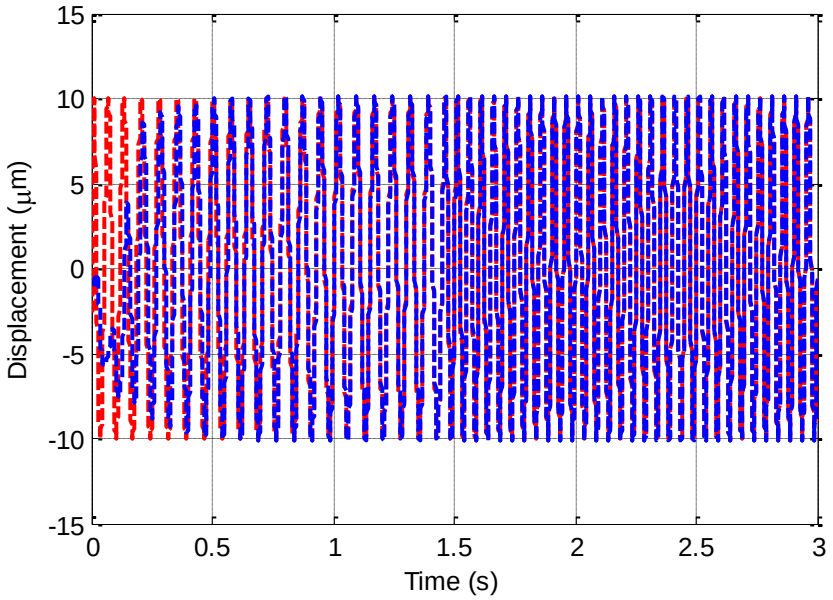

Fig. 5.15 Measured output and reference output at 30 Hz in MRAC

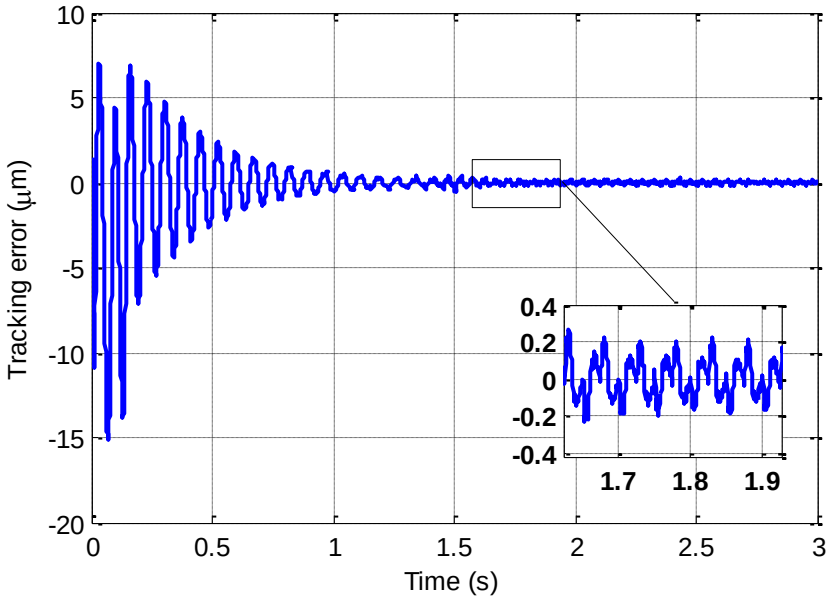

Fig. 5.16 Tracking error at 30 Hz in MRAC

In the experiment with $y_{d4}(k)$, the initial conditions of $\hat{\alpha}(k)$, $\hat{\beta}(k)$ and $\hat{\gamma}(k)$ are set to 0.5, 0.5, -0.7, respectively. The initial value of output $y(k)$ is assumed as 0. The adaptive gain Γ is chosen as 0.02.

Fig. 5.17 shows the control input $u(k)$. The estimates of parameters $\hat{\alpha}(k)$, $\hat{\beta}(k)$ and $\hat{\gamma}(k)$ are shown in Fig. 5.18. Fig. 5.19 shows the tracking result between reference and measured displacement. The tracking error for $y_{d4}(k)$ is shown in Fig. 5.20. It is observed that the maximum error is within $\pm 0.05\mu m$ when the system is at steady state.

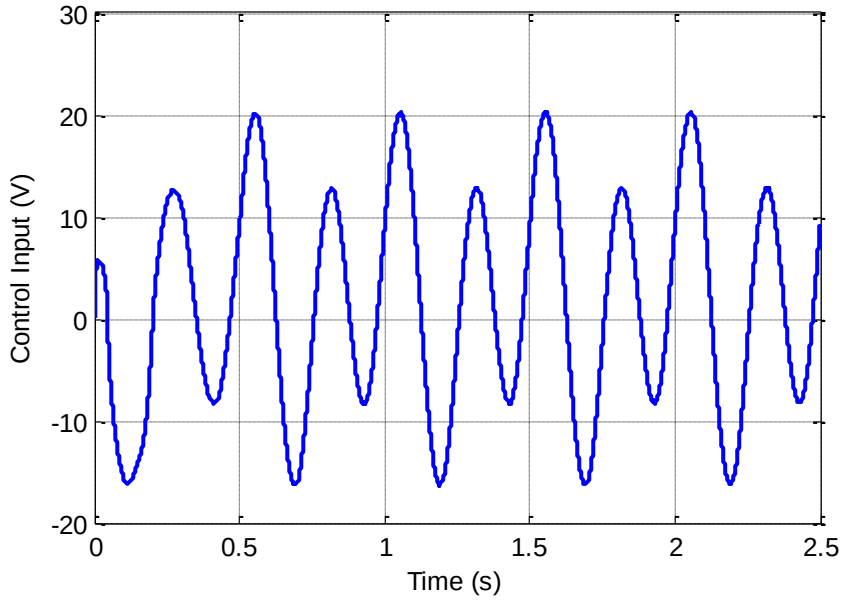

Fig. 5.17 Control input for multiple frequencies signal in MRAC

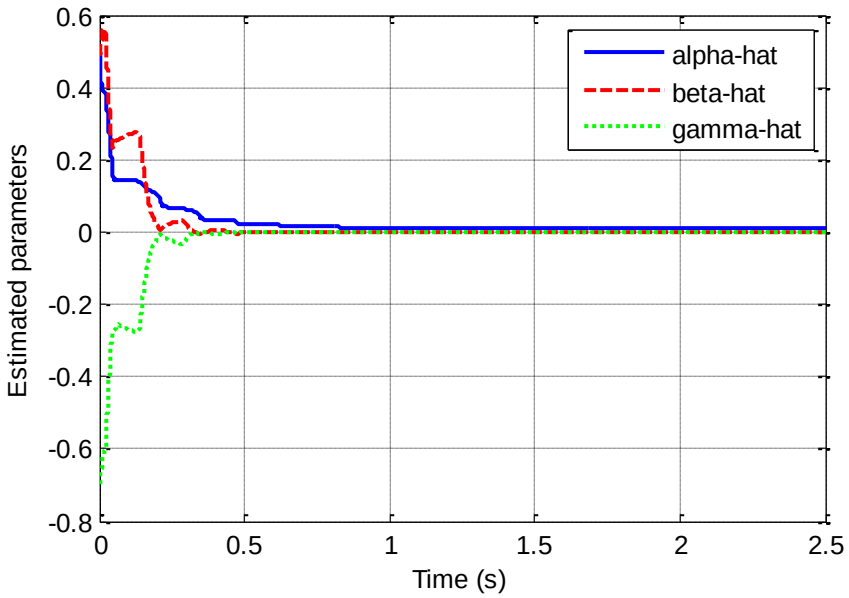

Fig. 5.18 Estimated parameters for multiple frequencies signal in MRAC

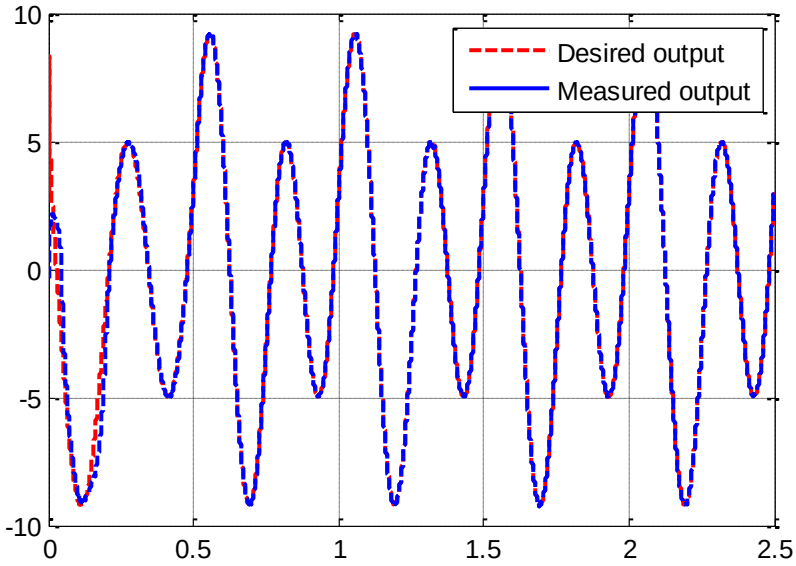

Fig. 5.19 Measured output and reference output for multiple frequencies signal in MRAC

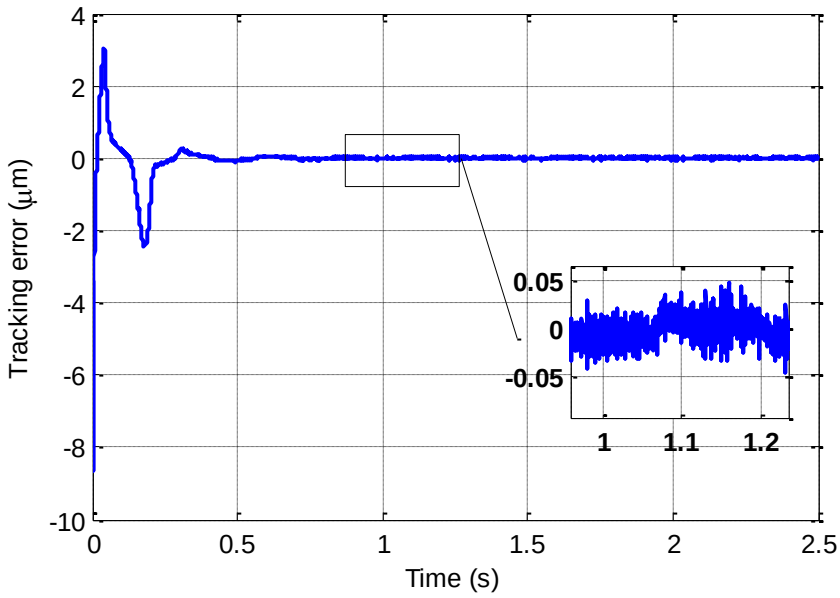

Fig. 5.20 Tracking error for multiple frequencies signal in MRAC

5.6 Discussion

MRAC shows that it has the best performance in term of tracking error among other control techniques. It's about 0.2% at 1 Hz frequency. Another advantage of MRAC is that, model parameters need not to be identified and the control algorithm is simple.

However, when frequency increases, in order to have a good tracking, the transient respond is slow (around 1 to 2 seconds). Thus, the overall performance is not so high.

Chapter 6: Conclusions and Future Works

6.1 Comparison Analysis

This thesis has discussed the control design and experimental results on PEAs of five model based control methods, which are open-loop feedforward compensation based on PI model, conventional PI control, model predictive control, adaptive model predictive control and model reference adaptive control based on pseudo discrete-time Bouc-Wen model.

The experiments are conducted with four difference frequency reference signals, which are 1Hz, 10Hz, 30Hz and the combination of two sinusoid signals with different frequencies. Experimental results show that the performance of open-loop control is poor even at low frequency. On the other hand, PID control has good results at low frequency, fast transient respond, and the controller is simple. However, PID control fails to get a good performance at higher frequency. At 30 Hz frequency reference signal, the maximum tracking error is within $\pm 20\%$.

Comparing to PID control, MPC and AMPC has a good control performance for low or high frequency, such as small tracking error, smooth tracking, and good transient respond. However, MPC is based on linear identified model; it will not work well in case the hysteresis nonlinearity is strong. Another disadvantage of MPC is the computation cost. The performance can be higher when the numbers of predicted steps are bigger, but the amount of calculation is also larger. Designers have to pay attention to this matter because when the calculation time increases, the sampling time also has to increase.

Lastly, the MRAC based on pseudo discrete-time Bouc-Wen model has the best tracking error, but the transient respond is slow. Thus, the performance is not so high. The advantage

of MRAC is that, the model parameters need not to be identified. Moreover, all of system signals can be proved to be bounded, and the system is stable.

Table 6.1 shows the comparison of control techniques.

Table 6.1 Comparison between control methods

	1Hz	10Hz	30Hz	Multiple frequencies signal
Feedforward control	10	15	21	16
PI control	1	6	20	1
MPC	3	4	18	4
AMPC	0.4	4	8	0.8
MRAC	0.2	1	2	0.5
	Maximum error (%)	Maximum error (%)	Maximum error (%)	Maximum error (%)

6.2 Conclusions

PEAs have been widely employed in various nano-positioning applications. However, hysteresis and other nonlinear effects greatly degrade the performance of PEAs. To exploit the full potential of PEAs in nano-positioning applications, this work presents the development of the model and its corresponding control schemes.

Firstly, the PEAs are modeled using linear identified model. Even though this model cannot describe the hysteresis nonlinearities in PEAs, it can be used as nominal model for control purpose. In order to describe the hysteresis, classical Prandlt-Ishlinskii model using play operator is adopted. This model is validated experimentally. Another hysteresis model is introduced; it is the Bouc-Wen model. Comparing to PI model, Bouc-Wen model is

differential-equation-based hysteresis model, and it has less parameters. This model is modified into discrete-time form for control purpose.

Secondly, several control methods are discussed and compared, which are feedforward compensation base on linear identified model, conventional PI control, model predictive control, adaptive model predictive control and model reference adaptive control. Each method has its own strength and weakness. Feedforward compensation with the explicit inversion of PI model shows that it can be used directly in open-loop control as in Chapter 2. However, the accuracy is not high. Another weakness of this model is that that classical PI model is limited to symmetric hysteresis, thus it is inappropriate to use this model for other types of smart actuators, such as magnetostrictive actuators which has an asymmetric hysteresis phenomenon. For the PI control as in Chapter 3, it is simple to design the controller and easy to be implemented. However, the system tracking performance is bad when the experiment is conducted at high frequency reference signals. It can be seen in Chapter 4 that the MPC and the AMPC show their effectiveness in control PEAs at various frequencies. But it is sensitive to system unknown effect, also the computation cost is needed to consider. Lastly, MRAC in Chapter 5 is proved to achieve the best results in tracking error performance, simple controller design, system stability is guaranteed, but it need long time to achieve steady state.

6.3 Future Work

- The tracking performance with feedforward compensation could be improved by combining it with feedback control techniques. Moreover, classical PI model can be modified so that it has ability to describe asymmetric hysteresis in other types of smart actuators.

- As a further extension of this work, it would be interesting to extend feedforward compensation method and adaptive control method to other types of hysteresis models such as Preisach model, Duhem model, Maxwell model, etc.

- This work only concerns the displacement control of PEAs without load. The tracking control of piezo-actuated system with load would be considered.

References

[1] D. Croft, G. Shed and S. Devasia, "Creep, Hystereis, and Vibration Compensation for Piezoactuators: Atomic Force Microscopy Application," *Journal of Dynamic Systems, Measurement, and Control*, Vol. 123, No.1 , 2001, pp 35-43.

[2] Q. Zou, K. K. Leang, E. Sadoun, M.J. Reed and S. Devasia, "Control Issues in High-Speed AFM for Biological Applications: Collagen Imaging Example," A*sian Journal of Control*, Vol. 6, No. 2, 2004, pp. 164-178.

[3] R. Kassies, K. O. Van der Werf, A. Lenferink, C. N. Hunter, J. D. Olsen, V. Subramaniam and C. Otto, "Combined AFM and Confocal Fluorescence Microscope for Application in Bio-Nanotechnology," *Journal of Microscopy*, Vol. 217, No. 1, 2005, pp. 109-116.

[4] H. Song, G. Vdovin, R. Fraanje, G. Schitter and M. Verhaegen, "Extracting Hysteresis from Nonlinear Measurement of Wavefront-Sensorless Adaptive Optics System," *Optics Letters*, Vol. 34, No. 1, 2009, pp. 61-63.

[5] W. Yang, S.-Y. Lee and B.-J. You, "A Piezoelectric Actuator with a Motion-Decoupling Amplifier for Optical Disk Drives," *Smart Materials and Structures*, Vol. 19, No. 6, 2010, pp. 1-10.

[6] G. Stöppler and S. Douglas, "Adaptronic Gantry Machine Tool with Piezoelectric Actuator for Active Error Compensation of Structural Oscillations at the Tool Centre Point," *Mechatronics*, Vol 18, No. 8, 2008, pp. 426-433

[7] S. R. Viswamurthy, A. K. Rao and R. Ganguli, "Dynamic Hysteresis of Piezoceramic Stack Actuators Used in Helicopter Vibration Control: Experiments and Simulations," *Smart Materials and Structures*, Vol. 20, No. 4, 2009, pp 387-399.

[8] M. S. Senousy, F. X. Li, D. Mumford, M. Gadala and R. K. N. D. Rajapakse, "Thermo-Electro-Mechanical Performance of Piezoelectric Stack Actuators for Fuel Injector Applications," *Journal of Intelligent Material Systems and Structures*, Vol. 20, No.4, 2007,pp. 1109-1119.

[9] J.–J. Wei, Z.-C. Qiu, J.-D. Han and Y.-C. Wang, "Experimental Comparison Research on Active Vibration Control for Flexible Piezoelectric Manipulator Using Fuzzy Controller," *Journal of Intelligent and Robotic Systems*, Vol. 59, No. 1, 2010, pp.31-56.

[10] P. Ge and M. Jouaneh, "Tracking Control of a Piezoceramic Actuator," *IEEE Transactions on Control Systems Technology*, Vol. 4, No.3, 1996, pp.209-216.

[11] P. Instrumente, "The World of Nanopositioning and Micropositioning 2005/2006," Physik Instrumente, Karlsruhe, 2005

[12] I. Mayergoyz and G. Bertotti, "The Science of Hysteresis," Vol.3, Elsevier, St. Louis, 2005.

[13] IEEE, "ANSI/IEEE std. 17601987: IEEE Standard on Piezoelectricty," The Institute of Electrical and Electronics Engineers, New York, 1988.

[14] D. C. Jiles nad D. L. Atherton, "Theory of Ferromagnetic Hysteresis," *Jounal of Magnetism and Magnetic Materials*, Vol 61, No.1, 1986, pp. 48-60.

[15] R. Smith, and A. Ounaie, "A Domain Wall Model for Hysteresis in Piezoelectric Materials," *Journal of Intelligent Material Systems and Structures*, Vol. 11, No. 1, 2000, pp. 62-79.

[16] R. C. Smith, "Smart Material System: Model Development," *SIAM*, Philadelphia, USA, 2005.

[17] T. L. Jordan, Z. Ounaies, "Piezoelectric Ceramics Characterization," *ICASE*, NASA Langley Research Center, Virginia, USA, 2001.

[18] A. Visintin, “Differential Models of Hysteresis,” Springer-Verlag, Berlin, Germany, 1994.

[19] Y. Shan, “Repetitive Control for Hysteretic Systems: Theory and Application in Piezo-based Nanopositioner,” Reno, University of Nevada, USA, 2011.

[20] W. S. Galinaitis, “Two Methods for Modeling Scalar Hysteresis and Their Use in Controlling Actuators with Hysteresis,” Virginia Polytechnic Institute and State University, USA, 1999.

[21] C. Y. Su, Y. Stephanenko, J. Svoboda and T. P. Leung, “Robust Adaptive Control of a Class of Nonlinear Systems with Unknown Backlash-like Hysteresis,” *IEEE Transactions on Automatic Control*, Vol. 45, No. 12, 2000, pp 2737-2432.

[22] I. Mayergoyz, “Mathematical Models of Hysteresis and Their Applications,” Elsevier, Netherlands, 2003.

[23] J. W. Machi, P. Nistri and P. Zecca, “Mathematical Models for Hysteresis,” *SIAM Review*, Vol. 45, No. 12, 1993, pp. 94-123.

[24] I. Mayergoys, “Preisach Models of Hysteresos,” *IEEE Transactions on Magnetics*, Vol. 37, No. 1, 1988, pp. 2925-2927.

[25] Y. H. Yu, X. Xiao, N. G. Naganathan, R. V. Dukkipati, “Dynamic Preisach Modelling of Hysteresis for the Piezoceramic Actuator System,” *Mechanism and Machine Theory*, Vol. 37, No. 1, 2002, pp. 75-89.

[26] M. A. Kranosklskii and A. V. Poorovskii, “System with Hysteresis,” Springer-Verlag, Berlin, German, 1989.

[27] YK. Wen, “Method for Random Vibration of Hysteresis System,” *Journal of Engineering Mechanics. ASCE*, Vol 102, 1976, pp.249-263.

[28] M. Ismail, F. Ikhouane, J. Rodellar, “The Hysteresis Bouc-Wen Model, a Survey,” *Arch Comput Methods Eng 16*, Barcelona, Spain, 2009, pp.161-188.

[29] R. Bouc, "Forced Vibration of Mechanical System with Hysteresis," *in Fourth Conference on Nonlinear Oscillation*, Prague, Czechoslovakia, 1976, pp.315.

[30] C. Lin and S. Yang, "Precise Positioning of Piezo-Actuated Stages using Hysteresis-Observer Based Control", *Mechatronics*, Vol. 16, 2006, pp.417-426.

[31] A. K. Padthe, B. Drincic, J. Oh, D. D. Rizos, S. D. Fasssois, and D. S. Bernstein, "Duhem Modelling of Friction-Induced Hysteresis," *IEEE Control Systems*, Vol. 28, No. 5, 2008, pp. 90-107.

[32] M. F. M. Naser and F. Ikhouane, "Consistency of the Duhem Model with Hysteresis," *Mathematical Problems in Engineering*, 2013.

[33] Dutta, M. Sushant, "Dynamic hysteresis modelling and applications," Master thesis, Rice University 2004.

[34] J. H. Oh and D. S. Bernstein, "Semilinear Duhem Model for Rate-Independent and Rate-Dependent Hysteresis," *IEEE Transactions on Automatic Control*, Vol. 50, No. 5, 2005, pp. 631-645.

[35] R. Bouc, "Modèle mathématic d'hystérésis ," *Acustica*, Vol.21, 1971, pp. 16-25

[36] G. S. Choi, H-S. Kim, G. H. Choi, "A Study on Position Control of Piezoelectric Actuators," *Proceedings of the IEEE International Symposium on Industrial Electronics*, Guimaraes, Portugal, 1997, pp. 851-855.

[37] S. H. Chang, C. K. Tseng, and H. C. Chien, "An Ultra-Precision XYΘZ Piezo-Micropositioner Part II: Experiment and Performance," *IEEE Transations on Ultrasonics, Ferroelectrics, and Frequency Control*, Vol. 46, No. 4, 1999, pp 906-912.

[38] Y. Haddab, N. Chaillet, and A. Bourjault, "A Microgripper Using Smart Piezoelectric Actuators," *Proceedings of the 2000 IEEE/RSJ International Conference on Intelligent Robots and Systems*, Takamatsu, Japan, 2000, pp. 659-664.

[39] P. Kallio, M. Lind, Q. Zhou, and H. N. Koivo, "A 3 DOF Piezohydraulic Parallel Micromanipulator," *Proceedings of the 1998 IEEE International Conference on Robotics and Automation*, Leuven, Belgium, 1998, pp. 1823-1828.

[40] F. Khorrami, "Adaptive Nonlinear Control for End-Effector Position Tracking of Multilink Flexible Manipulators with Embedded Active Materials," *Proceedings of the 33rd Conference on Decision and Control*, Florida, USA, 1994, pp 103-108.

[41] S.-S. Ku, U. Pinsopon, S. Cetinkunt, and S. Nakajima, "Design, Fabrication, and Real-time Neural Network Control of a Three-Degrees-of-Freedom Nanopositioner," I*EEE/ASME Transactions on Mechatronics*, Vol. 5, 2000, pp 273-280.

[42] J.-F. Li, K. Takagi, M. Ono, W. Pan, R. Watanabe, A. Almajid, and M. Taya, "Fabrication and Evaluation of Porous Piezoelectric Ceramics and Porosity-graded Piezoelectric Actuators," *Journal of the American Ceramic Society*, Vol, 86, 2003, pp 1094-1098.

[43] H. hu and R. Ben Mrad, "A discrete-Time Compensation Algorithm for Hysteresis in Piezoceramic Actuators," *Mechanical Systems and Signal Processing*, Vol. 18, No. 1, 2004, pp 169-185.

[44] S. Bashash and N. Jalili, "A Polunomial-Based Linear Mapping Strategy for Feedforward Compensation of Hysteresis in Piezoelectric Actuators," *Journal of Dynamic Systems, Measurement, and Control*, Vol. 130, No. 3, 2008, pp 1-10.

[45] U.-X. Tan, W. T. Latt, C. Y. Shee, C. N. Riviere and W. T. Ang, "Feedforward Controller of Ill-Conditioned Hysteresis Using Singularity-Free Prandlt-Ishlinskii Model," *IEEE/ASME Transactions on Mechatronics*, Vol 14, No 5, 2009, pp. 398-605

[46] C. Ru and L. Sun, "Hysteresis and Creep Compensation for Piezoelectric Actuator in Open-loop Operation," *Sensors and Actuators A: Physical*, Vol.122, No. 1, 2005, pp. 124-130.

[47] W. T. Ang, F. A. Garmón, P. Khosla and C. N. Riviere, "Modelling Rate-Dependent Hysteresis in Piezoelectric Actuators," *2003 IEEE/RSJ International Conference on Intelligent Robots and Systems*, Las Vegas, USA, 2003, pp 1975-1980.

[48] W. T. Ang, P. Khosla, C. N. Riviere, "Feedforward Controller with Inverse Rate-Dependent Model for Piezoelectric Actuators in Trajectory-Tracking Applications," *IEEE/ASME Transactions on Mechatronics*, Vol. 12, No. 2, 2007, pp 134-142.

[49] J. Lin, H. Chieng and C. C. Lin, "Tuning PID control Gains for Micro Piezo-Stage in using Grey Relational Analysis," *2008 International Conference on Machine Learning and Cybernetics*, Kunming, China, 2008, pp. 3863-3868.

[50] H.-J. Shieh, Y.-J. Chiu and Y.-T. Chen, "Optimal PID Control System of a Piezoelectric Micropositioner," *2008 IEEE/SICE International Symposium on System Integration*, Nagoya, Japan, 2008, pp. 1-5.

[51] D. Y. Abramovitch, S. Hoen and R. Workman, "Semi-Automatic Tuning of PID Gains for Atomic Force Microscopes," *Asian Journal of Control*, Vol. 11, No. 2, 2009, pp 188-195.

[52] K. K. Tan, T. H. Lee and H. X. Zhou, "Micro-Positioning of Linear-Piezoelectric Motors Based on a Learning Nonlinear PID Controller," *IEEE/ASME Transactions on Mechatronics*. Vol. 6, No. 4, 2001, pp 428-436.

[53] W. S. Oates and R. C. Smith, "Nonlinear Control Design for Piezoelectric-Driven Nanopositioning Stage," Pentagon Technical Report A591444, 2005.

[54] C. Edward and C. Edwards and S. K. Spurgeon, "Sliding Mode Control: Theory and Applications," Taylor & Francis, Abingdon, 1998.

[55] P.-K. Huang, P.-H. Shieh, F.-J. Lin and H.-J. Shieh, "Sliding-Mode Control for a Two-Dimensional Piezo-Positioning Stage," *Control Theory & Applications, IET*, Vol. 1, No. 4, 2007, pp. 1104-1113.

[56] J.-C. Shen, W.-Y. Jywe1, C.-H. Liu, Y.-T. Jian and J. Yang, "Sliding-Mode Control of a Three-Degrees-of-Freedom Nanopositioner," *Asian Journal of Control*, Vol. 10, No. 3, 2008, pp. 267-276.

[57] J.-C. Shen, J.-C. Shen, H.-K. Chiang and Y.-L. Shu, "Precision Tracking Control of a Piezoelectric-Actuated System," *Precision Engineering*, Vol. 32, No. 2, 2008, pp. 71-78.

[58] Q. Xu and Y. Li, "Dynamics Modelling and Sliding Mode Control of an XY Micropositioning Stage," *The 9th International Symposium on Robot Control (SYROCO'09)*, Gifu, Japan, 2009, pp. 781-786.

[59] Y. Li and Q. Xu, "Adaptive Sliding Mode Control with Perturbation Estimation and PID Sliding Surface for Motion Tracking of a Piezo-Driven Micromanipulator," *IEEE Transactions on Control Systems Technology*, Vol. 18, No. 4, 2010, pp. 798-810.

[60] H. C. Liaw, B. Shirinzadeh and J. Smith, "Sliding-Mode Enhanced Adaptive Motion Tracking Control of Piezoelectric Actuation Systems for Micro/Nano Manipulation," *IEEE Transactions on Control Systems Technology*, Vol. 16, No. 4, 2008, pp. 826-833.

[61] X. Chen and T. Hisayama, "Adaptive Sliding-Mode Posi- tion Control for Piezo-Actuated Stage," *IEEE Transactions on Industrial Electronics*, Vol. 55, No. 11, 2008, pp. 3927-3934.

[62] C. J. Li, H. S. M. Beigi, S. Li and J. Liang, "Nonlinear Piezo Actuator Control by Learning Self Tuning Regulator," *Journal of Dynamic Systems, Measurement, and Control*, Vol. 115, No. 4, 1993, pp. 720-723.

[63] H.-J. Shieh, F.-J. Lin, P.-K. Huang and L.-T. Teng, "Adaptive Tracking Control Solely Using Displacement Feedback for a Piezo-Positioning Mechanism," *IEEE Proceedings of Control Theory and Applications*, Vol. 151, No. 5, 2004, pp. 653-660.

[64] X. Tan and J. S. Baras, "Adaptive Identification and Con- trol of Hysteresis in Smart Materials," *IEEE Transactions on Automatic Control*, Vol. 50, No. 6, 2005, pp. 827-839.

[65] H. C. Liaw and B. Shirinzadeh, "Enhanced Adaptive Motion Tracking Control of Piezo-Actuated Flexure-Based Four-Bar Mechanisms for Micro/Nano Manipulation," *Sensors and Actuators A: Physical*, Vol. 147, No. 1, 2008, pp. 254-262.

[66] Y. Cao, L. Cheng, X. B. Chen, and PJ. Y. Peng, "An Inversion-Based Model Predictive Control With an Integral-of-Error State Variable for Piezoelectric Actuators," *IEEE/ASME Transactions on Mechatronics*, Vol 18, No. 3, 2013, pp 895-904.

[67] V. A. Neelakantan, G. N. Washington, and N. K. Bucknor, "Model Predictive Control of a Two Stage Actuation System using Piezoelectric Actuators for Controllable Industrial and Automotive Brakes and Clutches," *Journal of Intelligent Material Systems and Structures*, Vol. 19, No. 7, 2008, pp845-857.

[68] R. H. Comstock and W. Acton, "Charge Control of Piezoelectric Actuators to Reduce the Hysteresis Effects," United State Patent, 1981.

[69] R. Banning and W. L.de Koning et.al. "State-space Analysis and Identification for a Class of Hysteresis System," *Automatica*, Vol. 37, 2001, pp. 1883-1892.

[70] B. Bhikkaji, M. Ratnam, A. J. Fleming and S. O. R. Moheimani, "High-Performance Control of Piezoelectric Tube Scanners," *IEEE Transactions on Control System Technology*, Vol.15, No.5, 2007, pp. 853-866.

[71] A. J. Fleminga and S. O. R. Moheimani, "A Grounded-load Charge Amplifier for Reducing Hysteresis in Piezoelectric Tube Scanners," *Review of Scientific Instruments 23876*, 073707,2005

[72] A. J. Fleming and S. O. R. Moheimani, "Improved Current and Charge Amplifiers for Driving Piezoelectric Loads, and Issues in Signal Processing Design for Synthesis of Shunt Damping Circuits," *Journal of Intelligent Material Systems and Structures*,Vol. 15, 2004, pp. 77-92

[73] M. Brokate and J. Sprekeis, "Hysteresis and Phase Translations," Springer, New York, USA, 1996.

[74] P. Krejci and K. Kuhnen, "Inverse Control of Systems with Hysteresis and Creep," *IEEE Proceedings of Control Theory and Applications*, Vol. 148, No. 3, 2001, pp. 185-192.

[75] Ljung, "System Identification," Birkhäuser, Boston, USA, 1998.

[76] E. F. Camacho and C. Bordons, "Model Predictive Control," Springer-Verlag, London, England, 2007.

[77] C. Lin and S. Yang, "Precise Positioning of Piezo-Actuated Stages using Hysteresis-Observer Based Control," *Mechatronics*, Vol. 16, 2006, pp.417-426.

[78] F. Ikhouane, V. Manosa, J. Rodella, "Adaptive Control of a Hysteretic Structural System", *Automatica*, Vol. 41, 2007, pp.225-231.

[79] Y. Li and Q. Xu, "Adaptive Sliding Mode Control With Perturbation Estimation and PID Sliding Surface for Motion Tracking of a Piezo-Driven Micromanipulator," *IEEE Transaction on Control Systems Technology*, Vol. 18, No. 4, 2010, pp 798-810.

[80] M. Rakotondrabe, "Bouc-Wen Modeling and Inverse Multiplicative Structure to Compensate Hysteresis Nonlinearity in Piezoelectric Actuators", *IEEE Transaction on Automation Science and Engineering*, Vol. 8, 2011, pp.428-431.

[81] J. Zhou, C. Wen, T. Li, "Adaptive Output Feedback Control of Uncertain Nonlinear Systems with Hysteresis Nonlinearity," *IEEE Transaction on Automatic Control*, Vol. 57, No.10, 2012, pp. 2627-2633.

[82] F. Ikhouane, and J, Rodellar, "Systems with Hysteresis: Analysis, Identification and Control Using the Bouc-Wen Model," John Wiley & Sons Ltd, West Sussex, England, 2007.

[83] G. C. Goodwin and K. S. Sin, "Adaptive Filtering Prediction and Control," Dover, New York, USA, 2009.

[84] R. P. Agarwal, "Difference Equations and Inequalities – Theory, Methods, and Applications", Marcel Dekker, New York, USA, 2000.

Appendix A

Levenberg–Marquardt algorithm

The curvefitting toolbox in MathLab uses Levenberh-Marquardt (LM) algorithm to identify parameters.

The problem for which the LM algorithm provides a solution is called Nonlinear Least Squares Minimization. This implies that the function to be minimize is of the following special form:

$$f(x)=\frac{1}{2}\sum_{j=1}^{m} r_j^2(x) \tag{A1}$$

Where $x=(x_1,x_2,...,x_n)$ is a vector, and each r_j is a function from $R^n \to R$. The r_j are referred to as a residuals and it is assumed that $m \geq n$.

To make matters easier f is represented as a residual vector r: $R^n \to R^m$ defined by

$$r(x)=(r_1(x),r_2(x),...,r_m(x)) \tag{A2}$$

Now, f can be rewritten as $f(x)=\frac{1}{2}\|r(x)\|^2$. The derivatives of f can be written using the Jacobian matrix J defined as $J(x)=\frac{1}{2}\frac{\partial r_j}{\partial x_i}$, $1 \leq j \leq m, 1 \leq i \leq n$.

Appendix

Consider the linear case where every r_j function is linear. Here, the Jacobian is constant and we can represent r as a hyperplane through space, so that f is given by the quadratic $f(x) = \frac{1}{2}\|Jx + r(0)\|^2$. We also get $\nabla f(x) = J^T(Jx + r)$ and $\nabla f(x) = J^T J$. Solving for the minimum by setting $\nabla f(x) = 0$, we obtain $x_{\min} = -(J^T J)^{-1} J^T r$, which is the solution to the set of normal equations.

Returning to the general, nonlinear case, we have

$$\nabla f(x) = \sum_{j=1}^{m} r_j(x) \nabla r_j(x) = J(x)^T r(x) \tag{A3}$$

$$\nabla^2 f(x) = J(x)^T J(x) + \sum_{j=1}^{m} r_j(x) \nabla^2 r_j(x) \tag{A4}$$

The distinctive property of least squares problems is that given the Jacobian matrix J, we can essentially get the Hessian ($\nabla^2 f(x)$) for free if it is possible to approximate the r_j by linear function ($\nabla^2 r_j(x)$ are small) or the residuals ($r_j(x)$) themselves are small. The Hessian in this case simply becomes

$$\nabla f(x) = J(x)^T J(x) \tag{A5}$$

which is the same as for the linear case.

The common approximation used here is one of near-linearity of the r_j near the solution so that $\nabla^2 r_j(x)$ are small. It is also important to note that (A5) is only valid if the residuals are small. Large residual problems cannot be solved using quadratic approximation, and consequently, the performance of the algorithms presented is poor in such cases.

Appendix B

Projection Algorithm

Consider a nonlinear deterministic dynamical systems can be described by a model:

$$y(k) = \phi(k-1)^T \theta_0 \tag{B1}$$

where $y(k)$ denotes the system output at time t, $\phi(k-1)$ denotes a vector that is a nonlinear function of output and input $\phi(k-1) = \{u(k-1), u(k-2), ..., y(k-1), y(k-2), ...\}$ and θ_0 is unknown parameters vector.

The, projection algorithm is followed:

$$\hat{\theta}(k) = \hat{\theta}(k-1) + \frac{a\phi(k-1)}{c + \phi(k-1)^T \phi(k-1)} \left[y(k) - \phi(k-1)^T \hat{\theta}(k-1) \right] \tag{B2}$$

with $\hat{\theta}(0)$ is given and $c > 0 ; 0 < a < 2$.

Introduce the following notation:

$$\tilde{\theta}(k) = \hat{\theta}(k) - \phi_0 \tag{B3}$$

$$\begin{aligned} \varepsilon(k) &= y(k) - \phi(k-1)^T \hat{\theta}(k-1) \\ &= -\phi(k-1)^T \tilde{\theta}(k-1) \end{aligned} \tag{B4}$$

Lemma 2: For the algorithm (B2) and subject to (B1), it follow that

(i) $\left\| \hat{\theta}(k) - \theta_0 \right\| \le \left\| \hat{\theta}(k-1) - \theta_0 \right\| \le \left\| \hat{\theta}(0) - \theta_0 \right\|; k \ge 1$ (B5)

Appendix

$$\text{(ii)}\ \lim_{N\to\infty}\sum_{k=1}^{N}\frac{\varepsilon(k)^2}{c+\phi(k-1)^T\phi(k-1)}<\infty \tag{B6}$$

and this implies

$$\text{(a)}\ \lim_{k\to\infty}\frac{\varepsilon(k)}{\left[c+\phi(k-1)^T\phi(k-1)\right]^{1/2}}=0 \tag{B7}$$

$$\text{(b)}\ \lim_{N\to\infty}\sum_{k=1}^{N}\frac{\phi(k-1)^T\phi(k-1)\varepsilon(k)^2}{\left[c+\phi(k-1)^T\phi(k-1)\right]^2}<\infty \tag{B8}$$

$$\text{(c)}\ \lim_{N\to\infty}\sum_{k=1}^{N}\left\|\hat{\theta}(k)-\hat{\theta}(k-1)\right\|^2<\infty \tag{B9}$$

$$\text{(d)}\ \lim_{N\to\infty}\sum_{k=p}^{N}\left\|\hat{\theta}(k)-\hat{\theta}(k-p)\right\|^2<\infty \tag{B10}$$

$$\text{(e)}\ \lim_{k\to\infty}\left\|\hat{\theta}(k)-\hat{\theta}(k-p)\right\|=0 \tag{B11}$$

for any finite p.

Proof: (i) Subtracting θ_0 from both sides of (B2) and using (B1) and (B3), the following is obtained

$$\tilde{\theta}(k)=\tilde{\theta}(k-1)+\frac{a\phi(k-1)}{c+\phi(k-1)^T\phi(k-1)}\phi(k-1)^T\tilde{\theta}(k-1) \tag{B12}$$

Hence, using (B4),

$$\left\|\tilde{\theta}(k)\right\|^2-\left\|\tilde{\theta}(k-1)\right\|^2=a\left[-2+\frac{a\phi(k-1)^T\phi(k-1)}{c+\phi(k-1)^T\phi(k-1)}\right]\frac{\varepsilon(k)^2}{c+\phi(k-1)^T\phi(k-1)} \tag{B13}$$

Since $0<a<2$ and $c>0$, it gives

$$a\left[-2+\frac{a\phi(k-1)^T\phi(k-1)}{c+\phi(k-1)^T\phi(k-1)}\right]<0 \tag{B14}$$

and then (B5) follows from (B13).

(ii) Observe that $\left\|\tilde{\theta}(k)\right\|^2$ is a bounded nonincreasing function, and by summing (B13), its gives

$$\left\|\tilde{\theta}(k)\right\|^2 = \left\|\tilde{\theta}(0)\right\|^2 + \sum_{j=1}^{k} a\left[-2 + \frac{a\phi(k-1)^T\phi(k-1)}{c+\phi(k-1)^T\phi(k-1)}\right]\frac{\varepsilon(k)^2}{c+\phi(k-1)^T\phi(k-1)} \tag{B15}$$

Since $\left\|\tilde{\theta}(k)\right\|^2$ is nonnegative, and since (B14) holds, (B6) can be concluded.

(a) Equation (B7) follows immediately from (B6).

(b) Noting that

$$\frac{\varepsilon(k)^2}{c+\phi(k-1)^T\phi(k-1)} = \frac{\left[c+\phi(k-1)^T\phi(k-1)\right]\varepsilon(k)^2}{\left[c+\phi(k-1)^T\phi(k-1)\right]^2}$$

Equation (B8) can be established by using (B6).

(c) Equation (B8) immediately implies (B9) by noting the form of the algorithm (B2).

(d) It is clear that

$$\left\|\hat{\theta}(k)-\hat{\theta}(k-p)\right\|^2 = \left\|\hat{\theta}(k)-\hat{\theta}(k-1)+\hat{\theta}(k-1)-\hat{\theta}(k-2)\ldots\hat{\theta}(k-p+1)-\hat{\theta}(k-p)\right\|^2$$

Then, using the Schwarz inequality,

$$\left\|\hat{\theta}(k)-\hat{\theta}(k-p)\right\|^2 \le p\left(\left\|\hat{\theta}(k)-\hat{\theta}(k-1)\right\|^2 + \ldots + \left\|\hat{\theta}(k-p+1)-\hat{\theta}(k-p)\right\|^2\right)$$

Since p is finite, the results follows immediately from (B9).

(e) Equation (B11) follows immediately from (B10)

List of Publication

Journal papers (peer-reviewed)

T. V. Minh, X. Chen, "Precision Tracking Control for Piezoelectric Actuator Using Pseudo Discrete-time Bouc-Wen Model," International Journal of Advanced Mechatronic Systems, accepted as Regular Paper waiting for appearance.

Conference papers (peer-reviewed)

T. V. Minh, X. Chen, "Adaptive Control Using Discrete-Time Bouc-Wen Model for Piezoelectric Actuator," IEEE International Conference on Robotics and Biomimetics (ROBIO 2014), 5th -10th December 2014, Bali, Indonesia.

T. V. Minh, N. M. Linh, X. Chen, "Tracking Control of Piezoelectric Actuator Using Adaptive Model," International Conference on Real-time Computing and Robotics (RCAR 2015), 23rd – 27th June 2015, Changsha, China.

N. M. Linh, T. V. Minh, X. Chen, "Precise Tracking Control for Piezo-actuated Stage Using Inverse Compensation and Model Predictive Control," 2015 International Conference on Advanced Mechatronic Systems (ICAMECHS 2015), 21th-25th August 2015, Beijing, China.